ELECTRONIC AND OPTICAL PROPERTIES OF 2D MOLECULAR SYSTEMS

PAOLA MOCCI

Dottorato di Ricerca XXXII ciclo

Università degli studi di Cagliari
Facoltà di Scienze
Dipartimento di Fisica

Relatori:
Prof. Giancarlo Cappellini
Prof. Matteo Ceccarelli

Coordinatore:
Prof. Paolo Ruggerone

Esame Finale A.A. 2018 – 2019
Difesa Tesi: Sessione Gennaio-Febbraio 2020

[November 23, 2019 at 16:41 – classicthesis version 4.2]

Alla mia famiglia
A voi

Dedicated to my family: the only thing important in my life

ABSTRACT

This Thesis presents and explores the attractive landscape of the reduced dimensionality systems world, focusing in particular, on 2D materials. We analyze the effects of partial/complete atomic substitution and specific chemical functionalization on the electronic (ground and excited-state) and optical properties of nanometric portions of 2D compounds, that are of interest for both fundamental research and potential use in technological devices and applications.
In particular, we have considered the class of PAHs, concentrating our attention on the Circumacenes molecules (e.g. Coronene, Ovalene, Circumanthracene, Circumtetracene, Circumpentacene are the first five members). For these systems we have studied the effects induced by different substitutions: insertions of Silicon atoms, total substitutions of Boron and Nitrogen to form the Boron-Nitride (BN) counterpart and total replacement of peripheral H atoms with F atoms on several physical properties.

In the first part of this Thesis we report a systematic comparative study of Coronene and Ovalene molecules (the first two members of the Circumacenes family) analyzing the effects of Si-atoms substitutions (single, double and triple insertions) on the ground-state electronic and optical properties of these systems. We have performed all-electrons density functional theory (DFT) and time-dependent DFT (TDDFT) calculations to quantify the effects of morphology and chemical modifications on different physical observables, such as electron affinity, ionization energy, quasi-particle energy gap, optical absorption, exciton binding energy. For this part of the work we used the hybrid exchange-correlation functional B3LYP in combination with a gaussian localized basis-set. This adopted union functional/basis-set has proven to produce good results for polycyclic aromatic hydrocarbons and their derivatives. Globally, for this first part of the work we have used *NWChem* computational code.

In the second part, using the same theoretical framework (Density Functional Theory (DFT) and Time-Dependent DFT (TDDFT)), we study the electronic and optical properties of the Boron-Nitride counterparts of the five first members of the Circumacenes (from Coronene to Circumpentacene). In addition, we also select the case of the smallest molecule of the cluster to deepen the perfluorination effects on the same observables. We investigate in a comparative approach the molecular properties of these compounds, presenting the trend for different observables like: electron affinities, ionization energies, quasi-particle energy-gaps, optical absorption spectra, exciton binding energies and comparing with the corresponding results for the Carbon-

made original parents, as well as with the available data from the literature. For this part of the Thesis, globally, we have used an all-electrons gaussian-based computational package, namely *Gaussian-16*.

In the last part of this Thesis we present a comparative study focused on the C-made linear Acenes and their Si/Ge-based counterparts. We have quantified the effects of complete substitution on the electronic and optical properties of these systems, showing the behavior of the above mentioned observables as a function of the molecular size for each cluster and the differences among clusters of different atomic type at fixed molecular size. In this last part of the work we have implemented DFT and TDDFT calculations through *Gaussian* computational code.

Overall, the results obtained in this Thesis can be synthesized by the following points:

- We have found that the presence of Si-atoms into Circumacenes could alter in some cases (starting for trimer-substituted configurations) the planar appearance typical of these systems, showing that evident distortions in the 'out-of-plane' directions take place. We have found larger values of the ground-state energies for all the substituted configurations with respect to the original counterparts. In both Coronene and Ovalene molecules, we recorded a general reduction of the fundamental gap and optical onset energies as a consequence of the chemical modification.
  For what concerns the optical spectra, we have found that the insertion of Silicon in the C-based matrix provoke an enrichment of the absorption structure and a general redshift of the onsets and of the main peaks (the absorption is mainly translated towards the visible up the IR with a remodeling of the main peaks intensity).

- Analyzing the case of the Circumacenes as compared to their BN-made counterpart, the most considerable result concerns the optical properties: the absorption of the BN systems is in the UV range, with a general blueshift of the absorption features of the C-based materials. In particular, thanks to their UV-absorption feature here analysed, these BN nanomaterials keep a promising role in the technology linked to UV optoelectronics, beyond Graphene applications.
  Dealing with the electronic properties, we have found that a lowering of the vertical electron affinities and a rise of the ionization energies and QP gaps take place passing from the C-made to the BN-based systems. For what concerns the optical properties, we observed that the absorption is localized in the UV for all the BN-based molecules, unlike their C-made parents which

present an absorption spectrum located in the visible range. In this case, we have verified a blueshift of the optical onsets and the dominant peaks for the BN-made molecules with respect to the original C-made parents.

- Finally, for the linear clusters, comparing the C-made original molecules with the Si/Ge-made analogues, one of the principal results concerns the morphological properties. The analysis on this feature has confirmed that, while the carbon-based compounds preserve the planar appearance from the first to the last system, for both the silicon-made and germanium-made families, distortions in the out-of-plane direction take place ever since from the smallest molecule of the family. According to the data from the literature, extending ideally to the infinite dimension the previous molecules, a rippled surface of Si and Ge could be formed. This fact is in accordance with the finding of ripple surfaces either for Si or Ge.
  For what concerns the electronic properties, as a function of the molecular size, we have found for each species, a general increase (decrease) of the vertical electron affinities (ionization energies) and deviations of the fundamental gaps of the same order of magnitude. Dealing with the optical properties, we have observed a general redshift for both the optical onsets and the dominant peaks positions, as a function of the molecular size, independently by the nature of the constituent atom.

In conclusion, using state-of-the-art computational techniques, this Thesis presents original results on key molecular properties of different Polycyclic Aromatic Hydrocarbons, considered as nanometric portions of their infinite successful counterparts. We performed a systematic comparative investigation to evaluate, from a quantitative point-of-view, the effects of different chemical modifications (partial/total substitutions of different atomic types or perfluorination) on the electronic, optical and structural properties of different systems which are the building blocks of materials widely employed in molecular electronics. Our findings can be possibly used to select tailored chemical modifications to specific compounds for future electronic and optical applications.

PUBLICATIONS

The results of this Thesis have been published in the following papers:

[1] **P.Mocci**, R. Cardia, G. Cappellini, "Inclusions of Si-atoms in Graphene nanostructures: a computational study on the ground-state electronic properties of Coronene and Ovalene", *Journal of Physics: Conference Series* **956**,012020 (2018)

[2] **P.Mocci**, R. Cardia, G. Cappellini, "Si-atoms substitutions effects on the electronic and optical properties of coronene and ovalene", *New Journal of Physics* **20**,
DOI:https://dx.doi.org/10.1088/1367-2630/aae7f0(2018)

[3] **P.Mocci**, R. Cardia, G. Cappellini, "A computational investigation on the electronic and optical properties of Coronene and its Boron-Nitride and perfluorinated couterparts", *Journal of Physics: Conference Series* **1226**,012016 (2019)

[4] **P.Mocci**, R. Cardia, G. Cappellini, "A computational study on the Electronic and Optical properties of Boron-Nitride (BN) Circumacenes", *Phys. Chem. Chem. Phys.*, DOI:0.1039/C9CP01038F (2019)

Submitted Works

[1] **P. Mocci**, R. Cardia, A. Bosin, G. Cappellini, "Optical and Electronic properties of BN-ring insertions in Circumacenes: the case of Coronene and Ovalene" , **SUBMITTED** for *Journal of Physics: Conference Series –,–*

Works in Preparation

[1] **P. Mocci**, A. Bosin, G. Malloci, G. Cappellini, "Electronic and Optical properties of Linear Carbon Acenes and the Si/Ge-made analogous" , **IN PREPARATION FOR PCCP** –,–

CONFERENCES AND SEMINARS

Conferences, Talks and Posters

1. **Attended Conference and Poster Contribution P. Mocci**, R. Cardia and G. Cappellini. 'Electronic and optical properties of Si-atoms substituted Graphene nanoribbons " - Presented at: 8^{th} *YOUNG RESEARCHERS MEETING - Cagliari, Italy 29/05-1/06/17*.

2. **Attended Conference and Poster Contribution P. Mocci**, R. Cardia and G. Cappellini. "Si-atoms substitutions in Graphene nanoribbons: a study of electronic and optical properties " - Presented at: 7^{th} *ETSF- YOUNG RESEARCHERS MEETING - Tarragona, Spain 4-9/06/17*.

3. **Poster P. Mocci**, R. Cardia and G. Cappellini "Electronic and Optical Properties of Si-atoms substituted Graphene Nanoribbons" - Presented at: *Open days della ricerca scientifica-Cagliari, Italy 16-20/04/2018*.

4. **Attended Conference and Oral Contribution (Talk) P. Mocci**,R. Cardia and G. Cappellini "A computational investigation on the electronic and optical properties of Coronene and its Boron-Nitride and perfluorinated couterparts " -Presented at: 9^{th} *YOUNG RESEARCHERS MEETING - Salerno, Italy 9-14/07/2018*

5. **Attended Conference and Oral Contribution (Talk) P. Mocci**,R. Cardia, A. Bosin and G. Cappellini "Optical and Electronic properties of BN-ring insertions in Circumacenes: the case of Coronene and Ovalene " - Presented at: 10^{th} *YOUNG RESEARCHERS MEETING - Roma, Italy 18-21/06/2019*

Other Contributions

1. **Invited Speaker** G. Cappellini, R. Cardia, **P. Mocci** "Optical and electronic properties of BN nanoflakes: a DFT and TD-DFT computational study " - Presented at: *Congress on New Advances in Condensed Matter Physics, Kunming, Yunnan, PRC (CINA), 21-23 August, 2018*. [Presenting Author G. Cappellini]

2. **Invited Speaker** G. Cappellini, R. Cardia, **P. Mocci** "Optical and electronic properties of BN nanoflakes: a DFT and TDDFT computational study " - Presented at: *Istituto Tecnologico de Areonautica di Sao José dos Campos, - Sao Paolo, Brasil 9/2018*. [Presenting Author G. Cappellini]

3. **Invited Speaker** G. Cappellini, **P. Mocci** R. Cardia "Electronic and Optical properties of BN nanoflakes" - Presented at: *IFTO-FSU - Jena, Germany 15 January, 2019*. [Presenting Author G. Cappellini]

4. **Invited Speaker** G. Cappellini, **P. Mocci** R. Cardia "A DFT and TD-DFT computational study on the electronic and optical properties of BN nanoflakes: the case of Circumacenes" - Presented at: *CV Congresso SIF - L'Aquila, 23-27 September, 2019*. [Presenting Author G. Cappellini]

- **P. Mocci**, R. Cardia, A. Bosin and G. Cappellini "Silicon atoms insertions in Graphene nanoribbons: electronic and optical properties", **ISCRA C** Class Project; ID: SIGREOP - HP10CS13XP, *2017*
- **P. Mocci**, R. Cardia, A. Bosin and G. Cappellini "Optical and Electronic of Silicene Clusters", **ISCRA C** Class Project; ID: OESICLU - HP10CJTAHH, *2018*

ACKNOWLEDGEMENTS

Innanzitutto, vorrei ringraziare i miei supervisori Prof. Giancarlo Cappellini e Prof. Matteo Ceccarelli, per avermi condotto alla meta finale di questo percorso di crescita culturale e umana.
Un grazie speciale va a Roberto, che fin dall'inizio si è preso cura di me, insegnandomi i "trucchi del mestiere", aiutandomi nelle difficoltà e rendendosi disponibile per ogni spiegazione ed estremamente paziente nei momenti più critici.
Desidero ringraziare anche Dr Andrea Bosin e Dr Giuliano Malloci per aver dedicato parte del loro tempo a collaborare con il nostro piccolo gruppo di ricerca, mostrando immensa gentilezza e disponibilità in qualsiasi momento.
Infine, ma non per questo meno importante, il grazie principale è ovviamente rivolto ai miei genitori e ai miei fratelli, Stefano e Daniele, che da sempre mi hanno supportata, ancor di più sopportata, incoraggiandomi costantemente e amorevolmente, durante questi tre anni: grazie infinite "Family".
Inoltre, ringrazio con tutto il cuore, mia nonna Giovanna, che con le sue preghiere mi ha sostenuta e incoraggiata sempre e soprattutto nei momenti più negativi; ringrazio i miei zii, Marcello e Maria, per essermi stati affettuosamente ed energicamente vicini e con cui ho condiviso ansie e tormenti, oltre a gioie e piccole soddisfazioni.
La presente tesi è stata prodotta durante la frequenza del corso di dottorato in Fisica dell'Università degli Studi di Cagliari, A.A. 2016/2019 - XXXII ciclo, con il parziale supporto di borsa di studio finanziata con le risorse del P.O.R. SARDEGNA F.S.E. 2007-2013 - Obiettivo competitività regionale e occupazione, Asse IV Capitale umano, Linea di Attività l.3.1 "Finanziamento di corsi di dottorato finalizzati alla formazione di capitale umano altamente specializzato, in particolare per i settori dell'ICT, delle nanotecnologie e delle biotecnologie, dell'energia e dello sviluppo sostenibile, dell'agroalimentare e dei materiali tradizionali". P M ringrazia con gratitudine il Governo Regionale della Sardegna per il parziale supporto finanziario del suo corso di Dottorato.

CONTENTS

LIST OF FIGURES

LISTINGS

ACRONYMS

MO Molecular Orbital

HOMO Highest Occupied Molecular Orbital

LUMO Lowest Unoccupied Molecular Orbital

TFT Thin Film Transistor

FET Field Effect Transistor

LED Light Emitting Diode

OFET Organic Field Effect Transistor

OTFT Organic Thin Film Transistor

OLED Organic Light Emitting Diode

PV Photovoltaic

OPV Organic Photovoltaic

LMCDs Layered Metal Dichalcogenides

IE Ionization Energy

EA Electron Affinity

UV Ultra-Violet

IR Infrared

PAH Polycyclic Aromatic Hydrocarbon

CNT Carbon Nanotubes

BN Boron-Nitride

BNNR Boron-Nitride Nanoribbon

BNNT Boron-Nitride Nanotube

BNNS Boron-Nitride Nanosheet

TMD Transition metal dichalcogenides

LMDCs Layered Metal Dichalcogenides

DFT Density Functional Theory

XC Exchange-Correlation

QP Quasi-Particle

LDA Local Density Approximation

TDDFT Time-Dependent DFT

VdW Van der Waals

BSE Bethe-Salpeter Equation

SCF Self Consistent Field

Part I

SCIENTIFIC CONTEXT AND THEORETICAL BACKGROUND

1 INTRODUCTION

1.1 TECHNOLOGICAL BACKGROUND: TWO DIMENSIONAL (2D) MATERIALS BEYOND GRAPHENE

Two-dimensional (2D) materials (like Graphene and Silicene)[48, 76], which are one of the most extensively studied classes of systems, thanks to their attractive physical and chemical properties, actually occupy more than ever a central role, in both fundamental physics research and technological applications. Their importance, rapidly increased during the recent past, is now in incessant development, thanks to their advantageous electronic, optical and mechanical properties (planar feature, flexibility, mechanical resistance....). These materials are, in fact, considered among the most promising candidates for a multiplicity of different technological optoelectronic devices. They also exhibit unusual physical phenomena that occur, for example, when charge and heat transport is confined in a plane: from this fact, the third dimension can be considered as negligible. Commonly, low-dimensional materials can be distinguished in terms of dimension, into the following categories: 0D, 1D and 2D [98]. Low-dimensionality effects, as the basis of nano-optics and nano-electronics, for example, are well recognized to make group-III nitrides interesting for highly efficient light emitting diodes (LEDs) and a series of optoelectronic devices, since the high tunability of their properties [110, 123].
Many materials with properties dominated by their 2D structural units, such as the layered metal dichalcogenides (LMDCs), copper oxides and iron pnictides, present correlated electronic phenomena, among which charge density waves and high-temperature superconductivity [14].
The discovery in 2004 [101] of single-layer Graphene by Novoselov and Geim has shown that, not only it is possible the exfoliation of stable, single-atom or single-polyhedral-thick 2D materials from Van der Waals (VdW) solids (molecular solids in which the dominant cohesive force is the VdW interaction), but also that these systems can exhibit unique and fascinating physical properties. Considering, for example, single-layer Graphene's band structure, the linear dispersion at the K point generates original phenomena, like the anomalous room-temperature quantum Hall effect, implicating the birth of a new category of "Fermi-Dirac" physics. Even at one-atom thick, Graphene is an excellent thermal and electronic conductor material: for these reasons, Graphene-based systems have been proposed for a

wide range of applications (from transparent conductors to thermal interface materials to barristor transistor-like devices[67, 121, 141]). However, since single-layer Graphene is entirely surface area, its properties and reactivity are deeply dependent on the substrate, as also its local electronic environment and mechanical deformation: not only, several crystalline solid-state materials existant, which have their own different electronic, mechanical and transport properties, could be considered as the possibility to create single-atom or few-atom polyhedral thick 2D layers from any material. Some years ago, in this context, it has shown by Frindt *et* al. that layered VdW materials, like Layered Metal Dichalcogenides (LMCDs), could be mechanically and chemically exfoliated into few and single layers [43, 59].
Moreover, in the context of optoelectronics in connection with 2D-materials operations, also Silicon play a dominant role: this element is one of the most useful to mankind, covering a considerable position for a lot of reasons, especially for those linked to its electronic and optical properties that can be easily modulated and controlled [35]. In fact, optoelectronics, which is a branch based on the study and the operation of electronic devices, that produce, detect and control light, actually is an esteemed and rapidly growing field [138]: recently, 2D materials, carbon nanotubes and semiconductor quantum dots became elements of great attention thanks to their potential use in nano and optoelectronic devices.

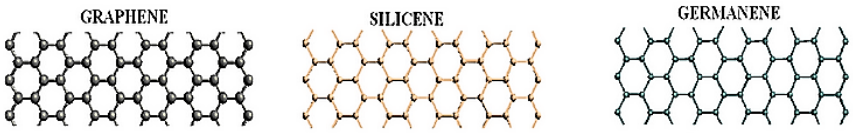

Figure 1: Representation of Graphene, Silicene and Germanene (figure from Ref.[130]).

However, it is certain that the recent surge of intense research on Graphene has stimulated the investigation on the general potential of other novel 2D materials. Moreover, during the last years, Graphene research has yielded lot of different methods of synthesis, transfer, detection, characterization and manipulation of layered VdW materials properties. Furthermore, many novel emerging materials beyond Graphene, that had been initially considered to exist only theoretically, have been synthesized. These include, for example, groups IV and VI semiconductor analogues of Graphene/Graphane (the sp^2/H-terminated sp^3 derivatives) such as Silicene [2] and Germenane [10] (see Fig. 1 that gives an illustration). Similarly to Graphene, their properties at the single layer are distinct from the bulk. Furthermore, these 2D materials are useful building blocks that can be restacked

and integrated into composites for a wide range of applications [14]. Compared with the intensive research focus on Graphene, investigations on Graphene-analogous materials is just at the beginning, and many challenges exist, such as their large-scale fabrications and definitive characterizations with desired thickness. Besides, many properties of graphene-analogous materials still remain unexplored, such as the practically measured mechanical, electronic, magnetic, and optical properties, and their possible applications are still waiting for the further explorations. However, it is highly expected that this emerging rich field has a promising future and will rapidly grow to be an advancing area to generate exciting properties and amazing applications.

1.1.1 *PAHs as finite portions of 2D materials*

In this field, the position occupied by polycyclic aromatic hydrocarbons (PAHs), also known as polynuclear aromatic hydrocarbons or polyarenes, in their crystalline and thin-film state has largely increased of importance. In fact, they are usually employed as active elements in several optoelectronic applications, ranging from LEDs, solar arrays, transparent and flexible displays to organic thin-film field-effect transistors and liquid crystals [21]. This large class of organic compounds is made up by molecules formed and released into the environment either through natural or man-made sources. Natural sources include volcanoes and forest fire, while the artificial sources come from wood burning, automobile exhaust, industrial power generators, incinerators, production of coal tar, coke, asphalt and petroleum, incomplete combustion of coal, oil, gas, garbage, tobacco and charbroiled meat [28]. These small-size molecules, with respect to polymers, offer several advantages, such as the possibility to be easily purified through various techniques and to be tractable by both evaporation and solution methods [84].

Among them, the *Circumacenes* (Coronene, Ovalene, Circumanthracene, Circumtetracene, and Circumpentacene are the first five members considered in the present work) have recently aroused scientific interest [84, 111]. These systems are here considered for their interesting and promising properties connected to the world of 2D materials: they are the smallest in size among the Circumacenes, showing a nanometric dimension with a characteristic symmetric structure and a planar geometry (e.g. see Fig. 2). Furthermore, these molecules are interesting in many domains of research (from solid state physics to astrochemistry) and also for condensed matter phyiscs applications [56].

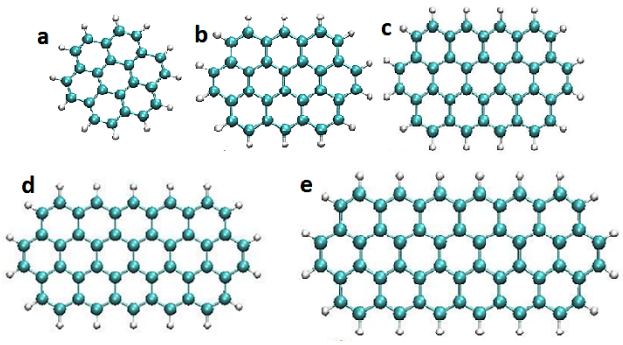

Figure 2: Representation of the five first members of Circumacenes (Coronene (a), Ovalene (b), Circumanthracene (c), Circumtetracene (d), and Circumpentacene (e)). C atoms are displayed in light-blue, while the peripheral H in white.

One of the goals of this work is focused on the analysis of finite-size effects on the electronic and optical properties of the nanometric portions of Graphene compounds after different atomic substitutions, with possible subsequent extentions to their infinite counterparts and in connection with other previous studies [91, 122, 144]. In this Thesis, we present a brief state-of-the art of 2D materials beyond Graphene, concentrating our attention on the study of the electronic and optical properties of the nanometric substructures of these compounds (from Silicene to Germanene and Boron-Nitride (BN) nanostructures), as fundamental units of their successful infinite analogues.

1.2 A BRIEF OVERVIEW ON GRAPHENE-ANALOGOUS EMERGING LOW-DIMENSIONAL MATERIALS

The explosive studies on Graphene have stimulated new interests towards Graphene- analogous materials: actually many of such systems have been fabricated from a large variety of layer and non-layer materials or others have been expected from the computational point-of-view. In these sections, we briefly summarize the recent progress on Graphene-analogous low-dimensional materials (e.g. 2D nanosheets and 1D nanoribbons) from both experimental and computational side, briefly mentioning some of their potential applications as well as the comparison with Graphene. It is highly expected that a more comprehensive review might be useful for both experimental and theoretical peers and provide a directional guide for the bright future of this emerging new area of research [8, 125]. In fact, these novel materials have very good properties and promising applications. For example, BN nanosheets (BNNSs) are highly insulating, and exhibit extreme chemical, thermal and oxidation stability, and possess a mechanical strength and thermal conductivity comparable to those own

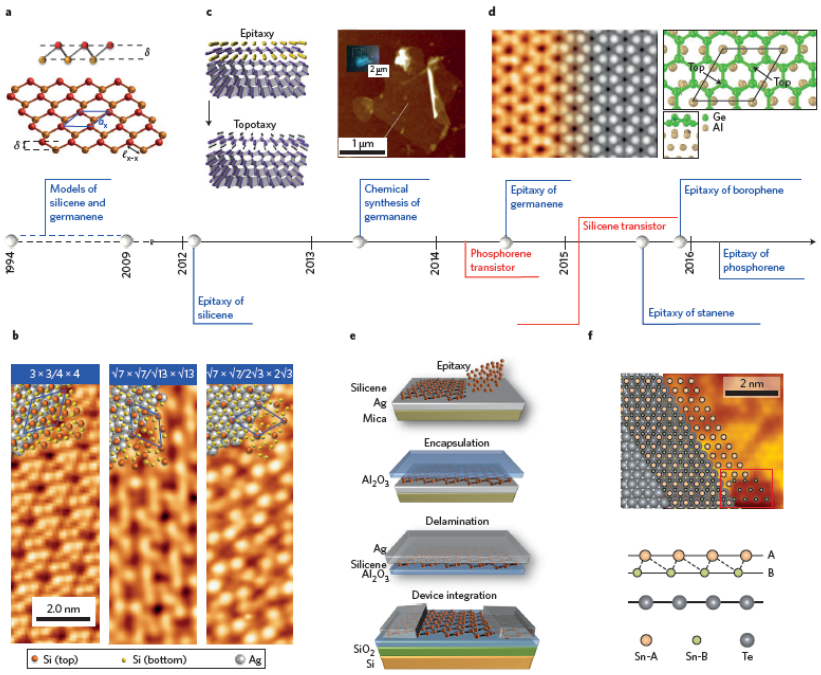

Figure 3: Evolutionary overview of 2D-Xene materials (X=Si, Ge, Sn and so on). a) Atomic configuration of a free-standing 2D-Xene lattice (top:side view, bottom:perseptice view), where red and orange spheres represent X atoms at the top and bottom positions, respectively; b) Silicene epitaxy on Ag(111) substrates as a representative case of Xene-on-substrates systems. c) Topotactic exfoliation of Germanene as a first example of chemical exfoliation of a Xene sheet: (left) process schematics, (right) optical microscopy image of a single hydrogen-terminated Germanene sheet. d) Representative case of germanene on metal substrates: STM topography and simulation (image size 5.64 nm $\times$ 8.10 nm) of an extended Germanene sheet on Al(111) (left) and *ab initio* atomic model (right). e) Silicene integration into a transistor device. f) Epitaxy of stanene on Bi_2Te_3 substrates based on STM identification of a buclked and unreconstructed lattice structure (top). Sketch of the Sn atom arrangement in the stanene lattice (A and B denote upper and lower positions, respectively) grown on Te-terminated Bi_2Te_3 (bottom). Figure taken from Ref. [96].

of Graphene. These excellent properties promote the uses of layered BN as thermal radiators, ultraviolet-light laser and emitter devices, as thermoconductive fillers in polymer or ceramic composites, and as dielectric substrate for Graphene-based electronics [77]. As other 2D materials of emerging importance there are the Transition Metal Dichalcogenides (TMDs), generally expressed by the formula MX_2 (M = Mo, W, V, Nb, Ta, Ti, Zr, Hf, and X = S, Se, Te), which constitute an intriguing family of materials with perspectives for a broad range of unique properties and applications [125]. TMD materials present a layered structures consisting of stacks of X–M–X sandwiches held together by VdW forces. Depending on the different compositions,

TMDs can have hexagonal or rhombohedral symmetry, and the central metal atoms can form octahedral or trigonal prismatic coordination configuration. Due to their weak interlayer interactions, isolated sheets of TMDs can be splited along the layer plane similar to graphite, and these mono- or fewlayer structures are considered as non-planar Graphene analoguos. Among the large class of layered TMDs, we remind MoS_2 and WS_2 since they are the two most widely studied materials in the last few years (see e.g. Fig. 4).

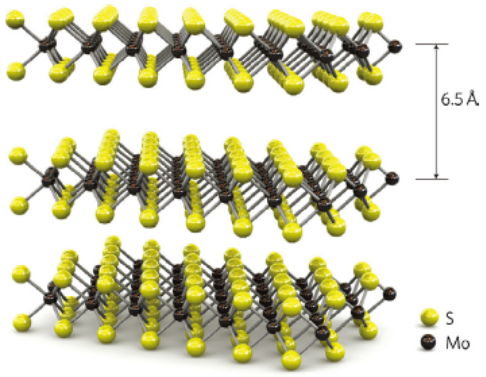

Figure 4: Layered structure of MoS_2, and its single layer has a thickness of 6.5 Å. (figure from Ref.[125]).

From the computational side, many Graphene-like materials have been explored and designed, and fascinating properties distinctive from Graphene are predicted even anticipating experiments. For example, unlike Graphene, all BN monolayers have closed-shell singlet ground states, and those with long zig-zag edges have slightly larger band gaps [46]. For BN nanoribbons (BNNRs), the electronic properties are heavily dependent on the edge states [143]. Moreover, hydrogenation can right modulate the electronic and magnetic properties of BN nanoribbons by controlling hydrogenation ratios [26]. Aside from these materials, many other 2D compounds have also gained recent interest [125].
In the following subsections, we will turn our attention to atomic structures, material properties, and potential applications of various 2D and 1D materials beyond Graphene and Graphene nanoribbons, which are divided, for brevity, among the myriad of materials (e.g. including also hypothetical planar materials that have not been experimentally realized, here not treated), into planar Graphene analogues (see the following subsections 1.2.1) and Silicene, the succesfull Si-made countepart of Graphene (see subsection 1.2.2).

1.2.1 *Planar Graphene analogues: "White Graphene"- BN nanosheets and nanoribbons*

BN nanomaterials ear particular attention since they are carbon's isoelectronic analogues. In fact, BN exhibits various crystalline forms in many ways analogous to carbon, including diamond-like cubic-BN (c-BN), graphite-like hexagonal-BN (h-BN), wurtzite-like BN, onion-like fullerenes, and BN nanotubes (BNNTs)[125]. Among these polymorphs, h-BN is thermodynamically the most stable and softest form, and has attracted increasing attention. Bulk h-BN presents a similar layered structure like graphite (the only exception is that the basal planes in h-BN are positioned directly on top of each other, with the electron-deficient B atoms in one layer lying over and above the electron-rich N atoms in adjacent layers, as Fig. 5 shows).
For graphite, however, the adjacent layers are stacked offset, and alternating C atoms lie above and beneath the hexagon centers. Both bulk h-BN and graphite show very similar lattice constants and interlayer distances (lattice constants: a = 2.456 Å (a = 2.504 Å), c = 6.696 Å (c = 6.661 Å) for graphite (bulk h-BN); interlayer distances: 3.33–3.35 Å (3.30–3.33 Å) for graphite (h-BN)). Due to their close structural similarity, monolayer h-BN can thus be regarded as a structural counterpart of Graphene where the C-C bonds are substituted by alternating B-N pairs. In analogy to the common denomination of "white graphite" for bulk h-BN, the monolayer h-BN is known as *White Graphene* [142].
Despite of their resemblance from the structural point-of-view, h-BN nanosystems show unexpected different properties from its carbon-made counterparts. The difference in electronegativity between boron and nitrogen induces a ionic nature, which is responsible for narrowing of sp^2 derived p bands and the corresponding loss of conductivity, causing h-BN, in contrast to semimetallic graphite, to be highly insulating. In fact, h-BN based materials, either 3D bulk, 2D sheets, or 1D nanotubes, are all electrically insulating with a wide band gaps of 5–6 eV.

On the other hand, h-BN systems also demonstrate advantageous and useful properties. For example, BN materials are thermally and chemically more stable than carbon analogues and possess a high thermal conductivity, high mechanical robustness, excellent resistance to oxidation (until temperature over 800 °C) [142]. The high thermal stability of h-BN is given by the strong covalent network in the plane and the high polarizability of individual layers. Note that, due to their oxidation resistance, thin h-BN nanosheets can not be prepared by the oxidation/exfoliation methods as widely adopted for large-quantity fabrication of Graphene.

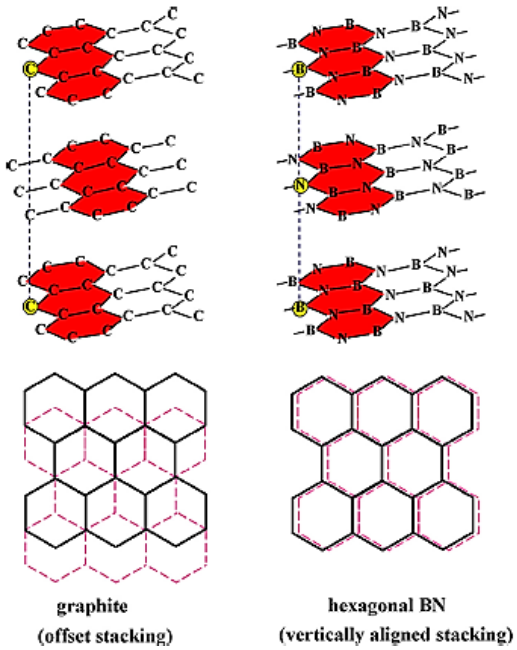

Figure 5: Graphitic structures for carbon and h-BN. (figure from Ref.[125]).

The unique and exceptional property with respect to the mechanical, electronic, thermal, and chemical aspects favor BN nanosheets (BNNSs) for use in an extended range of electronic and composite applications. For example, h-BN nanosheets are widely used as ultraviolet-light laser devices [46], field emitters, semiconductor diodes [145], and insulating thermoconductive nanofillers in polymer or ceramic composites [66]. For example, ultrathin BN nanosheets producted from Si_3N_4 nanowires [145] or BN fibers[27], as well as porous BN nanospheres [126], display excellent field emission performance with electron emission property comparable to that of carbon nanotubes. On the other hand, due to its attractive combination of electrical insulation, high thermal conductivity and optical transparency, layered h-BN holds great promise in applications as polymeric composite fillers. Moreover, functionalized BN nanosheets also demonstrated great potential to fabricate polymer composites [79].In addition, BNNSs are also a promising alternative of Graphene in plane electronics, where lithography technique can be conveniently employed, as superhydrophobic surface coating, and as nanoscale support for metal and metal oxide catalysts. For example, the BN nanomesh deposited into transition metal surfaces is thermally very stable and serves as a template for surface self-assembly of well-ordered organic molecules [31], water molecules [32], rare gas atoms [139], transition metal atoms [99], or metallic nanoparticles [135].
These substrate-supported molecular or atomic arrays can be used to produce functional supramolecular BN nanostructures, which demon-

strate great potential in catalytic and sensing applications. For instance, a theoretical study by Gao *et al.* [45] suggested that Au supported on BN surface exhibits enhanced adsorption and catalytic activation for O_2 molecule. Experimentally, Wang *et al.*[136] showed that Au- and Pt nanoparticles loaded into BN nanosheets function as efficient catalysts towards CO oxidation. Apart from the catalytic applications, Lin *et al.* [78] reported the fabrication of Ag nanoparticle-decorated BN nanosheets, which were further transferred into quartz substrates to fabricate reusable and oxidation-resistant surface enhanced Raman spectroscopy (SERS) sensor devices. Note that, the 1D BN nanoribbons are theoretically predicted to have significant potentials in the area of nano-electronics and spintronics; however, their realistic applications remain currently less explored by experimentalists. This challenge is possibly due to the large experimental difficulty in producing high-quality BNNRs with uniform and smooth edges.
On the other hand, also MoS_2 and WS_2 have been demonstrated to posses significant applications: in devices as field effect transistor (FET) [137], sensors [74], electrodes of Li-ion batteries [75] and PV cells [118]. Similarly, MoS_2 nanosheets were explored as high-temperature solid lubricants, nanoelectronics, electrode materials for Li-ion batteries, and catalysts. MoS_2 monolayer with a direct band gap of 1.8 eV serves as a semiconducting rival of Graphene, particularly considering that the zero-band-gap character of the latter poses a severe drawback for its applicability in logic devices. Actually, a MoS_2-based transistor with a room-temperature mobility of more than 200 $cm^2/(V \cdot s)$ and current on/off ratios of up to 1:108 has been fabricated, which is demonstrated to be comparable to thin Si films or Graphene nanoribbons (GNRs).

1.2.2 *Silicene*

Silicene, a one-atom-thick silicon sheet ordered in a 2D honeycomb lattice, is the newest allotrope of silicon, similar to Graphene (see Fig. 6). Because of its structural appareance, single-layer Silicene is also alternatively considered as the Si-made 2D counterpart of Graphene. However, unlike Graphene, Silicene favors to adopt a low-corrugated honeycomb configuration (presenting a buckling of about 0.44 Å) [16] rather than a planar one, forming a mixed sp^2–sp^3 like hybridized state [64]. This difference derives from the fact that for C atoms, the fully sp^2-hybridized state is more stable than the sp^3-hybridized state, while for Si the situation is opposed.
Due to this peculiar bonding behavior, bulk-Si can not form a layered phase like graphite: the only exception is represented by the layered Si atoms that can exist in alkaline-earth-metal silicides (such as $CaSi_2$), which are structurally composed of alternative layer-by-layer pack-

ing of hexagonal alkaline-earth-metal layers and corrugated Si(111) atomic layers.

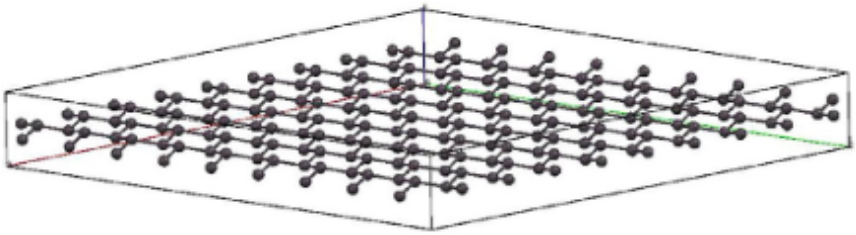

Figure 6: Schematic representation of Silicene sheet (figure from Ref.[64]).

As an important structural analogous of Graphene, Silicene shows amazing electronic properties and its reactive surface can be modified through many methods. Furthermore, it is advantageous that Silicene can be easily integrated into Si-based semiconductor industries. Although the current progress on Silicene is still at the beginning, this material is expected to be developed for many technical prospects [63]. For example, due to its high electron mobility, an intrinsic opening of spin–orbital band gap, and tunable electronic structures, Silicene could be employed in nanoelectronics, spintronics, and photonic devices [64].
Thermal transport computations by Pan *et al.* [104] suggested that armchair Silicene nanoribbons may be used as high performance thermoelectric materials. Hu *et al.* [55] showed that Silicene with divacancy defects exhibits high selectivity for H_2 over H_2O, N_2, CO, CO_2, and CH_4, and can be potentially used as hydrogen purification membrane.
Moreover, since Si-based nanomaterials have been largely explored for Li-ion battery anodes, thanks to their high energy density, Silicene sheets should also be a promising anode candidate for Li-ion batteries, because of its large specific surface area allowing for occupation of more Li ions and contributing to a higher energy density. However, unlike Graphene, which can form a free-standing sheet, Silicene has only been found to grow on metal substrates. Anyhow, to promote Silicene into the next phase for nanoelectronic infrastructure, it is of great importance to grow Silicene on insulator substrates, and these synthesis challenges would encourage more theoretical and experimental studies in the future [125]. Finally, these above presented peculiarties of Silicene are extendible in a very similar way to Germanene (the Ge-based analogous to Graphene), and for these reasons here not treated in details.

1.3 STRUCTURE OF THIS THESIS

The aim of the present Thesis is centred on study of the electronic and optical properties of some representative finite portions (with a nanometric size) of the infinite 2D counterparts (e.g. Graphene, Silicene, Germanene, BN systems). We analyze the effects of atomic substitutions (partial/total conversion of C-made molecule into BN/Si/Ge-made ones) and perfluorination, on the morphological, electronic and optical properties of systems based on specific Polycyclic Aromatic Hydrocarbons (PAHs.) In particular, we have chosen some members among the Circumacenes family (from Coronene up to Circumpentacene) and the Linear acenes Clusters (up to the sixth molecule-hexacene) as prototypes of compounds used in organic electronics, since the importance of PAHs employed in this field.

With this purpose we have selected a set of theoretical and numerical tools based on DFT and TDDFT.

More specifically we focused on the following points:

- **Electronic, Optical and Morphological Properties of Si-atoms substitutions in Circumacenes**:

  Study of Si-atoms substitutions (single, double and triple atomic insertions) effects on the Ionization Energy (IE), Electron Affinity (EA), Quasi-Particle gap (QP_{Gap}), in the case of Coronene and Ovalene molecules.

  Study of the effects of Si-atoms substitutions (single, double and triple atomic insertions) on the structural properties of the same molecules.

  Calculations of the optical absorption spectra and the optical observables (E_{opt}, E_{bind}) for all the systems under study.

- **Morphological, Electronic and Optical Properties of BN-Circumacenes**

  Investigation, for the same molecular familiy (Circumacenes-from Coronene to Circumpentacene) and the same observables (IE, EA, Quasi-Particle gap (QP_{Gap}), of the effects of global substitution of B and N atoms to study the Boron-Nitride (BN) counterparts and compare them to the C-based original parents.

  In this last case, we select the Coronene molecule to study also the effect of perfluorination (total peripheral substitution of H atoms with F ones), comparing the BN system with the C-based original parents under halogenation.

- **Morphological, Electronic and Optical Properties of C/Si/Ge Linear Clusters**

  Study of the differences in terms of atomic type (C vs Si and Ge) analyzing the ground/excited-state properties and the optical absorption spectra as a function of the molecular size.

Chapter 2 contains the detailed explanation of the theoretical tools used in all parts of this work. Some secondary computational details are contained in the first part of each Chapter 3, 4, and 5. The investigation on morphological, electronic properties and optical spectra of Coronene and Ovalene with Silicon atoms insertions are presented in Chapter 3. The study of the electronic and optical properties of Boron-Nitride Circumacenes are contained in Chapter 4. The same Chapter reports also the results of perfluorination effect, limited on the case of Coronene and BN-made Coronene. Finally, Chapter 5 presents the results obtained for the C-made linear acenes clusters as compared to their Si/Ge-made counterparts on the morphological, electronic and optical properties. The study has been performed as a function of the molecular size and fixing the molecular dimension, comparing the C/Si/Ge structures.

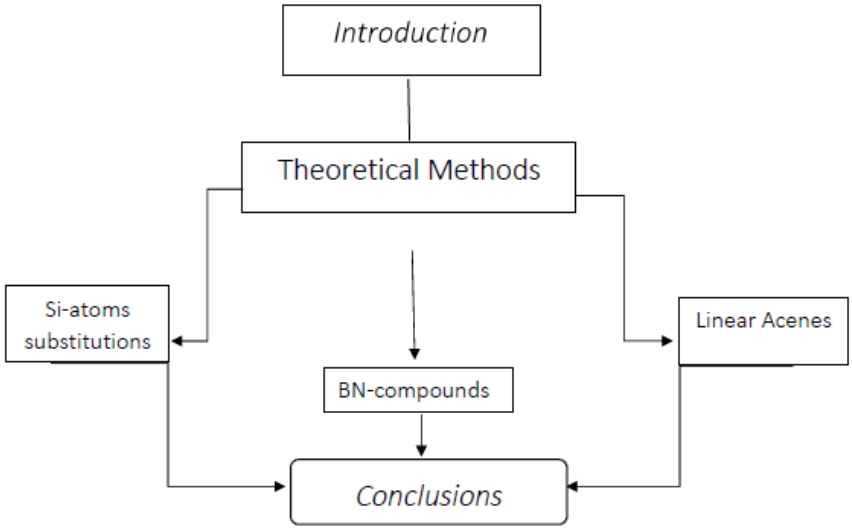

Figure 7: Structure of the Thesis.

2

THEORETICAL METHODS

Ab initio (or first-principle) simulations owe their name since are focused on a physical-mathematical theory, from which the properties of the system are derived without the recourse to empirical parameters. Currently, the density functional theory DFT is probably one of the most helpful theory to perform atomistic ab-initio simulations, thanks to the advantageous scalability of the computational time as a function of the number of electrons in the system analyzed [69]. The DFT, in fact, is able to give a reliable prediction of the ground-state properties for a large class of materials/molecules. Moreover, its time-dependent counterpart, Time-dependent density functional theory TDDFT extends the DFT to the study of excited states of the considered system and the related observables[112]. In this chapter we present an overview of the theoretical methods adopted in this Thesis.

2.1 INTRODUCTION

As it is known from classical physics, the time evolution of bodies positions and velocities are uniquely determined by Newton law or more generally by Lagrange or Hamilton equations. On the contrary, in Quantum Mechanics, the situation is reversed, since (QM) particle trajectories do not exist anymore and the time evolution of the system can be described by a mathematical tool, which characterizes the state of the system, the so called wavefunction $\Psi(\mathbf{r}, t)$.

The time evolution of $\Psi(\mathbf{r}, t)$ for a single particle can be found solving the *time-dependent* Schrödinger equation:

$$i\hbar\frac{\partial}{\partial t}\Psi(\mathbf{r}, t) = -\frac{\hbar^2}{2m}\nabla^2\Psi(\mathbf{r}, t) + V(\mathbf{r}, t)\Psi(\mathbf{r}, t) = \mathbf{H}(\mathbf{r}, t)\Psi(\mathbf{r}, t) \quad (1)$$

where $\hbar$ is the reduced Planck constant and $V(\mathbf{r}, t)$ the potential depending on the position of the particle and the time. The sum of the last two terms represents the time-dependent *Hamiltonian* of the system $\mathbf{H}(\mathbf{r}, t)$.

The resolution of the Schrödinger equation permits the knowledge of the electronic properties of atoms and molecules from first principles. Generally, many phenomena under exam in molecular physics and quantum chemistry can be considered stationary (the potential does not depend on the time parameter, but only on the position of

the particles). The Eq. 1 is traceable to the *time-independent* equation written for a molecular system:

$$\mathbf{H}\Psi(\bar{R},t) = E_{tot}\Psi(\bar{R},t) \tag{2}$$

where $\Psi(\bar{R},t)$ is the *total wavefunction* of the molecular system that depends on both **r** and **R** ($\bar{R} = [\mathbf{r},\mathbf{R}]$) which are respectively the electron and the nuclei spatial coordinates; E_{tot} is the *total energy* of the system and **H** the *total Hamiltonian* of the molecular system containing M nuclei and N electrons. The global hamiltonian for a multielectronic molecular system can be written as the following expression:

$$\begin{aligned}\mathbf{H} &= T_e + T_N + V_{eN} + V_{ee} + V_{NN} \\ &= -\frac{\hbar^2}{2m_e}\sum_{i=1}^{N}\nabla_i^2 - \hbar^2\sum_{a=1}^{M}\frac{1}{2m_a}\nabla_a^2 \\ &- \frac{1}{4\pi\varepsilon_0}\sum_{i=1}^{N}\sum_{a=1}^{M}\frac{e_i Z_a}{r_{ia}} + \frac{1}{4\pi\varepsilon_0}\sum_{i=1}^{N}\sum_{j>i}^{N}\frac{e_i e_j}{r_{ij}} \\ &+ \frac{1}{4\pi\varepsilon_0}\sum_{A=1}^{N}\sum_{b>a}^{M}\frac{Z_a Z_b}{r_{ab}}\end{aligned} \tag{3}$$

where the sum of the electronic (T_e) and nuclear (T_N) kinetic energies gives the *total kinetic energy*; the *total potential energy* is the sum of three components: the attractive interactions between nuclei and electrons (V_{eN}), the repulsive electron-electron interactions (V_{ee}) and the repulsive interactions between the nuclei (V_{NN}). $Z_{a,b}$ are the nucleic charge of atoms A and B, $m_{e,a}$ are the mass of electron and of the atom A, r_{ab} is the distance between nuclei A and B, r_{ia} is the distance between nucleus A and electron i and finally r_{ij} is the distance between electrons i and j. In particular, in the previous expressions we choose not to include intentionally the spin dependence inside the wavefunction because the Hamiltonian operator here presented is independent on it.

Analytical solutions of Eq. 2 (with associated expressions of the eigenfunctions and energies) can only be obtained in a few cases, among them we remind:

- A particle in one, two or three dimensional box submitted to a zero potential inside the box and infinite at the boundaries;
- Single atom with non interacting electrons;
- Hydrogen atom;
- Hydrogenoid atomic systems[1]

1 Similar class of problems as the hydrogen atom with the same number of electrons but different nuclear charge.

2.1.1 *The Born-Oppenheimer Approximation*

The Schrödinger equation for a multielectronic system is a very hard problem to solve, since it consists in the search of stationary states of interacting nuclei and electrons. From the conservation of the momentum and the consistent difference between the nuclei masses and the electrons (at least, the proton mass excedes by a factor of 1832 the electron one), nuclei are expected to be much slower than electrons. This fact allows one to neglet the kinetic energy of the nuclei (T_N), since they are considered roughly in stasis. According to this approximation, the electrons move in the field created by the fixed nuclei and are supposed to rearrange immediately after any displacement of the atoms. It commonly said that electrons follow adiabatically the movement of the nuclei and for this reason, the approximation is called the *Born-Oppenheimer approximation* or *adiabatic approximation*[11]. The stationary states and eigenvalues of the energy become function of the atomic positions. From this evidence it is possible define an electronic Hamiltonian which carries a parametric dependence on the nuclear coordinates and depends explicitly on the electron coordinates:

$$\mathbf{H}_{el} = T_e + V_{eN} + V_{ee} \tag{4}$$

Moreover, the total wavefunction can be factorized as a combination of the electronic wavefunction ($\phi_i(\mathbf{r}, \mathbf{R})$) and the nuclear wavefunction ($\zeta_i(\mathbf{R})$), where the sum goes over all the electronic states:

$$\Psi(\mathbf{r}, \mathbf{R}) = \sum_i \phi_i(\mathbf{r}, \mathbf{R})\zeta_i(\mathbf{R}) \tag{5}$$

If we consider the total wavefunction in the form expressed by Eq. 5, the Schrödinger equation can be rewritten as:

$$\mathbf{H}\Psi(\mathbf{r}, \mathbf{R}) = [H_{el}(\mathbf{R}) + T_N + V_{NN}] \sum_i \phi_i(\mathbf{r}, \mathbf{R})\zeta_i(\mathbf{R}) \tag{6}$$

Applying the Born-Oppenheimer approximation, neglecting the term T_N, the previous equation becomes:

$$\mathbf{H}\Psi(\mathbf{r}, \mathbf{R}) = [\mathbf{H}_{el}(\mathbf{R}) + V_{NN}] \sum_i \phi_i(r, R)\zeta_i(\mathbf{R}) \tag{7}$$

from which a set of equations completely independent by the nuclear wavefunction can be obtained:

$$\mathbf{H}_{el}\phi(\mathbf{r}, \mathbf{R}) = E_i^{el}(\mathbf{R})\phi_i(\mathbf{r}, \mathbf{R}) \tag{8}$$

where $E_i^{el}(\mathbf{R})$ is the electronic energy for the i-th state. The adiabatic energy E_{ad} (distinguished from the total energy by neglecting the nuclear kinetic energy contribution) is obtained as:

$$\sum_i [E_i^{el} + V_{NN}]\phi_i(\mathbf{r}, \mathbf{R})\zeta_i(\mathbf{R}) = E_{ad} \sum_i \phi_i(\mathbf{r}, \mathbf{R})\zeta_i(\mathbf{R}) \tag{9}$$

Multiplying Eq. 6 by $\phi_j^\star(\mathbf{r},\mathbf{R})$ and integrating with respect to r, we obtain:

$$\begin{aligned}\int \phi_j^\star(\mathbf{r},\mathbf{R})\mathbf{H}\Psi(\mathbf{r},\mathbf{R})dr &= [E_j^{el}(\mathbf{R}) + V_{NN}]\zeta_j(\mathbf{R}) \\ &+ \sum_i \int \phi_j^\star(\mathbf{r},\mathbf{R})T_N\phi_j(\mathbf{r},\mathbf{R})\zeta_j(\mathbf{R})dr \\ &= E_{Tot}\zeta_j(\mathbf{R})\end{aligned} \tag{10}$$

In equation 10 the first term of the second member represents the adiabatic energy mentioned above. The second term can be rewritten in another form to let appear the non-adiabatic coupling Θ_{ij}. From these algebraic manipulations, the complete nuclear equation is given by:

$$[T_N + E_j^{el}(\mathbf{R}) + V_{NN}]\zeta_j(\mathbf{R}) + \sum_i \Theta_{ij}\zeta_i(\mathbf{R}) = E_{Tot}\zeta_j(\mathbf{R}) \tag{11}$$

The non-adiabatic coupling accounts for the coupling between electronic and nuclear states and is responsible of the transitions between electronic states induced by nuclear motions. Generally, these terms are of weak importance, so much to be often neglected. However, the non-adiabatic coupling has to be taken into account in order to achieve a good description when electronic states are close to one other or for avoiding crossings.

Through Born-Oppenheimer approximation, the Schrödinger equation has been divided in two independent parts, electronic and nuclear; the electronic equation being solved in the field of fixed nuclei, but even using this approximation the problem of finding an analytical solution of the Eq.2 remains unaffordable.

However, despite of this approximation, the electronic equation remains solvable only in few cases:

- The problem of M nuclei and one electron (such as the ion H_2^+);
- Within the independent model which is the problem of N non interacting electrons and M nuclei.

The last example introduces important notions in quantum-chemistry and is treated more in details in the next section (see section 2.1.2).

2.1.2 *Independent Electron Model*

In 1928, Hartree [50, 51] trying to approximate a multielectronic wavefunction, introduced the idea of a self-consistent field referring to valence electrons and groups of core electrons. The wavefunction of an electron ψ_i is determined from the field of the nucleus and the

other electrons through a self-consistent approach. Starting with an approximate field, this procedure constist in the continous iteration until output fields for all electrons become coincident to the input. In this approach the wavefunction of the N-electron system can be approximated by the product of N single-particle functions:

$$\Psi(\mathbf{r}_1, \sigma_1; \mathbf{r}_2, \sigma_2; \ldots; \mathbf{r}_N, \sigma_N) = \psi_1(\mathbf{r}_1, \sigma_1)\psi_2(\mathbf{r}_2, \sigma_2)\ldots\psi_N(\mathbf{r}_N, \sigma_N) \tag{12}$$

where r_i is the i^{th} electron coordinate and σ_i is the spin term [2].

Each wavefunction $\psi_i(\mathbf{r}_i, \sigma_i)$ is solution of the single electron Schrödinger equation:

$$\hat{h}_i\psi_i(\mathbf{r}_i, \sigma_i) = \left(-\frac{\hbar^2}{2m}\nabla^2 + \Phi_i + V_{ext}\right)\psi_i = \varepsilon_i\psi_i \tag{13}$$

where ε_i is the energy eigenvalue of the single electron state ψ_i, $\hat{h}$ is the one-electron hamiltonian, V_{ext} is the nuclei potential and Φ_i is the "Hartree" potential due to the interaction with other electrons.

According to the *Pauli exclusion principle*, a multifermionic wavefunction must be antisymmetric, i. e.

$$\Psi(\mathbf{r}_1, \sigma_1; \ldots; \mathbf{r}_i, \sigma_i; \mathbf{r}_j, \sigma_j; \ldots; \mathbf{r}_N, \sigma_N) = -\Psi(\mathbf{r}_1, \sigma_1; \ldots; \mathbf{r}_j, \sigma_j; \mathbf{r}_i, \sigma_i; \ldots; \mathbf{r}_N, \sigma_N) \tag{14}$$

but the product wavefunction 12 does not respect this antisymmetry. Fock [42] and Slater[120] (1930) demonstrated that replacing Eq. 12 by a determinant of such functions led to equations that were only a little more complicated, while satisfying the Pauli principle. This determinantal function is known as *Slater Determinant*[120] and can be written as follows:

$$\Psi(\mathbf{r}_1, \sigma_1; \ldots; \mathbf{r}_N, \sigma_N) = \frac{1}{\sqrt{N!}}\begin{vmatrix} \psi_1(\mathbf{r}_1, \sigma_1) & \psi_1(\mathbf{r}_2, \sigma_2) & \ldots & \psi_1(\mathbf{r}_N, \sigma_N) \\ \psi_2(\mathbf{r}_1, \sigma_1) & \psi_2(\mathbf{r}_2, \sigma_2) & \ldots & \psi_2(\mathbf{r}_N, \sigma_N) \\ \vdots & \ddots & \ddots & \vdots \\ \vdots & \ddots & \ddots & \vdots \\ \vdots & \ddots & \ddots & \vdots \\ \psi_N(\mathbf{r}_1, \sigma_1) & \psi_N(\mathbf{r}_2, \sigma_2) & \ldots & \psi_N(\mathbf{r}_N, \sigma_N) \end{vmatrix} \tag{15}$$

2 Indeed the single electron wavefunction $\psi_1(\mathbf{r}_1, \sigma_1)$ can be factorized as $\psi_i(\mathbf{r}_i, \sigma_i) = \psi_i(\mathbf{r}_i)\sigma_1(\omega_i)$ in which $\psi_i(\mathbf{r}_i)$ indicates the spatial wavefunction and $\sigma_1(\omega_i)$ is spin wavefunction

This expression satisfy the condition required for a multi-fermionic system expressed by Pauli's principle, according to which any two electrons can not occupy the same spin-orbital. This follows immediately from the fact that the determinant in equation 15 vanishes if any two spinorbitals are identical.

2.2 DENSITY FUNCTIONAL THEORY (DFT)

The density functional theory (DFT) [69] is founded on the hypothesis that a multi-electron system and all the related observables can be described univocally by its electronic density $n(r)$. For a N-electrons system, for example, this signifies that, instead of calculating the multielectronic wavefunction $\Psi(\mathbf{r}_1, \mathbf{r}_2, \ldots, \mathbf{r}_N)$ (that is a function of $3N$ variables) one can calculate the density $n(r)$ (depending only on three variables). This possibility implicates that the DFT method is advantageous from a practical point of view, since the computational cost of the variational procedure grows relatively slowly as a function the number N of electrons in the system (operation which results more clear in the following text). It can be demonstrated [69] that the computational time t follows the relationship:

$$t \sim N^{\alpha} \tag{16}$$

with $\alpha \simeq 2 \div 3$.

The first steps towards the Density Functional Theory were developed by the Thomas-Fermi model [39, 127] and later by the Thomas-Fermi-Dirac model, which succeeded in giving quantitative results of atomic properties. However, these earlier versions were not yet able to give a description of molecules that were predicted to be unstable. The modern version of DFT starts with the publication of the demonstrations of the two Hohenberg and Kohn theorems [54]:
For any system of interacting particles in an external potential, $V_{ext}(\boldsymbol{r})$, the potential $V_{ext}(\boldsymbol{r})$ is determined uniquely, except for a constant, by the ground state particle density $n_0(\boldsymbol{r})$. An universal functional for energy $E[n]$ in terms of the density $n(\boldsymbol{r})$ can be defined, valid for any external potential $V_{ext}(\boldsymbol{r})$. For any particular $V_{ext}(\boldsymbol{r})$, the exact ground-state energy of the system is the global minimum value of this functional, and the density $n(\boldsymbol{r})$ that minimizes the functional is the exact ground state density $n_0(\boldsymbol{r})$.

The variational principle on the energy represents the basis of the formulation of the exact density functional formalism given by Hohenberg and Kohn (1964) [54]. Firstly they showed that there is a one-to-one relationship between the external potential $V_{ext}(\mathbf{r})$ and the (non-degenerate) ground state wavefunction Ψ, and that there is

a one-to-one relationship between Ψ and the ground state density $n(\mathbf{r})$ of an N-electrons system:

$$n(\mathbf{r}) = N \int \mathbf{r}_2 \dots \mathbf{r}_N \Psi^*(\mathbf{r}, \mathbf{r}_2 \dots \mathbf{r}_N)\Psi(\mathbf{r}, \mathbf{r}_2 \dots \mathbf{r}_N) \tag{17}$$

where the spin coordinates are not shown explicitly. From the knowledge of the density then it is possible determine the external potential within a constant, so that all terms in the Hamiltonian are known.

These ideas can be applied to the total energy using the variational principle and for this purpose, Hohenberg and Kohn defined the functional $F[n(\mathbf{r})]$, which is "universal" , that it is valid for any external potential $V_{ext}(\mathbf{r})$. This functional can be expressed as:

$$F[n(\mathbf{r})] = \langle \Psi_N | T + V_{ee} | \Psi_N \rangle \tag{18}$$

and showed that the energy functional $E[n(\mathbf{r}), V_{ext}(\mathbf{r})]$ satisfies a variational principle:

$$E_{GS} = \min_{n(\mathbf{r})} E[n(\mathbf{r}), V_{ext}(\mathbf{r})] \tag{19}$$

where

$$E[n(\mathbf{r}), V_{ext}(\mathbf{r})] = F[n(\mathbf{r})] + \int d\mathbf{r} V_{ext}(\mathbf{r}) n(\mathbf{r}) \tag{20}$$

The minimization is performed over all nondegenerate densities that can be derived from the ground-state of some external potential.

2.2.1 *The Kohn-Sham equations*

To find good approximations to the energy functional $E[n, V_{ext}]$ it is useful and easier restoring to the decomposition introduced by Kohn and Sham (1965) [68]:

$$F[n] = T_s[n] + \frac{1}{2} \int n(\mathbf{r}) \Phi(\mathbf{r}) d\mathbf{r} + E_{xc}[n(\mathbf{r})] \tag{21}$$

where T_s is the kinetic energy that a system with density n would have in a situation where electron-electron interactions are absent, Φ is the classical Coulomb potential for electrons, and E_{xc} defines the exchange-correlation (XC) energy.[3] T_s is not the real kinetic energy

3 In the framework of wave functions, the "correlation energy" can be defined as the difference between the exact and Hartree-Fock (variationally optimized single Slater determinant) energies.

T, but it is of comparable magnitude and is treated here without approximation. In Eq. 21 all the terms different from the exchange-correlation energy E_{xc} can be evaluated exactly, so that approximations for this term are crucial in density functional applications. The variational principle applied to Eq. 20 yields [61]:

$$\frac{\delta E[n, V_{ext}]}{\delta n(\mathbf{r})} = \frac{\delta T_s}{\delta n(\mathbf{r})} + V_{ext}(\mathbf{r}) + \Phi(\mathbf{r}) + \frac{\delta E_{xc}[n]}{\delta n(\mathbf{r})} = \epsilon \tag{22}$$

where ϵ is the Lagrange multiplier associated with the requirement of constant particle number.

Comparing this last with the corresponding equation for a system with the same density in an external potential $V(\mathbf{r})$, but without electron-electron interactions, we obtain:

$$\frac{\delta E[n]}{\delta n(\mathbf{r})} = \frac{\delta T_s}{\delta n(\mathbf{r})} + V(\mathbf{r}) = \epsilon \tag{23}$$

Note that the mathematical problems are identical and provided that:

$$V(\mathbf{r}) = V_{ext}(\mathbf{r}) + \Phi(\mathbf{r}) + \frac{\delta E_{xc}[n]}{\delta n(\mathbf{r})} \tag{24}$$

The solution of Eq. 23 can be found by solving the Schrödinger equation for a non-interacting particles system:

$$\left[-\frac{1}{2}\nabla^2 + V(\mathbf{r})\right] \phi_i(\mathbf{r}) = \varepsilon_i \phi_i(\mathbf{r}) \tag{25}$$

yielding:

$$E = \sum_{i=1}^{N} \varepsilon_i + E_{xc}[n(\mathbf{r})] - \int V_{xc}(\mathbf{r}) n(\mathbf{r}') d\mathbf{r}' + \frac{1}{2} \int \frac{n(\mathbf{r}) n(\mathbf{r}')}{|\mathbf{r} - \mathbf{r}'|} d\mathbf{r} d\mathbf{r}' \tag{26}$$

and

$$n(\mathbf{r}) = \sum_{i=1}^{N} |f_i \phi_i(\mathbf{r})|^2 \tag{27}$$

The functions ϕ_i are the Kohn-Sham orbitals, and the occupation numbers f_i are noninteger at zero temperature, when the orbitals are degenerate at the Fermi level and Fermi-Dirac occupancies at nonzero temperatures. The condition 24 can be satisfied in a self-consistent procedure.

The solution of this system of equations leads to the energy and density of the lowest state and all quantities derivable from them.

The analyzed formalism can be generalized to the lowest state with a given symmetry[49] or other constraints [30]. Instead of seeking these quantities by determining the wave function of the system of interacting electrons, the DFT method reduces the problem to the solution of a single-particle equation of Hartree form.

The exchange-correlation term $E_{xc}[n(\mathbf{r})]$ is the responsible of the difficulty in finding the self-consistent solution of the KS equations and actually it remains unknown. In principle, if one were able to determine $E_{xc}[n(\mathbf{r})]$ exactly, the Kohn-Sham equations would include all the many-body effects. However, the complexity of the multielectrons interaction prevents an exact solution and approximations needs to be adopted to solve the problem.

2.2.2 *Exchange-Correlation energy approximations*

For various class of materials (especially metals), the screening effect on a reference electron exerted by the other electrons is sufficient to screen it completely on a distance of the order of the Fermi wavelength ($\lambda_F(r) = [3\pi^2 n(r)]^{1/3}$).

Consequently, a reference electron is not affected by the charge distribution for distances longer than λ_F (the so called ''nearsightedness'' of the electron). Hence, its exchange-correlation (XC) energy only depends on the charge distribution $n(r)$ in its proximity.

These considerations are at the basis of the *Quasi-Local Approximation*(QLA) for the XC energy $E_{xc}[n(\mathbf{r})]]$:

$$E_{xc}[n(\mathbf{r})] = \int e_{xc}(\mathbf{r}, [n(\tilde{\mathbf{r}})])n(\mathbf{r})d\mathbf{r} \tag{28}$$

where e_{xc} is the one-electron XC energy. This approximation is called *quasi-local* because e_{xc} in the coordinates $\mathbf{r}$ depends only by the charge distribution in $\tilde{\mathbf{r}}$, where $\tilde{\mathbf{r}}$ differs from $\mathbf{r}$ for a distance of the order of λ_F. The QLA can be implemented in a code for atomistic simulations in different ways: the *Local Density Approximation* (LDA), for example, which assumes that the one electron XC energy e_{xc} in $\mathbf{r}$ with density $n(\mathbf{r})$ is the same of a uniform electron gas with density $n(\mathbf{r})$:

$$E_{xc}^{LDA}[n(\mathbf{r})] = \int e_{xc}(\mathbf{r}, [n(\mathbf{r})])n(\mathbf{r})d\mathbf{r} \tag{29}$$

In the case of homogeneous electrons gas the XC energy can be considered as the sum of the exchange energy and the correlation energy ($e_{xc} = e_x + e_c$), which are given by [82, 140]:

$$e_x(n) = -\frac{0.458}{r_s} \tag{30a}$$

$$e_c(n) = \frac{0.44}{r_s + 7.8} \tag{30b}$$

where r_s indicates the radius of the average sphere of volume occupied by each electron. In the case of not uniform density the Eqs. 30a and 30b can still be adopted, but considering $r_s(\mathbf{r})$ as variable. This is a reasonable approximation in some cases: if the density is almost constant [54], as well as at high densities, where the kinetic energy dominates the exchange and correlation terms [68].

Typically, in molecular systems, the electron density is spatially not uniform and the LDA is consequently subject to limitations. One way to improve the description of the exchange-correlation functional is given by the so called *Generalized Gradient Approximation* (GGA) [106]:

$$E_{xc}^{GGA}[n(\mathbf{r}, \nabla n(\mathbf{r}))] = \int e_{xc}(\mathbf{r}, [n(\mathbf{r})], \nabla n(\mathbf{r}))n(\mathbf{r})d\mathbf{r} \tag{31}$$

According to this the exchange-correlation functional is not only depending on the local density $n(\mathbf{r})$, but also on the direction of the density gradient $\nabla n(\mathbf{r})$, in some extent to region of space where the density is not uniform. Most of the exchange-correlation functionals are then constructed adding a correction term to the LDA functional. Among all the exchange or correlation potentials, a distinction has to be made between those containing experimental parameters and those which do not contain any of them. The GGA functionals has been implemented in a lot of ways, with different complexity, accuracy and computational cost. Among the most widespread implementations, we remind the Vosko-Wilk-Nusair (1980)[133] functional, the Perdew-Burke-Ernzerhof (1996) [105] and the Lee-Yang-Parr (1988) [73] functional, which is used in a part of this work. It is possible improve the GGA functional allowing the exchange-correlation functionals to depend on high order derivative of the electronic density.

2.2.3 *Hybrid Functionals*

The *Adiabatic Connection Method* represents the basis for the composition of the hybrid functional, which is a system composed by a N-electrons set with other interacting electrons. In this situation a smoothly passage from a non-interacting system to a fully interacting one has to be considered. Restoring to the Hellmann-Feynman

theorem[40], the exchange-correlation energy can then be computed as:

$$E_{xc} = \int_0^1 \langle \psi(\alpha)| V_{xc}(\alpha) |\psi(\alpha)\rangle \, d\alpha \tag{32}$$

where α describes the extent of electronic interactions ranging from 0 to 1 (in which 0 and 1 corresponds to no-interactiong and fully interacting system, respectively). If $\alpha = 0$ the system is without correlation and the wavefunction of the system corresponds to a Slater determinant and the exchange-correlation potential reduces to the Hartree-Fock exchange potential.

In other terms *Hybrid Functionals* (sometimes called also *Hyper-GGA functionals*) include a portion of exact exchange from the Hartree-Fock theory with the approximate exchange and correlation estimated using LDA, GGA, etc. The exact exchange functional is expressed in terms of Kohn-Sham orbitals instead of the density and, for this reason, it is also referred as *Implicit Density Functional*.

Since either the exchange-correlation potential and the wavefunction for $\alpha \neq 0$ are unknown, the value of the integral can only be approximated. Different attempts were made with a weighted sum of the L(S)DA and GGA exchange and correlation functionals, giving rise to the development of several important hybrid functionals, among which for example the B3LYP (Becke 3-parameter Lee-Yang-Parr)[6]: this is one of the most used hybrid functionals and has been extensively employed also in the present Thesis. The B3LYP, which incorporates the 20 % of the exact Hartree-Fock exchange, can be described by the following expression:

$$E_{XC}^{B3LYP} = E_X^{LDA} + \alpha(E_X^{HF} - E_X^{LDA}) + \beta(E_X^{GGA} - E_X^{LDA}) + E_C^{LDA} + \gamma(E_C^{GGA} - E_C^{LDA}) \tag{33}$$

with: $\alpha = 0.2$, $\beta = 0.72$ and $\gamma = 0.81$. These mixing parameters are obtained by fitting experimental atomic energies, electron affinities and ionization potentials. The hybridization procedure permits an improvement of the estimate of many chemical and physical properties, such as the molecular energy levels and the bond lengths of different molecular compounds [17, 21, 22, 84].

2.3 EXCITED STATES

2.3.1 Δ-*Self Consistent Field Method*

If on one side, it has been demonstred that Density Functional Theory (DFT) is a successfull method to obtain the ground-state electronic properties of countless materials and molecules, on the other side, it is well recognized that the use of Kohn-Sham eigenvalues

to determine the quasi-particle properties of many-electrons systems inevitably lead to results not in accordance with experimental data [62]. One example is given by the band-gap problem for bulk semiconductor: in this case a huge underestimat (even exceeding 50%) of the electronic excitation energies takes place with respect to available experimental results (optical absorption, direct and inverse photoemission)[5, 102]. In particular, considering optical absorption experiments, when an electron excited into a conduction state interacts with the resulting hole in the previously occupied state and two-particles (excitonic) effects must be properly considered [103].

For a finite system it is possible to obtain accurate excitation energies using the so-called "delta-self-consistent-field" (ΔSCF) approach[62, 103]. This method, successfully applied to obtain the quasi-particle energies for isolated molecules and a wide range of cluster [87, 88], consists in the evaluation of total energy differences between the self-consistent calculations performed for the system with N and $N \pm 1$ electrons, respectively.

In correspondence of the optimized geometry of the neutral system, it is possible calculate the vertical electron affinity (EA_V) and the vertical first ionization energy (IE_V) as a difference between the total energies of neutral (E_N) and charged molecules (the cation ($E^{(N)}_{N-1}$) and the anion ($E^{(N)}_{N+1}$)):

$$EA_V = E_N - E^{(N)}_{N+1} \tag{34a}$$

$$IE_V = E^{(N)}_{N-1} - E_N \tag{34b}$$

Through the same method, it is also possible the evaluation of the adiabatic observables: the adiabatic electron affinity (EA_A) and adiabatic first ionization energy (IE_A) are obtainable in the same way but considering the cation and anion total energies ((E_{N-1}) and (E_{N+1}) respectively) calculated at their proper optimized geometry:

$$EA_A = E_N - E_{N+1} \tag{35a}$$

$$IE_A = E_{N-1} - E_N. \tag{35b}$$

This allows the calculation of the quasi-particle-corrected HOMO-LUMO gap, E_{Gap}, (also known as "quasi-particle gap" QP_{gap}) of the neutral systems; this observable is usually referred to as the fundamental energy gap and is rigorously defined according to the ΔSCF scheme[62] as:

$$E_{Gap} = IE_V - EA_V = E^{(N)}_{N-1} + E^{(N)}_{N+1} - 2E_N \tag{36}$$

In the context of Δ-SCF, an alternative possible expression for E_{Gap} is given by:

$$E_{Gap} \simeq \varepsilon_{N+1}^{N+1} - \varepsilon_{N}^{N} \tag{37}$$

where ε_i^j are the i^{th} Kohn-Sham eigenvalue of the j-electron system. The results obtained using the above Eqs. 36 and 37 tend to coincide as a function of the system size and the orbitals become progressively more delocalized.

2.3.2 *Time-Dependent Density Functional Theory (TDDFT)*

The *Time-Dependent Density Functional Theory* (TDDFT) is the time-dependent counterpart of DFT, that can be considered its extention with the aim to investigate the properties and dynamics of multi-electron systems in the presence of time-dependent potentials (i.e. study of the excited states). Through the TDDFT technique it is possible calculate the excitation energies, frequency-dependent response properties and obtain the photoabsorption spectra of molecular systems. Similarly to DFT, TDDFT is founded on the fundamental hypothesis that the time-dependent wavefunction can be replaced by the time-dependent electronic density in order to derive the effective potential of a fictitious non-interacting system. In fact, TDDFT is based on an extension of the HK Theorems previously seen in the Sect. 2.2, known as *Runge-Gross Theorem*[112] (RG) which establishes that: *Given initial state at time* t_0, *the single particle potential* $V(\boldsymbol{r}, t)$ *leading to a given density* $n(\boldsymbol{r}, t)$ *is uniquely determined so that the map* $V(\boldsymbol{r}, t) \mapsto n(\boldsymbol{r}, t)$ *is invertible. As a consequence of the bijective map* $V(\boldsymbol{r}, t) \leftrightarrow n(\boldsymbol{r}, t)$, *every observable* $O(t)$ *is unique functional of the time-dependent electronic density* $n(\boldsymbol{r}, t)$.

From the RG theorem and in a similar way to the KS construction for the ground-state density, we may build a time-dependent KS scheme. With this proposal, an auxiliary system of N non-interacting electrons, subjected to an external potential v_{KS}, has to be introduced. This potential is unique, by virtue of RG theorem applied to the non-interacting system, and it has chosen such that the density of the KS electrons is the same as the density of the original interacting system. These Kohn-Sham electrons satisfy the time-dependent Schrödinger equation:

$$i\hbar\frac{\partial}{\partial t}\phi_i(\mathbf{r}, t) = \left[-\frac{\hbar^2}{2m}\nabla^2 + v_{KS}([n]; \mathbf{r}, t)\right]\phi(\mathbf{r}, t) = \mathbf{H}_{KS}([n]; \mathbf{r}, t)\phi_i(\mathbf{r}, t) \tag{38}$$

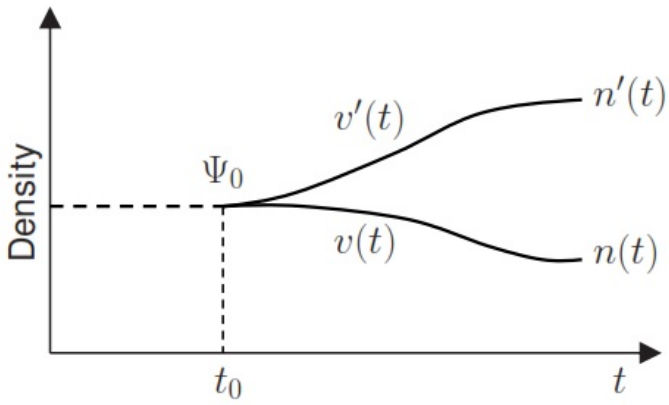

Figure 8: Illustration of the Runge-Gross theorem, which demonstrates that two different potentials can never give the same density. Figure taken from Ref. [23].

from which one can obtain the electronic density of the interacting system from the Kohn-Sham orbitals as:

$$n(\mathbf{r}, t) = \sum_{i=1}^{N} |\phi_i(\mathbf{r}, t)|^2 \tag{39}$$

The time-dependent Kohn-Sham potential (v_{KS}) in Eq. 38 is usually written as the sum of three terms:

$$v_{KS}([n]; \mathbf{r}, t) = v_{ext}(\mathbf{r}, t) + v_{Hartree}([n]; \mathbf{r}, t) + v_{XC}([n]; \mathbf{r}, t) \tag{40}$$

where the first one is the external potential (usually due to the nuclei), the second one (Hartree term) accounts for the classical electrostatic interaction between electrons:

$$v_{Hartree}([n]; \mathbf{r}, t) = \int \frac{n(\mathbf{r}, t)}{|\mathbf{r} - \mathbf{r}'|} d^3\mathbf{r}' \tag{41}$$

and the last term (XC potential) includes all the many-body effects. As previously seen for the ground-state DFT, also in this case, $v_{XC}([n]; \mathbf{r}, t)$ is functionally dependent (in a complex way) on the density. This dependence has a non-local nature, both in space and in time: i.e., the potential at time t and position $\mathbf{r}$ can depend on the density at all other positions and all previous times (due to causality principle).

2.3.3 *Absorption Spectra: Casida formalism*

The major application of TDDFT method consist in the calculations of the electronic absorption spectra commonly using the *Liner Response*

Theory, here not analyzed [89]. Hence, in this Thesis, to obtain all the optical absorption spectra of the molecular systems under study, we have performed TDDFT calculations following the *Casida* computational method, instead of the previously mentioned one [15]. According to this approach, the spectra are obtained from the calculations of the poles of the dynamic polarizability function, in the frequency domain, as a sum-over-states form in the case of finite systems and expressed by:

$$\alpha(\omega) = \sum_{I \neq 0} \frac{f_I}{\omega_I^2 - \omega^2}, \tag{42}$$

where ω_I and f_I are vertical excitation energies and the corresponding oscillator strengths, respectively. Finally, the Laurentzian broadened stick spectrum can be obtained considering [24],

$$S(\omega) = \frac{2\omega}{\pi} Im\alpha(\omega + i\eta). \tag{43}$$

In the reciprocal space, TDDFT calculations implementation computational costs scale steeply as a function of the number of required transition and electronic excitations are limited to the low-energy portion of the spectra. Such procedure offers the advantage of being able to go to calculate the absorption spectra of very large size molecules over a wide range of energies, albeit with not optimal spectral resolution.

2.4 COMPUTATIONAL DETAILS, NUMERICAL METHODS AND TOOLS

2.4.1 *Basis Sets*

Usually, in quantum chemistry, most computational methods represent the N-electron wavefunction as a linear combination of Slater determinants, combining one electron functions and the molecular spin orbitals. They are written in terms of atomic spin orbitals or similar functions, which are approximated as a linear combination of atomic orbitals LCAO (quantum superposition of atomic orbitals). For a given basis-set of atomic orbitals, namely $\{\phi_j\}$, the i^{th} molecular orbital ψ_i can be obtained as:

$$\psi_i = \sum_{j=1}^{k} c_{i,j}\phi_j \tag{44}$$

where $c_{i,j}$ is the coefficient of expansion and k the total number of atomic orbital functions, called *Basis Functions*. From the choice of an appropriate basis-set depends the quality and the accuracy of all the

results obtained in quantum chemistry calculations. In fact, an efficient basis-set should reproduce the physics of the problem, ensuring rapid convergence as a function of the number of basis function, allowing fast calculation of all the integrals involved (to save computational time) and vanishing at large distance from the nuclei. The two types of atomic orbital functions more commonly used to obtain the combination showed in Eq 44, are the Slater-Type Orbitals[119] (STO) and Gaussian-Type Orbitals[13] (GTO).

The STO basis functions (proposed by Slater in 1930) are based on hydrogenic-like wavefunctions and can be written in two possible forms (expressed in polar and cartesian coordinates, respectively):

$$\phi^{STO}_{\zeta,l,m}(r,\theta,\varphi) = Nr^{l}Y_{lm}(\theta,\varphi)e^{-\zeta r} \tag{45a}$$

$$\phi^{STO}_{\zeta,l_x,l_y,l_z}(x,y,z) = N\bar{x}^{l_x}\bar{y}^{l_y}\bar{z}^{l_z}e^{-\zeta|r|} \tag{45b}$$

On the other hand, the GTO basis functions (introduced in1950 by Boys) have the following forms:

$$\phi^{GTO}_{\zeta,l,m}(r,\theta,\varphi) = Nr^{l}Y_{lm}(\theta,\varphi)e^{-\zeta r^2} \tag{46a}$$

$$\phi^{GTO}_{\zeta,l_x,l_y,l_z}(x,y,z) = N\bar{x}^{l_x}\bar{y}^{l_y}\bar{z}^{l_z}e^{-\zeta r^2} \tag{46b}$$

In the Eq.s 45 and 46 $\bar{x},\bar{y},\bar{z} = (x_c - x_N, z_c - z_N, z_c - z_N)$ are the difference between the nuclei coordinates (subscript N) and the coordinates of the center of the function (subscript c), N is a normalization constant, $Y_{lm}(\theta,\varphi)$ is the angular part (a spherical harmonic function), $r^{l}e^{-\zeta r}$ is the radial part, l and m are the atomic quantum numbers and r and ζ are the radial distance and the orbital exponent, respectively. The orbital exponent, ζ, governs the size of the orbital (large ζ values gives tight function, while small ζ values diffuse function) and it is chosen for each (n, l) separately, where n is the principal quantum number. The terms l_x, l_y, l_z (referred to as angular momentum $L = l_x + l_y + l_z$) determines the type of orbital ($L = 0,1,2,3,4,5,6$ indicated as s, p, d, f, g, h, i).

Slater type orbitals posses the proper functional behavior next to the nucleus with a cusp in the origin, the correct $1/r$ decay at long distances and, in general, are more convenient when high accuracy is needed for atomic and diatomic systems (ab-initio methods), or where all three-and four-centre integrals are neglected (e.g. semi-empirical methods) as well as in cases where Coulomb energy is calculated by fitting the density into a set of auxiliary functions rather than computing the exact exchange energy (in DFT). However, the use of STO functions is time-consuming for computing the two-electron molecular integrals and difficult to be differentiated analytically.

For these reasons, in order to quicken molecular integral evaluation, it is more useful to restore to the Gaussian-type orbitals.

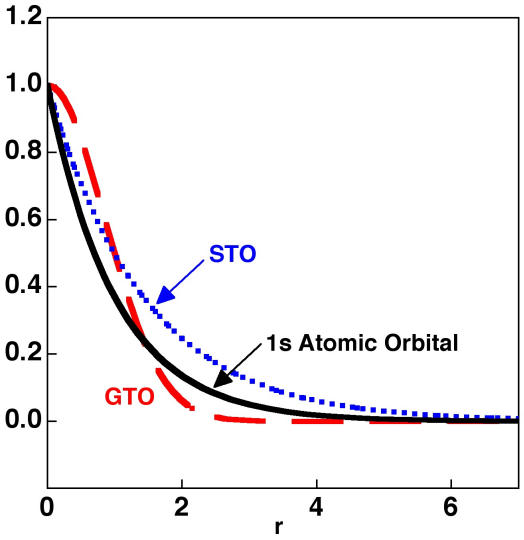

Figure 9: Gaussian (red) Slater (blue) type functions in comparison with an 1s type real atomic orbital. Figure from Ref. [20].

From a computational point of view, GTO functions are more simple to treat (this implies, for example, a rapid calculation of molecular integrals) and can be differentiated in an easy way any number of times. Gaussians are very useful and computationally efficient because satisfy definite properties: the product of any two gaussians is again another gaussian, and the sum of two gaussians is easily evaluated (see Fig. 10).

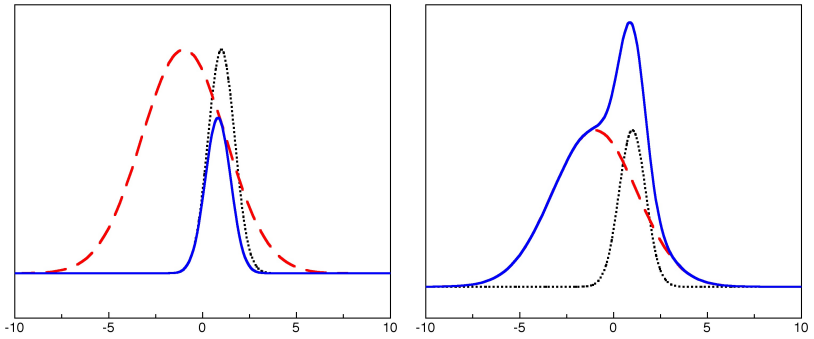

Figure 10: Product (left) and sum (right) of different GTO. Figures from Ref. [20].

This property is a crucial point in quantum chemistry where you need to evaluate integrals of the form given below. The first is called a

"4-center integral" and is easily reduced to a "2-center integral" when using gaussians.

$$\underbrace{\int \overbrace{g_1 g_2}^{g_a} \frac{1}{r_{12}} \overbrace{g_3 g_4}^{g_b} d\tau}_{\text{4-center integral}} = \underbrace{\int g_a \frac{1}{r_{12}} g_b \, d\tau}_{\text{2-center integral}} \tag{47}$$

in wich the terms g_k are GTO funtions.

On the other hand, despite of the numerical advantages, the GTO, present however some serious lacks, among which: the bad description of the electron density near the nuclei due to the fact that, unlike the STO, the GTO do not have a cusp at the origin, and have, instead, a too quick decay for $r \to \infty$ thus underestimating long range interactions [20]. For these reasons replacing a STO by a single Gaussian function unavoidable errors are made.

However, this problem can be overcome with the introduction of the *Contracted Gaussian-type Orbital* (CGTO) which is represented as a linear combination of primitive GTO functions that simulate the behavior of specific STO orbitals ($\phi_\mu^{STO}(\mathbf{r}, \zeta)$).

$$\phi_\mu^{CGTO}(\mathbf{r}, N, \{d_{p,\mu}, \zeta_{p,\mu}\}) = \sum_{p=1}^{N} d_{p,\mu} \phi_\mu^{GTO}(\mathbf{r}, \zeta_{p,\mu}) \tag{48}$$

where $d_{p,\mu}$ are the coefficients of the primitive gaussian functions $\phi_\mu^{GTO}(\mathbf{r}, \zeta_{p,\mu})$ and N is the number of functions in the combination.

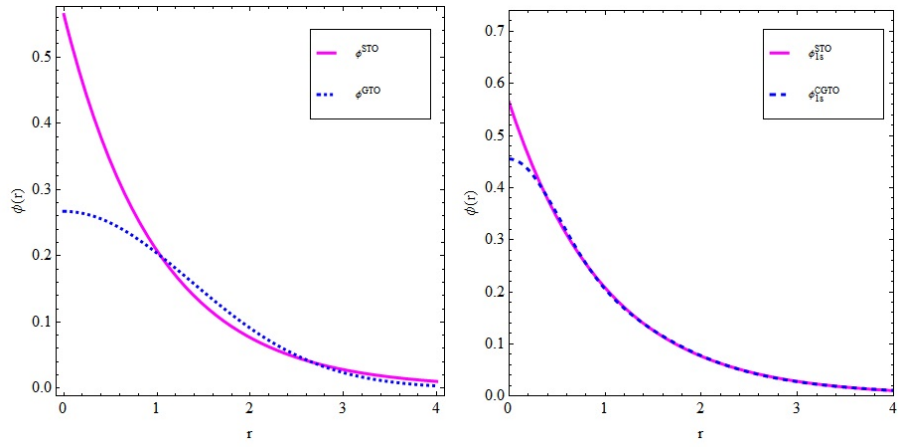

Figure 11: (left) Comparison between a Slater $\phi_{1s}^{STO}(1.0; \mathbf{r})$ and Gaussian $\phi_{1s}^{GTO}(0.270; \mathbf{r})$ functions.
(right) Comparison of the same Slater function ($\phi_{1s}^{STO}(1.0; \mathbf{r})$) (purple) and the Contracted GTO $\phi_{1s}^{CGTO}(\mathbf{r}) = 0.445\phi_{1s}^{GTO}(0.110; \mathbf{r}) + 0.535\phi_{1s}^{GTO}(0.406; \mathbf{r}) + 0.154\phi_{1s}^{GTO}(2.228; \mathbf{r})$ (blue). Figures taken from Ref. [20].

As Fig. 11 shows, a single GTO significantly differs from STO, while CGTO of three GTO shows a reasonable approximation of STO, except at very small and very large electron-nucleus separation (ideally considering an infinite range).

Aside from the choice of STO or GTO type of functions, the most important parameter to set is the number of basis functions used in the basis-set. According to this, the most frequently used basis-sets can be classified into the following classes:

MINIMAL BASIS SET: Represents the minimum number of basis functions needed to obtain the right numerical description of the atomic orbitals. A minimal basis set (MBS) contain the minimum number of basis functions required for each inner-shell and valence-shell orbital. In particular, if STO functions are employed, a MBS uses one STO to describe each atomic orbital in the ground state of an atom. For shells with more than one angular component, this implies one function for each angular component. On the contrary, for the use of GTO functions a minimal set can be obtained using the so called "STO-nG", in which each atomic orbital is expressed by a linear combination of n-gaussians, where the coefficients and exponents of the GTOs are fitted to the corresponding atomic orbital[4] (n usually assumes values in the range 1-6 and the computational cost does not increase linearly with n).

MULTIPLE ζ BASIS SET: These basis-set are constituted by replacing each GTO (or STO) of a minimal basis set by 2 (Double-ζ; DZ), 3 (Triple-ζ; TZ), 4 (Quadruple-ζ; QZ) or more (5-ζ, 6-ζ ecc.) GTOs (or STOs) each having different orbital exponent ζ. The use of multiple ζ basis-sets allows the required radial flexibility in the description of the electronic cloud. The tighter functions (closer to the nuclei, large exponent) can be used to describe the σ-bond with a large coefficient, while the more diffuse function (further from the nuclei, small exponent) can be used primarily for describing the π-bond. As the number of basis functions that describe the atomic orbitals increases, a better description of the situation in which the electron distribution is different in more directions, will be given [20].

SPLIT VALENCE: The core electrons (inner-shell) of an atom are less affected by the chemical environment with respect to the valence-shell electrons. A split valence basis set (SV) represents a numerical simplification of multiple ζ basis-sets, in which the core shells are treated with a minimal basis-set, while the valence shells are treated with a larger basis-set. In other words, each

4 More precisely the coefficients of each combination of GTO are fitted to the corresponding Slater type orbital of the minimal STO basis set that provides the best description of the orbital

orbital of a core-shell is represented by a single function, while two or more functions are used to describe each valence shell atomic orbital.

POLARIZATION FUNCTIONS: Considering the distortion in shape of the atomic orbitals and that their centers of charge are shifted upon molecule formation, the improvement of basi-set for this polarization can be done with the addition of higher angular momentum functions to the basis-set to allow angular flexibility. In these functions, l quantum numbers are greater than the maximum l of the valence shell of the ground-state atom (e. g.p functions for the hydrogen, d functions for carbon ecc.)[20] .

DIFFUSE FUNCTIONS: These functions, characterized by very small ζ exponents added to a split valence basis-set, are additional functions. Diffuse functions have small orbital exponent that reproduce a very broad electron distribution and are needed whenever loosely bound electrons are present (for example anions or excited states) or when the property of interest is dependent on the wave function tail (for example polarizability). In particular, it is necessary to restore to the diffuse functions to a correct description of anions and weak bonds (e.g. hydrogen bonds), to remove an anomaly typical of the negative charged species. Diffuse functions are often used to calculate physical properties (e. g.dipole moments, polarizabilities, etc.) and to treat atoms with a high electronegativity (e. g.fluorine).

In this Thesis, for the molecular calculations, we have used the so called *Pople type* [33] localized basis set 6-31+G*. The Pople basis-sets are usually identified by the notation n-ijk*w*G, where:

- n: defines the number of primitive Gaussians functions employed to describe the core atomic orbitals.
- i,j,k and *w* represent the number of primitives for contractions in the valence shell. The ij notation defines sets of valence double-ζ quality, ijk the triple-ζ valence sets, ijk*w* the quadruple-ζ quality and so on. Said otherwise, the number of digits after the symbol "-" identify the number of basis that compose the valence orbitals and the explicit value of i,j,k and w indicate the number of gaussian functions that represent the linear combination for each base.

This formalism provides also the use of the symbols "+" and "++" to indicate the presence of diffuse functions for heavier atoms (except hydrogen and helium) (+) and for all atoms (++), (including H and He), respectively. In the Pople notation other symbols used are "$\star$" and " $\star\star$", which denotes the inclusion of polarization functions.

Even in this case, the single symbol indicates the presence of these functions with the exception of lightest atoms; the double symbol, instead, confirms the presence of diffuse functions also for He and H. More details on the basis-sets and the convergence criteria adopted in this Thesis will be specified in the dedicated sections of the computational methods of each sigle chapter.
An alternative approach with respect to the basis functions (STOs or GTOs previously seen in Sect. 2.4.1) developed for the atomistic simulation of molecules and condesed phase systems with the DFT, is given by a technique which exploits plane waves (PW) aimed directly at the full system. Plane waves are more popular in solid state simulations because their application to periodic systems is straightforward and usually only DFT methods without Fock-exchange are employed [128]. Commonly, plane wave basis-sets tend to be highly larger as compared to typical Gaussian basis-sets (for example, a cutoff energy of $\sim$ 200 eV corresponds to a set of $\sim$ 20000 functions [58]). However, this approach is here not used, since not ideal to treat the systems analyzed (molecules), but it is very efficient and actually often employed when one need to describe more extended systems (see e.g. Ref. [91, 110, 122, 123]). The pros and cons of both the approach are briefly summarized by the following points [128]:

- PW calculations, in particular, for solid state systems, are usually faster than GTO ones, for both energy and gradient computation, even if they require much more main memory when norm-conserving pseudopotentials are adopted;
- Within the PW approach core electrons are not treated explicitly and their presence is accounted for by pseudopotentials.The projector augmented-wave method PAW for the explicit treatment of core electrons has also been implemented in some of the more advanced computer codes which greatly increases the accuracy of PW results;
- The calculation of atomic forces is simpler with PW because only Hellmann-Feynman forces are included. The evaluation of Pulay forces in GTO calculations is much more time-consuming, and also their coding is more involved;
- The quality of PW basis sets is simply specified by a single parameter (the electronic kinetic energy cut off E_{kin}). The higher E_{kin}, the better is the basis set. Standard GTO basis sets of increased quality have been developed for almost all atomic elements since the early days of quantum chemistry. Due to potential linear dependence problems, however, transferability to periodic systems is not immediate. In particular, basis sets including very diffuse Gaussian functions (for example, $6-31++G(d,p)$) are critical for periodic systems, and exponents of the most diffuse Gaussian functions should be properly regulated;

- With PW basis sets calculations are intrinsically periodic in three dimension (3D): the system, regardless of being a molecule, a two dimensional (2D) sheet or areal 3D crystal, is always defined in a 3D box which is uniformly filled with plane waves. By virtue of the local nature of Gaussian functions, in GTO calculations the true dimensionality of the system is always obeyed.

- Energies calculated with PW basis sets do not suffer from the basis set superposition error (BSSE). This is an extremely appealing feature of PW calculations, expecially, for studying adsorption processes characterized by interaction energies of moderate strength. In GTO calculations corrections for the BSSE can be made by the well known function *counterpoise method*. In most cases these corrections are *a posteriori* applied to uncorrected equilibrium structures ,i.e., potential energy surfaces are those computed without counterpoise correction;

- Due to extremely high computational costs when using delocalized basis sets exact (Fock-) exchange is rarely calculated with PW. This avoids the recourse to hybrid functionals (e.g. B3LYP), which in several respects are known to be more accurate than standard generalized gradient (GGA) functionals. Nowadays, the number of PW calculations employing hybrid functionals is still limited. On the contrary, exact exchange as well as hybrid functionals are standard in GTO based molecular computer codes as shown by a variety of studies on periodic systems.

Part II

RESULTS

3

SI-ATOMS INSERTIONS IN CIRCUMACENES

3.1 INTRODUCTION

The relevance of 2D systems (like Graphene and Silicene)[48, 76], in the last few years, has quickly and highly upgraded and is now in incessant evolution, since these systems show advantageous electronic, mechanical and optical properties (planar feature, ,flexibility, mechanical resistance....). These materials are, in fact, considered among the most promising candidates for several different forefront optoelectronic devices. Moreover, in this last context, Silicon is one of the most useful elements to mankind, covering a considerable position for several reasons, especially for those linked to its electronic and optical properties that can be easily modulated and controlled [35].
Furthermore, optoelectronics, the scientific branch based on the study and the operation of electronic devices that produce, detect, and control light, actually is an esteemed and rapidly growing field [138]: recently, 2D materials, carbon nanotubes, and semiconductor quantum dots have been elements of great attention thanks to their potential use in nano and optoelectronic devices.
In this field, the role of polycyclic aromatic hydrocarbons (PAHs) in their crystalline and thin-film state has largely increased: in fact, these compounds can be employed as active elements in several optoelectronic applications, ranging from light-emitting diodes (LEDs), solar arrays, transparent and flexible displays to organic thin-film field-effect transistors and liquid crystals. Among them, the "Circumacenes" (Coronene, Ovalene, Circumanthracene, Circumtetracene, and Circumpentacene) have recently manifested scientific interest in many contests of research (from condensed matter physics to astrochemistry) and also for solid state physics applications [56, 84, 111]. Among the Circumacenes, we have selected the Coronene (or ”superbenzene”), which is a symmetric molecule composed by the union of six benzene rings (with chemical formula $C_{24}H_{12}$) and Ovalene ($C_{32}H_{14}$), obtainable from Coronene by the addition of three lateral benzene rings (see Fig. 12) [25, 47, 109]. The first one occurs in nature as the very unusual mineral ”carpathite”, that is characterized by flakes of pure Coronene embedded in sedimentary rock and it can be synthesize through the petroleum-refining process of hydrocracking [57]; the second one appears as a reddish-orange compound and can be made through similar ways. As compared to polymers, these small-size molecules, offer several advantages, among which: they can be such easily purified through different techniques and tractable by both evaporation and

solution-processing methods [84].
The present part of the Thesis is focused on the study of the effects that Silicon-atoms substitutions induce in Coronene and in Ovalene molecules, considering their electronic and optical properties. We have evaluated single, double and triple-atom substitutions of Silicon into these molecules, with the aim to probe the resulting consequences. In fact, since one of the goals of this Thesis is the analysis of finite-size effects on the electronic and optical properties of the nanometric portions of Graphene compounds, in this case we study what happens after Silicon-atoms substitutions, with possible subsequent extensions to their infinite counterparts and in connection with other previous studies [91, 144]. Through the DFT (Density Functional Theory) technique [69] we have computed the ground-state morphological and electronic properties of the systems under exam (e. g. electron affinities, ionization energies, quasi-particle (QP) gaps) using a gaussian-based localized orbital all-electrons scheme. Via the TDDFT (Time Dependent Density Functional Theory) scheme[89] we have obtained the optical absorption spectra of the above clusters, trying to find possible trends and analyzing the behavior as a function of the different Silicon substitutions. Hence, a comparison of our results with existing outcomes of previous theoretical and experimental works has been done. This part of the Thesis has been object of the work contained in two of our previous mentioned publications and here presented incorporating the results from both the two (see Ref. [92] and [93]).

3.2 COMPUTATIONAL DETAILS

Keeping on previous works [84, 111], we have performed geometry optimizations using the hybrid exchange-correlation functional B3LYP [7, 73, 124], combined with the $6-31G^*$ basis-set (a valence double-ζ set augmented with d polarization functions for each atom). We have chosen the B3LYP exchange-correlation (XC) potential, since with respect to other possible alternatives (e.g. the PBE (Perdew−Burke−Ernzerhof) [38]), it has been established to reproduce better results for different families of PAHs molecules, for both the ground-state and the excited properties [17, 21, 22, 84]. All the molecular relaxations have been computed without symmetry constraints and using tight convergence criteria (specified by maximum and root mean square gradient thresholds of $1.5 \cdot 10^{-5}$ and $1.0 \cdot 10^{-5}$, respectively, and maximum and root mean square thresholds of the Cartesian step respectively of $6.0 \cdot 10^{-5}$ and $4.0 \cdot 10^{-5}$). All the values are reported in atomic units. At the optimized geometry of the neutral molecules, we have evaluated the vertical ionization energies (IE_V) and the vertical electron affinities (EA_V). This let the calculation of the quasi-particle gap (or "fundamental gap"), which is rigorously

defined in the ΔSCF scheme as [62, 87] in the eq. 36. To obtain the absorption spectra in the visible/near-UV regions, we have performed TDDFT calculations, using the frequency space implementation set in the computational package, at the same level $B3LYP/6-31G^*$ set for the electronic ground-state. According to this method, the poles of the linear response function correspond to the vertical excitation energies and the pole strengths represent the oscillator strengths [15]. In particular, knowing the first optically active transition from the spectrum, E_{opt}, we could estimate the exciton binding energy expressed by the following difference:

$$E_{bind} = E_{gap} - E_{opt} \tag{49}$$

It is well known that the technique here used to evaluate the exciton-binding energy is an approximated one to obtain the aforesaid observable. However, in the case of systematic studies based on several molecules, this method turns out to be particularly useful and straightforward to obtain the right trend and the order of magnitude of the physical observables, allowing one not to apply most demanding computational techniques [29, 103]. All the calculations have been performed using NWChem [132] computational package, that is based on a numerical resolution of the Khon-Sham equations after a DFT Hamiltonian [69], while the XC effects are treated appealing to a particular functional inserted inside the Hamiltonian after the B3LYP scheme [7, 73, 124].

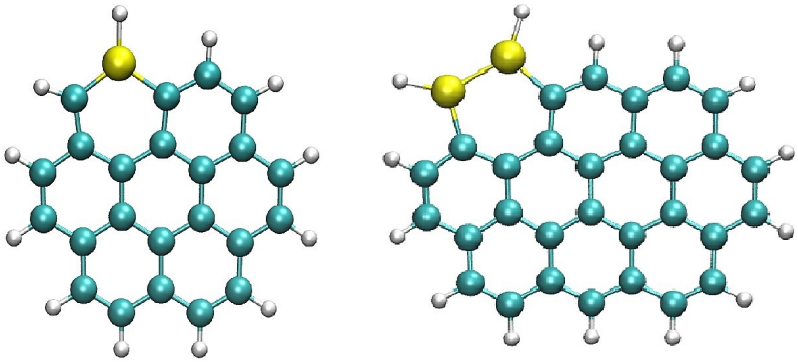

Figure 12: Coronene (left) and Ovalene (right) with Si-atoms insertions. C atoms are in cian, while Si atoms are in yellow and H atoms on the boundaries in white.

3.3 RESULTS AND DISCUSSION

3.3.1 *Silicon-atoms substituted configurations*

The possible non-equivalent insertions of Silicon atoms, according to the molecular symmetries, are the following ones (see Fig. 13):

- 6 (9) configurations as a result of single Si-atom substitutions in Coronene (Ovalene);
- 4 (9) configurations as a result of double Si-atom substitutions in Coronene (Ovalene);
- 4 (10) configurations as a result of triple Si-atom substitutions in Coronene (Ovalene).

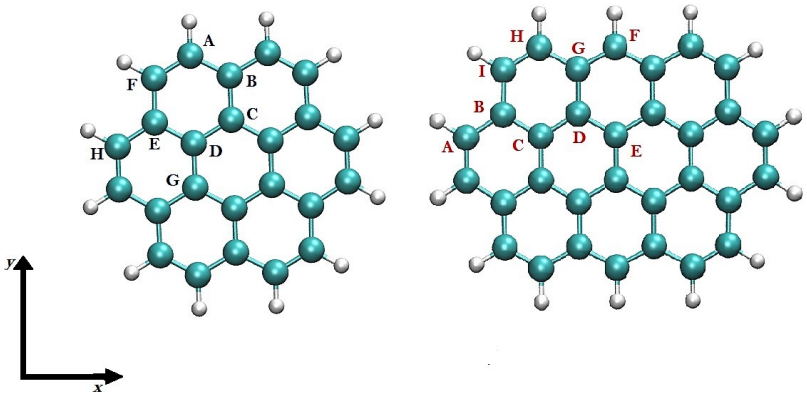

Figure 13: Coronene and Ovalene molecules. The C atoms selected to be replaced by Si atoms are indicated by letters from A to H for Coronene (left), while from A to I for Ovalene (right). Dimers and trimers are composed by the union of the adjacent individual ones.

In the case of Coronene, moreover, because of the equivalence between A-F, B-E and C-D atoms linked to symmetric reasons, the configurations number being reduced from 6 to 3 for single substitutions (see Fig. 13). On the contrary, considering Ovalene, the addition of three benzene rings in the structure implies an increase of the allowed configurations number, involving a reduction of the molecular symmetry. Among all these arrangements, in the following lines, we decide to present only one system for each substitution, for both Coronene and Ovalene, following a selection criterion based on the evaluation of the energy stability of the substituted clusters. In particular, we found that, from the energetic point of view, the most favorable configurations are the following ones: the atom placed in A (H)

position in the case of Coronene (Ovalene) for single substitutions, the dimer composed by A-F (H-I) atoms for Coronene (Ovalene) for the double insertions and finally, the trimer formed by the union of B-A-F (H-I-B) atoms for Coronene (Ovalene) for the triple substitutions [93]. We consider only the case for N=2, N=3 with insertions of adjacent individual Si-atoms.

In general, we verified that, in the modified systems with Silicon atoms, the energy stability tends to slack off from the external to the innermost molecular areas: this means that, the most stable configurations are potentially those in which the substitutional site is located in the peripheral molecular regions. A plausible physical explanation of this occurrence is that in the outer regions less constraints could bound the deformations after Si-atoms insertions. This fact could cause larger total energies when the substitutions are performed at the periphery of the cluster: Silicon has, in fact, with respect to Carbon, has, a larger covalent radius and therefore, if inserted in a carbonaceous matrix can provoke distortions of the original structure [93]. The substituted configurations were found to preserve the planar geometry of their parent molecules, after single and double Si-atoms inclusions: the deformations are, in these cases, planar and localized, close to the point in which the insertion has been made. On the contrary, in some cases of trimer insertion, for both Coronene and Ovalene, their planar appearance has been perturbed (Fig. 14 shows an example, reproducing the substitution of the trimer composed by the atoms placed on the central ring for Coronene and by the atoms B C D for Ovalene). In these particular cases the distortions are extended towards the "out-of-plane" directions. This effect seems to be more pronounced for Ovalene than for Coronene, as demonstrated by the variation of the interatomic bonds connecting Si-C atoms. Details of the Silicon insertions on the morphological properties will be given in the following dedicated section (see section3.4).

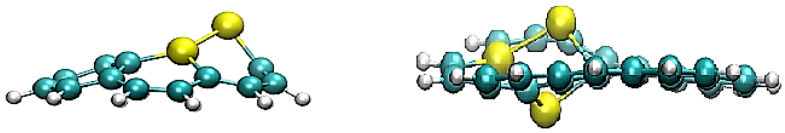

Figure 14: Lateral view of Coronene (left) and Ovalene (right) molecules with the Si-trimer substitution which do not preserve the planar geometry, as shown in Fig. 12.

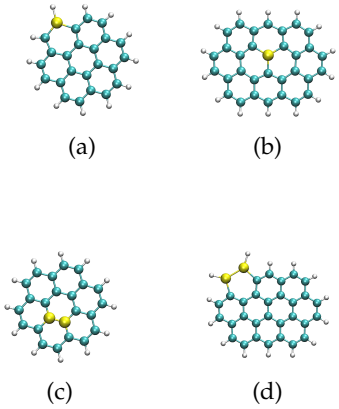

(a) (b)

(c) (d)

Figure 15: Coronene (a, c) and Ovalene (b, d) with single Si-atom inclusions and Si-dimers ones.

3.4 MORPHOLOGICAL PROPERTIES

In this section, which is part of the work came from Ref. [92], we have selected an example for both the molecules to show the effects induced on the structural properties by the Si-atoms insertions, analyzing the consequences as a function of the numbers of C-atoms replaced. In particular, we focus our attention on the trimer substitution for both the species, since this modified configuration largely loses the flatness typical of the Circumacenes (see Fig.16). For Coronene, we have chosen the configuration with the trimer substitution placed on the central ring (see Fig. 17, according to which the corresponding Si atoms are represented in yellow and indicated by numbers 1,2,3). In the case of Ovalene, the atoms labeled by B, C, D composed the substituted trimer. The interatomic bond lengths are shown in Tab. 1, where Si-C, Si-Si, C-C atomic distances are reported for these two specific configurations, labeling the selected atoms as indicated by Fig. 17. The percentage deviations of interatomic distance between C-C atoms that compose the parent molecules are also shown (the average C-C bond lenght value for the unperturbed compounds ($C - C_{unp}$) is 1.43 Å). We analyzed quantitatively how the distances in the ring in which Silicon atoms are inserted have been modified in comparison to the original structures. In the case of trimer substitutions, the distortions are consistent and concern the global structure, that clearly loses its planar appearance (see, for example, Fig. 16). On the contrary, in the case of some single and double substitutions, after the present calculations, minor strain of the rigid structure take place, but in general, for both Coronene and Ovalene, the deformations are only local and they determine a change of the interatomic bond lengths, without any loss of planar feature.

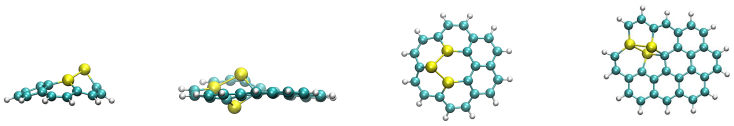

(a) (b) (c) (d)

Figure 16: Coronene (a,c) and Ovalene (b,d) with a Si-trimer substitution placed in an internal molecular area.

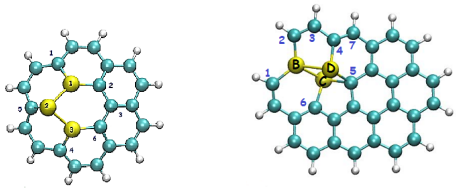

(a) (b)

Figure 17: Coronene (a) and Ovalene (b) with a Si-trimer substitution in which Si and C atoms are labeled by letters and numbers, as reported in Tab. 1.

In particular, the modifications imply that for Coronene the C-Si bond deviation with respect to the corresponding C-C bond of the unsubstituted system goes from ~ 20% to 26%. Similarly for Ovalene, the calculated percentage change of the C-Si bond in comparison with the C-C one results in the range of 22% − 30%. Moreover, the distance connecting two Si atoms (Si-Si bond) is larger in the case of Ovalene (with an increase of ~ 47% compared to the C-C bond) if compared to the Coronene one (~ 36%). Our results confirm larger deformation provoked by the insertion in Ovalene molecule (see Tab. 1). On the contrary, C-C bond length, in the case $C^2 - C^3$ and $C^4 - C^7$, in the substituted Ovalene is subjected to a reduction of ~ 4% as compared to the pure geometry, while for Coronene the C-C bond for $C^2 - C^3$ and $C^3 - C^6$ show a negligible variation (~ 1.4%). This result proves that, according to the chemical modification, different effects takes place depending on the position in which it has been made as well as on the system under study. After the presented outcomes for Si-atoms insertions the here considered isolated molecules seem to offer a different scenario in comparison to the infinite Graphene sheet [80, 144]. This point, therefore, needs additional focused experimental and theoretical studies to be completely understood.

3.5 ELECTRONIC PROPERTIES

From DFT calculations (see Tab.2), we observed that Ovalene ground-state total energy (-33.4 keV) exceeds by 33% the Coronene one (-

Table 1: Interatomic bond lengths between C-Si, Si-Si and C-C atoms for the two selected substituted molecules with a Si-trimer. The percentage variations with respect to the C-C unperturbed distance ($C - C_{unp}$) are also shown. Numerical and alphabetical labels are made according to Fig. 17.

CORONENE	Å	(%)	**OVALENE**	Å	(%)
$C - C_{unp}$	1.43	–	$C - C_{unp}$	1.43	–
$C^1 - Si^1$	1.78	19.7	$C^1 - Si^B$	1.84	22.3
$C^2 - Si^1$	1.80	25.9	$C^2 - Si^B$	1.84	22.3
$C^5 - Si^2$	1.92	25.5	$C^4 - Si^D$	1.92	25.5
$C^6 - Si^3$	1.80	25.9	$C^6 - Si^C$	1.92	25.5
$C^4 - Si^3$	1.78	19.7	$C^5 - Si^D$	2.04	29.9
$Si^1 - Si^2$	2.22	35.6	$Si^B - Si^C$	2.68	46.6
$Si^2 - Si^3$	2.22	35.6	$Si^B - Si^D$	2.69	46.8
$C^2 - C^3$	1.45	1.37	$C^2 - C^3$	1.37	-4
$C^3 - C^6$	1.45	1.37	$C^3 - C^4$	1.45	1.38
			$C^4 - C^7$	1.37	-4

25.1 keV): this is a consequence of the larger electrons numbers involved.Exploring the effects of Silicon insertions, we verified that the ground-state energy increases, in absolute value, in the range between $\sim 27 - 82\%$ ($\sim 20 - 61\%$) comparing the Coronene (Ovalene) and its modified configurations, from single to triple substitutions, respectively.
This signifies that in the case of each substituted configuration, the effects of Silicon inclusions imply a growth of the energy stability with respect the corresponding original parent and in addition, this result for Coronene is larger than Ovalene [93].

Tabs. 2 and 3 report the computed data for ground and excited states of Coronene and Ovalene and their selected substituted configurations, as previously indicated (the percentage deviations have been calculated with respect to Coronene).

Firstly, we consider the comparison between the original molecules, indicating the percentage variation for each observable, going from Coronene to Ovalene and then for their substituted geometries. In relation to ground-state total energies, all Ovalene configurations present deeper energies than those of Coronene (this is expressed with an increase, in absolute value, of the ground-state total energy (E_0^N) as a consequence of the increase in the number of electrons).
For Ovalene, EA_V is $\sim$ 26 times larger with respect to the Coronene one, while for the IE_V, the situation is reversed, since this observable results larger by $\sim$ 9.8% for Coronene (6.85 eV) than Ovalene (6.18 eV).

Table 2: Ground-state total energies, E_0^N, for Coronene and Ovalene substituted molecules (single (S), dimer (D) and trimer (T) Si-atoms insertions).The percentage deviation, calculated with respect to Coronene to the corresponding Ovalene molecule, is also reported.

Ground-state Total Energies		
	E_0^N (keV)	(%)
CORONENE	-25.1	-
S	-31.9	-
D	-38.8	-
T	-45.6	-
OVALENE	-33.4	+33%
S	-40.2	+26%
D	-47.1	+21.4%
T	-53.9	+18.2%

Consequently, the corresponding QP gaps (E_{gap}) are of the same order of magnitude, 6.82 (5.40) eV for Coronene (Ovalene), respectively. Note that, only in the case of Coronene EA_V, the calculation has been performed using the $6-31+G^*$ basis-set (which includes the atomic diffuse functions), instead of the $6-31G^*$, to overcome an anomaly in the value obtained for that observable [129], with the resultant value of EA_V=0.39 eV . All the data reported in Tab. 3 have been calculated for coherence with the same basis-set $(6-31G^*)$, but we decided that, to make possible a connection with the available theoretical/experimental data for the Coronene EA_V, the implementation of the diffuse functions included in the $6-31+G^*$ basis-set (see Tab. 4) has been required. Some of the same data are shown by Fig. 18 with an energy level depiction for Coronene and Ovalene [1].

Now we consider the effects induced by Si-atoms substitutions, switching from Coronene on Ovalene, followed by the same effects passing from the pure molecule to the substituted ones. As shown in Tab. 3, there is an increase in the vertical electron affinities, going from Coronene to Ovalene, for each type of substitution (from 45% to 600%), while, on the other hand, the vertical ionization energies and the fundamental gaps show a general lowering (of $\sim$ 7% and from $\sim$ 12% to 18%, respectively).The analysis of the substitutional effects on the electronic properties, with respect to its original compound, follows.

We found that for Coronene (Ovalene)EA_V the variation range oscillates between $\sim +300-1900\%$ $(4-13\%)$, considering the minimum

1 The illustration by Fig. 18 takes into account the Coronene $EA_V = 0.39$ as obtained with the $6-31+G^*$ basis-set, to make possible a more consistent link with the data from the literature reported in Tab. 4. For E_{opt} and E_{gap} see the dedicated following section.

Table 3: Vertical electron affinity (EA_V), ionization energy (IE_V) and fundamental gap (E_{gap}) for Coronene and Ovalene substituted molecules (with single (S), dimer (D) and trimer (T) insertions). The percentage deviation, passing from Coronene to Ovalene corresponding system, is also reported. All the values are given in eV.

	EA_V	IE_V	E_{gap}
CORONENE	0.03	6.85	6.82
S	0.11	6.43	6.32
D	0.31	6.37	6.06
T	0.6	6.24	5.64
OVALENE	0.77 –	6.18 (-9.8%)	5.38 (-20.8%)
S	0.80(+600%)	5.95 (-7.5%)	5.15 (-18.5%)
D	0.81 (+161%)	5.96 (-6.4%)	5.14 (-15.2%)
T	0.87 (+45%)	5.80 (-7%)	4.93 (-12.5%)

Table 4: Theoretical and experimental data (in brackets after literature) for the electron affinity (EA_V) and the ionization energy (IE_V) for Coronene and Ovalene, as obtained by Ref. [83] and Ref. [97], respectively.

	EA_V	IE_V
CORONENE	0.38 (0.47 $\pm$ 0.090)	7.08 (7.29 $\pm$ 0.03)
OVALENE	1.10 (–)	6.41 (6.71)

and the maximum value. For IE_V, we recorded a decrease included in the range of $\sim 6-9\%$ ($\sim 3-5\%$) for Coronene (Ovalene). The reduction of E_{gap} with respect to the corresponding original parent is of $\sim 7-10\%$ ($\sim 4.5-8.5\%$) in the case of Coronene (Ovalene).

Moreover, in Tab. 4 have been presented the theoretical and experimental data (in brackets) for EA_V and IE_V of Coronene and Ovalene, as obtained by Ref. [83] and Ref. [97], respectively. For the electron affinities, we have found that the theoretical (experimental) values differ from our calculated data by $\sim +2\%(-17\%)$ and by $+30\%$ for Coronene and Ovalene, respectively. While for the ionization energies we recorded theoretical (experimental) values larger by $+3.2\%$ ($+6\%$) and $+3.6\%(+8\%)$ for Coronene and Ovalene, respectively [93].

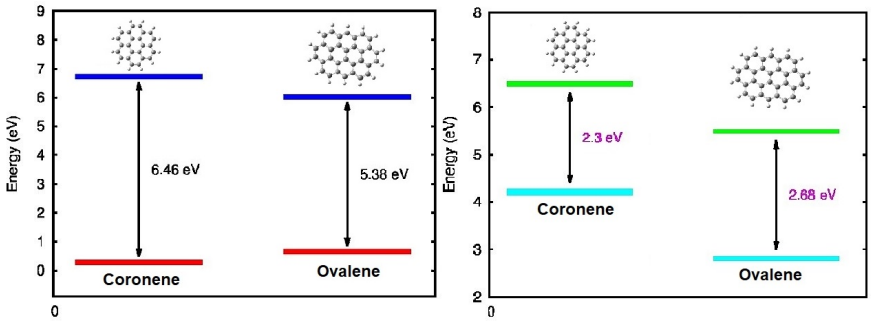

Figure 18: (Left) Vertical electron affinities (red lines), vertical ionization energies (blue lines) and fundamental gaps (black arrows) for Coronene (left) and Ovalene (right). (Right) Fundamental gaps (green lines), optical onsets (light blue lines) and exciton binding energies (black arrows) for Coronene (left) and Ovalene (right).

3.6 OPTICAL PROPERTIES

For the optical absorption of the modified systems we have performed the calculations for all the possible substitutions considered in the present work, but for brevity, we present the results for the selected systems, because of the large number of molecules (all the details can be found in the additional material of Ref. [93]). In what follows we particularly analyze the optical properties only of the modified systems selected with the criterion of the minimum ground-state total energy (see the dedicated subsection "Silicon-atoms substituted configurations"). In particular, our calculated spectra reproduce the absorption cross-section (in arbitrary units [a.u.]) as a function of energy (in [eV].) Fig.19 displays the pure molecules absorption spectra in comparison, while Fig. 20 and 21 show the absorption spectra for Coronene and Ovalene in the visible/near-UV region up to 5.5 eV, as obtained after B3LYP/$6-31G^*$ TDDFT calculations, for each substituted configuration with the corresponding original counterpart.

Tab. 5 reports the wavelengths of the main peaks appearing in the cross-section of Coronene and Ovalene here calculated with the main peak in the experimental absorbance of Graphene after Ref. [146]. While Coronene and Ovalene, can be considered as nanometric portions of infinite Graphene sheets, show spectra with a rich structure of different peaks, the experimental absorbance of Graphene is distinguished by the presence of a single dominant structure, quite broaden, which covers roughly the same wavelength range. In fact, the presence of only one absorption peak, located around 275 nm and the characteristic steep rise for wavelengths shorter than 250 nm, could be observed.

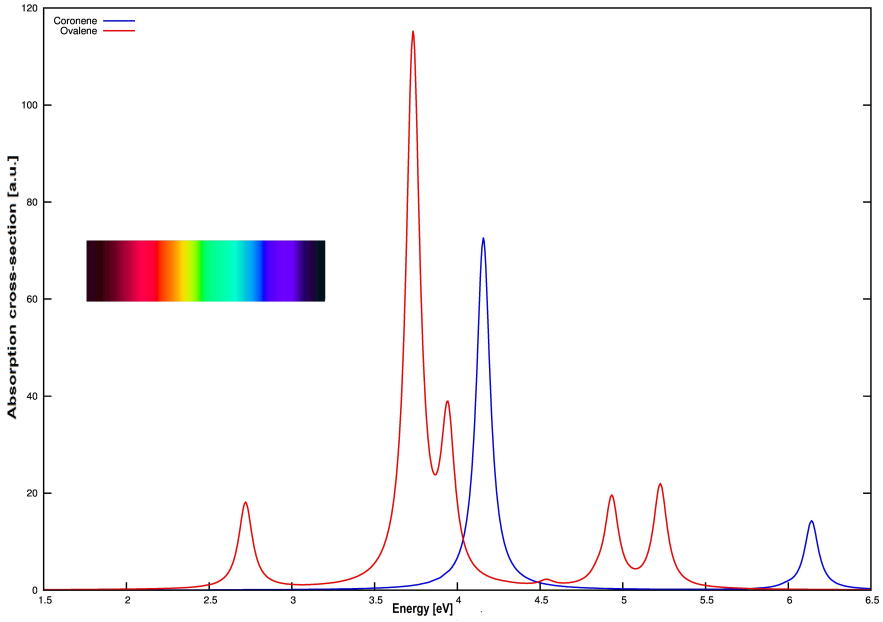

Figure 19: Absorption spectra of Coronene (blue) and Ovalene (red) after present calculations. The visible range is also highlighted. Figure taken from Ref. [93].

Table 5: Dominant peaks positions (in wavelength) in the cross-sections of Coronene and Ovalene, after the here presented calculations as compared to the experimental absorbance peak for Graphene as obtained by Ref. [146].

	λ (nm)
GRAPHENE	275
CORONENE	300
OVALENE	340

On the other hand, both Coronene and Ovalene, present the dominant peak at larger wavelengths, at around 300 and 340 nm. The computed data for the Coronene and Ovalene optical properties and those of their substituted systems are reported in Tab. 6. From these results we noted that a general reduction of the optical onsets (E_{opt}) and of the main peaks between the substituted-systems (for single, dimer and trimer insertions) and their original parent takes place as a function of the number of the inserted Silicon atoms, for both Coronene and Ovalene. In particular, in the case of Coronene (Ovalene) E_{opt} reduction oscillates in the range $27.6 - 37.3\%$ ($7.7 - 17.6\%$) considering the single and the triple Si-atoms substituted configurations. For what concerns the dominant peak position in energy the variation is included in the range of $\sim -7.2 - 6.3\%$ ($-4.3 - 10.8\%$), in

Table 6: Optical onset (E_{opt}), exciton binding energy (E_{bind}) and the energy corresponding to the dominant peak position (D. P. P.) in the absorption spectrum for Coronene and Ovalene substituted molecules (with single (S), dimer (D) and trimer (T) insertions). The percentage deviation has been calculated with respect to each Coronene configurations. All the values are given in eV.

	E_{opt}	E_{bind}	D. P. P.
CORONENE	4.16	2.66	4.16
S	3.01	3.31	3.86
D	2.87	3.19	3.62
T	2.61	3.03	3.48
OVALENE	2.72 (-35%)	2.68(+0.8%)	3.73 (-10%)
S	2.51 (-17%)	2.65(-20%)	3.57 (-8%)
D	2.49 (-13%)	2.64 (-17%)	3.41 (-6%)
T	2.24 (-14%)	2.69(-11%)	3.33 (-4%)

the case of Coronene (Ovalene). Finally, analyzing E_{bind}, for both the molecules deviations take place around $+13.9 - 24.4\%$ for Coronene and $+0.4 - 1.5\%$ for Ovalene, respectively.

More in detail, from Fig. 19, we observed that the absorption spectrum of Coronene is characterized by the presence of two principal peaks: the main one, corresponding to the optical onset (E_{opt}), falls at 4.16 eV and an other transition at 6.14 eV, both in the UV range. On the other hand, in the case of Ovalene, more peaks appear in the same considered range. In particular, E_{opt} of Ovalene is distinguished by the main peak and it is redshifted by 1.44 eV with respect to Coronene E_{opt}, with the main structure placed at 3.73 eV. Therefore, Ovalene starts to absorption in the visible, rather than in the UV, as Coronene. For the modified systems, for all the types of substitutions (single, dimer, trimer ones), we found that the insertion of Silicon atom/s has as general prevailing consequence the redshift of either the optical onsets or the dominant peaks. Hence, the optical absorption range of all the modified compound is redshifted with respect to those of the pure parents with a redistribution of the absorption structures in the UV range. At fixed substitution, the redshift of the absorption spectra, relative to the main peak, either for Coronene and Ovalene is of the order of $\sim$ 10%. In addition, we have also found that in one case of the trimer-substituted clusters, for both Ovalene and Coronene, the absorption edge takes place in the IR (at $\sim$ 1 eV).

The main tendency registered for the substituted molecules spectra is a reduction of the peaks amplitude, combined with a redistribution of the intensity in the considered energy range and a greater

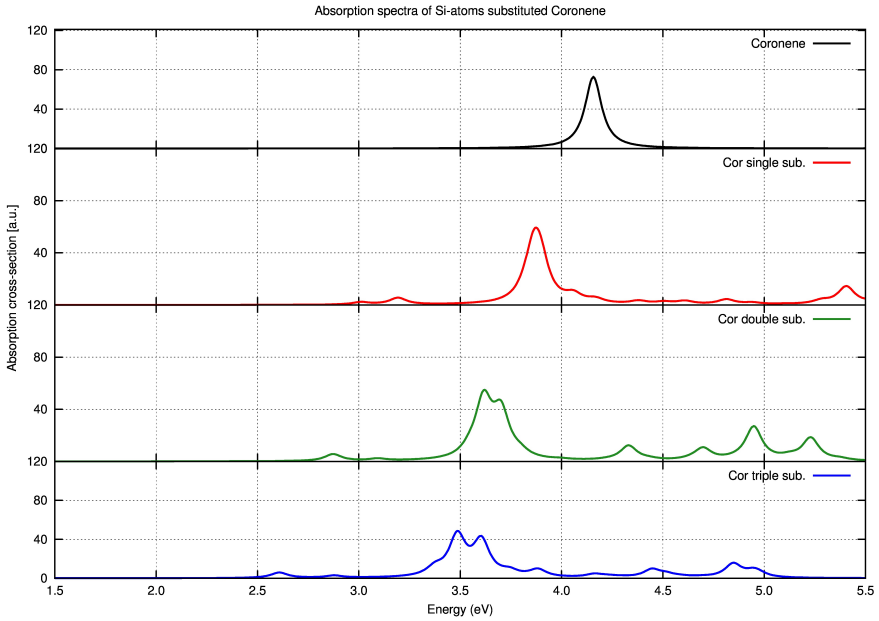

Figure 20: Absorption cross-sections [a.u.] of the selected Coronene substituted systems (with single, double and triple Si-atom insertions) as compared to the corresponding original compound (black curve).

structural richness with respect to the pure systems. The most consistent analogy between Coronene and Ovalene has found to be that all the Si-substituted clusters show optical absorption more focused in the UV, instead of in the visible. Moreover, a meaningful result after Silicon insertions, is represented by a translation of the optical absorption structure for the substituted systems with respect to their pure counterparts towards the visible. In particular, for both substituted Coronenes and Ovalenes, Silicon insertions give rise to a redshift of the absorption onset as predicted by the fundamental gap reduction reported by ΔSCF calculations [21] (see Tab.3).

3.7 FINAL DISCUSSION

We have presented a systematic comparative investigation on the electronic, optical and morphological properties of Coronene and Ovalene molecules in their original and substituted forms (with individual Silicon atoms, Si-dimers and Si-trimers). Concerning the morphological properties, we observed that some trimeric insertions (either for Coronene or Ovalene) are the responsible substitutions which provoke consistent deformations extended in the out-of-plane molecular directions. Other calculations, executed with different substitutional sites, have shown different behaviors in terms of out-of-plane distortions: for example, some peripheral substitutions did not manifest this effect, keeping the planar appearance. We expect that as a func-

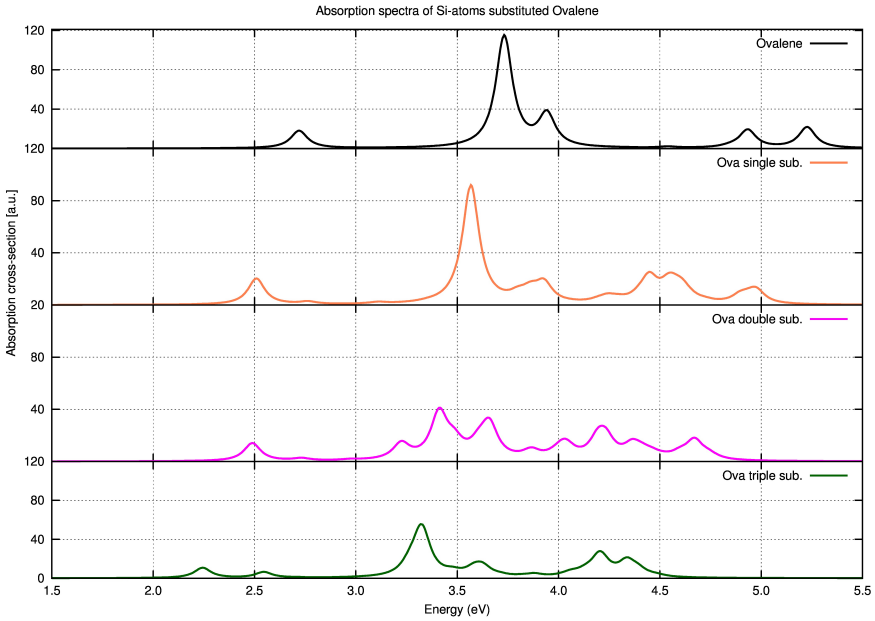

Figure 21: Absorption cross-sections [a.u.] of the selected Ovalene substituted systems (with single, double and triple Si-atom insertions) as compared to the corresponding original compound (black curve).

tion of increasing Si atoms substituted, there would be larger or morphologically different molecular deformations.
We have computed electron affinities, ionization energies, fundamental gaps, optical onset energies and absorption spectra. We have found larger values of the ground-state energies for all the substituted configurations with respect to the original counterparts. In both Coronene and Ovalene, we have ascertained a general reduction of the fundamental gap and optical onset energies as a consequence of the chemical modification.
Dealing with the optical properties, for each type of substitution, the absorption spectra present a redshift of the optical onsets and a remodeling of the main peaks intensity. In addition, in one case of Si-trimer substitution, for both Coronene and Ovalene, the absorption edge takes place in the IR (at $\sim$ 1 eV), rather than the in visible (Ovalene) or in the UV (Coronene).
The here presented evaluation on the Si-atoms substitutions effects on several physical observables, considering the two first members of Circumacenes, could be helpful in the choice of the best substitutional path to be found to enhance specific excitation properties of these molecules for both applications in optoelectronic devices and condensed matter physics fundamental research.

4

ELECTRONIC AND OPTICAL PROPERTIES OF BORON-NITRIDE (BN) CIRCUMACENES

4.1 INTRODUCTION

One of the main properties of PAHs is that they show tunable electronic and optical features and, as compared to polymers, their modification with strong electronegative substituents may be an effective approach for converting p-type organic semiconductors to n-type. Indeed, typically, n-type materials based on PAHs are obtained by the attachment of strong electron withdrawing groups, such as CN, to the conjugated core, or by the peripheral substitutions of hydrogens with halogen atoms (in particular F and Cl), as previous studies show (see Ref. [111]). It has also been established that an efficient strategy for tailoring the electronic, magnetic and physico-chemical properties of Graphene-related materials consists on the controlled introduction of substitutional defects (chemical doping)[108]. Among these compounds, the role played by the Circumacenes (Coronene, Ovalene, Circumanthracene, Circumtetracene, and Circumpentacene are the first five members of the family here analyzed) has recently pointed out, thanks to their promising properties [56, 111], as already mentioned. Moreover, these planar and symmetric molecules could cover a significant position since they can be considered as finite portions (typically with a nanometric size) of Graphene, their infinite counterpart [48]. Beginning with the surge of Graphene and Carbon-based material research, the way in the investigation of other 2D nanomaterials has soon opened: this is the case of the two-dimensional Nitrides (AlN, GaN, InN, TlN..) and in particular, in our case, the 2D Boron-Nitride (BN)[91],[41]. 2D materials over Graphene show several advantages: they show peculiar and versatile physical properties, like tunable band gap or electron conductivity and, for this reason, they can be employed in innovative optoelectronic or FET devices [131]. The BN, compound formed by the union of Boron and Nitrogen atoms in the same amount, presents different crystalline forms, isoelectronic with respect to the elementary Carbon-made structure, among which there are [18, 115]:

- the cubic form (c-BN), analogous of diamond (softer than diamond but with higher chemical and thermal stability);
- the hexagonal form (h-BN), the counterpart of the C-made graphite (this is the most stable and soft form among BN polymorphs);

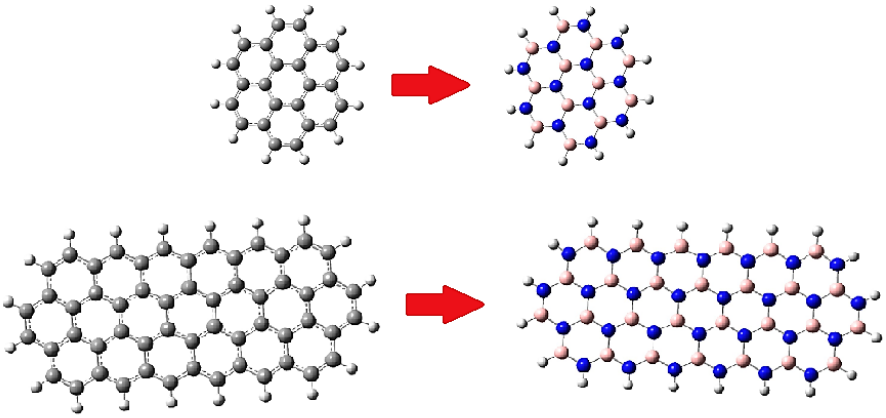

Figure 22: Coronene (up) and Circumpentacene (bottom) molecules and their BN counterparts (right), which are the smallest and the biggest member of the Circumacenes family here considered. C atoms are indicated in gray, H in white, N in blue and B in pink.

Furthermore, the BN compound is also renowned to be one of the most thermally and chemically resistant materials among those actually known [115]. c-BN shares many of its properties, structures, processing and applications with carbon. Its extreme hardness, wide energy band gap, low dielectric constant, and high thermal conductivity are very close to those own of diamond [19]. Nevertheless, despite of these structural analogies among the two species, many differences between the BN-made compounds and the C-based ones also take place, especially from a chemical-physical side. These divergences, manifested through properties own of each of the two materials, are mostly due to the different nature of the chemical bond involved: for example, while graphite is a conductive semi-metal, h-BN is an insulator [134]. However, it is certain that, 2D BN-based nanostructures are believed to be promising candidates for different technologic devices and applications: going from microelectronic devices, wear-resistant lubricants, vacuum technology to deep UV LED, Graphene-engineering, x-ray lithography masks [19]. Finally, their emerging role could open new way into biological and medical fields applications [77]. In this last context, the synthesized BN-nanotubes (BNNTs), were investigated for their potential use as drug and gene transporter in biomedical applications or tissue scaffolds, after the evaluation of their non-toxicity and their biocompatibility [65][34]. In particular, our results concerns the optical properties: we found that the substantial difference between the two families is that the BN molecules absorb in the UV, instead of in the visible as the C-made parents.
In the following discussion we expose a comparative computational

analysis on the electronic and optical properties of some representative BN planar molecules thanks to their attractive properties of interest for potential applications in condensed matter physics [9, 100, 113]. In particular, we have selected the first five members of the Circumacenes family (from Coronene to Circumpentacene (see Fig. 22), studying their BN-made counterparts. Our results with existing previous data from the literature, could have possible implications in different theoretical branches and experimental applications, opening new ways for a better comprehension of the BN clusters properties as compared to their C-made counterparts. Implications on the band-gap and exciton engineering behaviors, for example, could be useful to envision potential new optical applications [96].

This part of the work is contained in a publication under revision (see ...) focused on a systematic comparative study of BN-Circumacenes opto-electronic properties versus their original carbonaceous counterparts.

4.2 COMPUTATIONAL DETAILS

According to recent studies [21, 92–94, 111], we have performed geometric optimizations using a localized gaussian basis-set, $6-31+G^*$, in combination with the hybrid exchange-correlation functional B3LYP [7, 73, 124]. The basis-set is composed by a valence double-ζ set augmented with d polarization functions for each atom (the inclusion of the diffuse functions is indicated by the + sign) [3]. The B3LYP as exchange-correlation potential has been chosen, since, with respect to other possibilities (e.g. the PBE - Perdew-Burke-Ernzerhof [38]), reproduces better results for different clusters of PAHs molecules, for both the ground-state and the excited one, as it has been previously demonstrated[17, 21, 22, 71, 85] and presented in Chapter 3.
Actually, several works shows that even if B3LYP functional has been developed in principle for ground-state calculations, this hybrid functional also (in some limited cases) shows reliable behavior if employed to excited states calculations and yields accurate results in the case of low lying valence excited states of both closed-shell [4] and open-shell species [52, 53]. More precisely for the case of conjugate aromatic molecules the work of Ref. [85] and other papers previously published (see Ref. [21] and Ref. [22]) show a fair comparison between experimental and calculated ($B3LYP/6-31+G^*$ framework) values for electronic properties (e.g electron affinity, first and second ionization energy, QP gaps) and optical properties (optical onset and optical absorption spectra in the range of near IR, visible and near UV). For the above reason we decided to maintain the previous computational framework (basis-set and XC functional) for the calculations of the excited states of the molecules under study.
We performed all the DFT [69] and Time dependet-DFT (TDDFT)

[89] calculations as implemented in the Gaussian16 computational code[44] (an all electrons gaussian-based package). In particular, for the ground-state and the electronic properties (e.g electron affinities, ionization energies and quasi-particle (QP) gaps) the DFT method has been employed, for all the molecules analyzed. Subsequently, we have used the time-dependent DFT to obtain the optical properties (optical onsets, exciton binding energies) and to work out the absorption spectra from the visible up to the UV range (covering the middle ultraviolet (MUV [4.13-6.20 eV]) and far ultraviolet (FUV [6.20-10.16 eV])[70]). In particular, for the computation of the poles of the polarizability function in the frequency domain the Casida computational scheme has been used (these poles correspond to the vertical excitation energies, while their strengths represent the oscillatory strengths [15]).
Finally, we used the ΔSCF scheme[62, 87], through which the vertical electron affinities (EA_V) and ionization energies (IE_V) can be calculated as differences between the ground-state total energy of the neutral system, E_N^0, and the energies of the charged species (the anion E_A^0 and the cation E_C^0, respectively), at the neutral geometry.
According to the ΔSCF method, we can obtain the quasi-particle (QP) gap, as defined by the expression 36. Related to this, from the knowledge of E_{opt}, the first optically active transition from the absorption spectrum, an estimate of the exciton-binding energy could be given through the difference expressed by equation 49 [29, 71]. More in details, we have performed the geometrical optimizations for all the considered structures: for all of them (neutral and ± 1 charged) we used the *Tight* convergence criteria as implemented in Gaussian16 [44]. The numerical values of convergence parameters corresponding to the *Tight* keyword in the package are: *Maximum Force* 0.000015 Ha/Bohr, *RMS Force* 0.000010 Ha/Bohr, *Maximum Displacement* 0.000060 Åand *RMS Displacement* 0.000040 Å. Within TDDFT relatively to the frequency-space implementation, for the absorption spectra, we set the default integration grid of Gaussian16 and the default convergence criteria for the SCF cycles (more precisely these values are 10^{-6} for the energies ΔE_{tot} for each SCF cycle and 10^{-8} for the wavefunctions).

4.3 MORPHOLOGICAL PROPERTIES

Substitutions of carbon (C) with boron (B) and nitrogen (N), neighbors of C in the periodic table, in PAHs and in their functionalized compounds, have attracted a vivid interest for quite some years now. B-N is isoelectronic with C-C, and h-BN has similarities to graphite. B-N replacement of the C-C units in the PAHs, even if does not alter the structural appearance, provokes deep modifications in their chemical and physical properties [12].

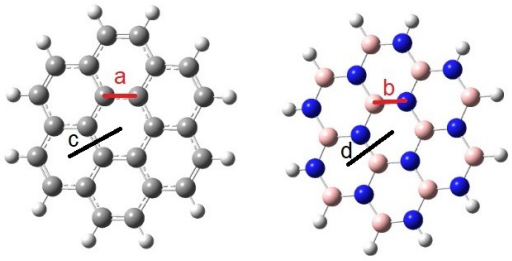

Figure 23: Coronene molecule (left) and BN-Coronene (right). C atoms are represented in gray, H in white, N in blue and B in pink. The distance a (b) connected two C-C (B-N) atoms is also indicated.

Table 7: Calculated interatomic distances (green) in comparison with the data as obtained by Ref. [114] (red). All the values are given in Å.

Molecule	Avg. A-A
C	1.41 1.41
BNC	1.44 1.38

In particular, we focus on the interatomic distances only in the case of the smallest molecules of the cluster: Coronene (C) and BN-Coronene (BNC) (see Fig. 23). After the optimization, we have calculated that the average bond length connected two C-C atoms, in the case of C, is $\bar{a} = 1.41$Å, while in the case of the distance between B-N atoms, for the BNC, the same length has found to be $\bar{b} = 1.44$Å.
The result for the C-made molecule is in accordance with that after Ref. [114] (in red in table), while for the BN-one the percentage deviation is of the order of 4%. We have also calculated the average distance between the two adjacent hexagons centers, indicated, as $\bar{c}$ and $\bar{d}$ for C and BNC, respectively (see Fig. 23). We found $\bar{c} = 2.48$ Åand $\bar{d} = 2.51$ Å, with a deviation of $\sim 1\%$. This fact is in analogy with the slight larger value of the in-plane lattice parameter of the bulk h-BN and that of graphite.
Finally, as previous our studies confirmed (see Ref. [92, 93]), all the molecules under exam preserve the planar appearance typical of the Circumacenes and this fact is valid also for each member of the BN-made family (see Ref. [94] focused on the case of Coronene). On the contrary, other calculations, performed considering Si-atoms substitutions (see Ref. [92, 93] for more details), have shown different behaviors in terms of distortions: some substituted configurations, for example, present large deformations extended in the 'out-of-plane' directions. This phenomenon did not manifested in the case of the BN compounds.

4.4 ELECTRONIC PROPERTIES

In the following discussion, for brevity, the molecules under exam will be indicated respectively by the acronyms in brackets: Coronene (C), Ovalene (O), Circumanthracene (CA), Circumtetracene (CT) and Circumpentacene (CP) and their corresponding Boron-Nitride counterparts by the same acronyms with the suffix "BN". Figs. 24 and 25 show the behavior of the electronic properties (vertical electron affinity (EA_V), vertical ionization energy (IE_V) and quasi-particle energy gap (E_{gap}) as a function of the molecular size for each family and respectively for the Circumacenes and their BN counterparts, as obtained after DFT calculations.

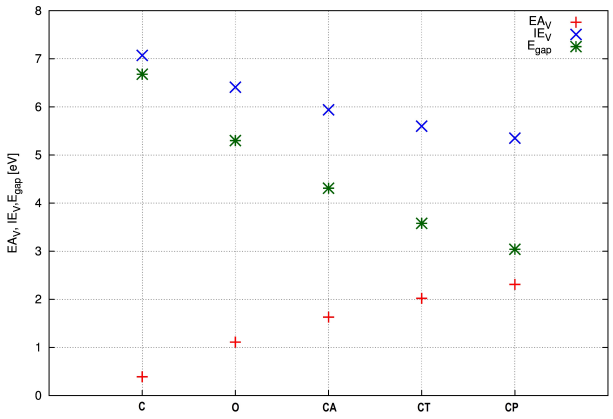

Figure 24: Computed electronic properties as a function of size for Circumacenes: vertical electron affinity (EA_V), vertical ionization energy (IE_V) and QP energy gap (E_{gap}). All data are reported in eV in Tab.8.

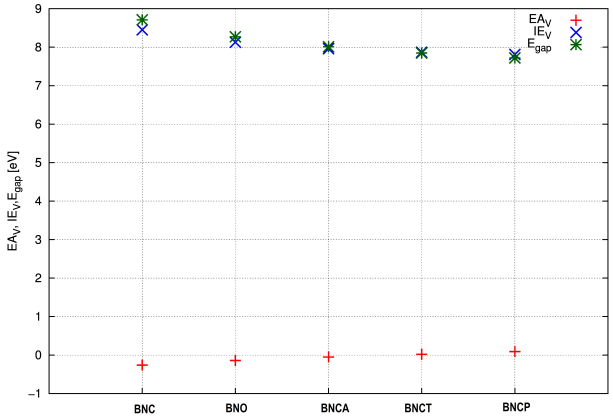

Figure 25: Computed electronic properties as a function of size for BN-Circumacenes: vertical electron affinity (EA_V), vertical ionization energy (IE_V) and QP energy gap (E_{gap}). All data are reported in eV in Tab. 8.

The same computed data are reported in Tab. 8, in which the deviation for each observable has been calculated with respect to the corresponding C-made parent. We firstly propose a description on the behavior of the electronic properties analyzed, separately, family by family, followed by a final comparison between the two species. From Fig. 24 we noted that an increase of EA_V, a decrease of IE_V and a consequent reduction of E_{gap}, take place as the molecular size rises. This trend for each electronic observable is similar in the case of the BN-made family, but with the difference that the deviations as a function of the molecular size are strongly reduced: in fact, as shown in Fig. 25 the trends of the points simulate curves almost flat as the molecular dimension increases. To show a comparative depiction about the size effects on the electronic properties, Fig. 26 presents the behavior of the above mentioned observables (EA_V, IE_V and E_{gap}) through a level representation, analyzing the smallest and the largest molecule of the two species (C vs BNC and CP vs BNCP, respectively). From C (BNC) to CP (BNCP), we observe a rise of the vertical affinity, a decrease of the ionization energy and a consequent lowering of the QP gap.

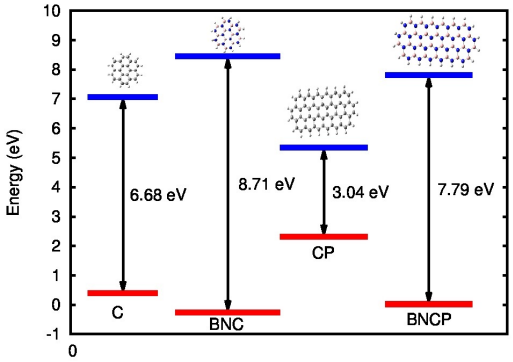

Figure 26: Vertical electron affinities (red lines), vertical ionization energies (blue lines) and fundamental gaps (black arrows) for C, BNC, CP and BNCP, from left to right, respectively.

These effects are lightly higher in the C-made family, considering that the percentage variation, going from C to CP, are $\sim +500\%$, -24% and -54% for EA_V, IE_V and E_{gap}vertical electron affinity, respectively. In the case of BN compounds, for the same observables, we found (going from BNC to BNCP) percentage deviations of the order of $\sim +135\%$, -7% and -11%. Passing from a C-made molecule to its corresponding BN-made counterpart, we found a general reduction of EA_V and a rise of IE_V and the E_{gap}, while an increase of IE_V and E_{gap} has been observed from the original Circumacenes to their BN analogues. In particular, in the case of the C-made family, we observed that EA_V presents always positive values, while for the BN-made counterparts this observable shows a change in the sign occurring inside the family. In fact, the first three molecules (BNC, BNO

Table 8: Vertical electron affinity (EA_V), vertical ionization energy (IE_V) and fundamental gap (E_{gap}) for C, O, CA, CT and CP molecules and their corresponding BN-made counterparts (BNC, BNO, BNCA, BNCT and BNCP). The (%) variation of each observable is computed with respect to the original C-made molecule. All the values are given in eV.

Molecule	EA_V	IE_V	E_{gap}
C	0.39	7.07	6.68
BNC	-0.26 (-167%)	8.45 (+19.5%)	8.71 (+30.4%)
O	1.11	6.41	5.30
BNO	-0.14 (-112%)	8.13 (+26.8%)	8.27(+56%)
CA	1.63	5.94	4.31
BNCA	-0.05 (-103%)	7.96 (+34%)	8.01 (+85.8%)
CT	2.02	5.60	3.58
BNCT	0.02 (-99%)	7.87 (+40.5%)	7.85 (+119%)
CP	2.31	5.35	3.04
BNCP	0.09 (-96%)	7.81 (+45.9%)	7.72 (+154%)

and BNCA) have a negative vertical electron affinity (in any case these last values are, however, close to zero), while BNCT and BNCP report positive values.
In general, the stability of either the neutrals or the anions increases with the dimension of the molecule: the only exceptions are the anions of BNC, BNO and BNCA, whose ground-state energies are lower with respect to those of the neutrals (for more details see the *Appendixl*). For what concerns IE_V, for both the families, this physical observable show a monotone decreasing trend as the molecular size increases. The effect of the trends for the ionization potential and the electron affinity cause a reduction of the QP-gap with respect to the rise of the cluster size. The other important point is that, considering the fixed dimension, in the passage from the carbonaceous to the BN-made molecules, a large increase of the QP gap takes place: e.g. going from CP to BNCP the QP-gap is more than doubled.

4.5 OPTICAL PROPERTIES

Figs. 27 and 28 display the optical absorption spectra for the Circumacenes and their BN-made counterparts, respectively, as obtained after TD-DFT calculations. The above mentioned spectra have been purposely represented with different x-ranges since the two families present a different absorption range: in particular, the absorption of

the Circumacenes takes place from the IR to the UV (~1-7 eV), while in the case of the BN-family it is shifted towards the UV region from 5 up to ~ 9eV. Figs. 29 and 30 show the optical properties (main peak position (M.P.), optical onset (E_{opt}) and exciton-binding energy (E_{bind}) as a function of the molecular size for each family and respectively for the Circumacenes and their Boron-Nitride counterparts, as obtained after TDDFT calculations. The same computed data are shown in details in Tab. 9, in which the deviation for each observable has been calculated with respect to the original corresponding C-made molecules. Similarly to the previous section, firstly, we propose a description of the observed trend for each family a part, followed by a comparison between the two species analyzed. From Fig. 27 a general redshift of the optical onsets takes place as a function of the molecular size (from 4.09 eV (C) to 1.18 eV (CP)) can be observed. The absorption concerns part of the visible and the UV range. The dominant peaks in the onset region are located in the range 2.87-4.09 eV with a trend that follows the molecular size. A similar behavior has been noted for the optical onsets and the exciton-binding energies (see Fig. 29). Moreover, a monotonous trend can be found also for the exciton-binding energies, as the molecular dimension increases, that oscillates between 1.86-2.61 eV, following the cluster size (see Fig. 29). Please, consider that only in the case of C E_{bind} has been calculated with respect to the first root of the absorption spectra (with O.S. smaller than 10^{-4}) for the sake of consistency with the trend found for also for the other member of the family.

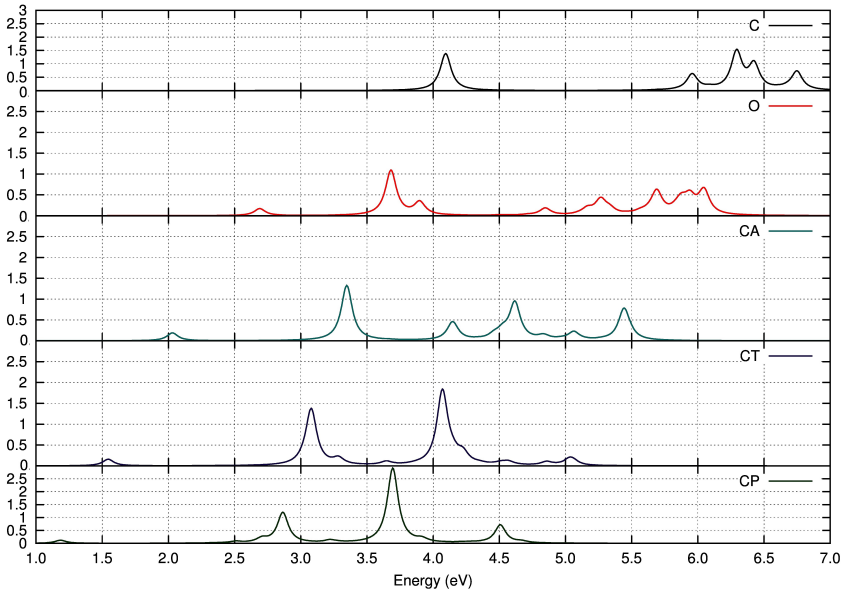

Figure 27: Absorption spectra (absorption cross-section [a.u.] as a function of energy [eV]) for the Circumacenes (from Coronene to Circumpentacene from top to bottom, respectively).

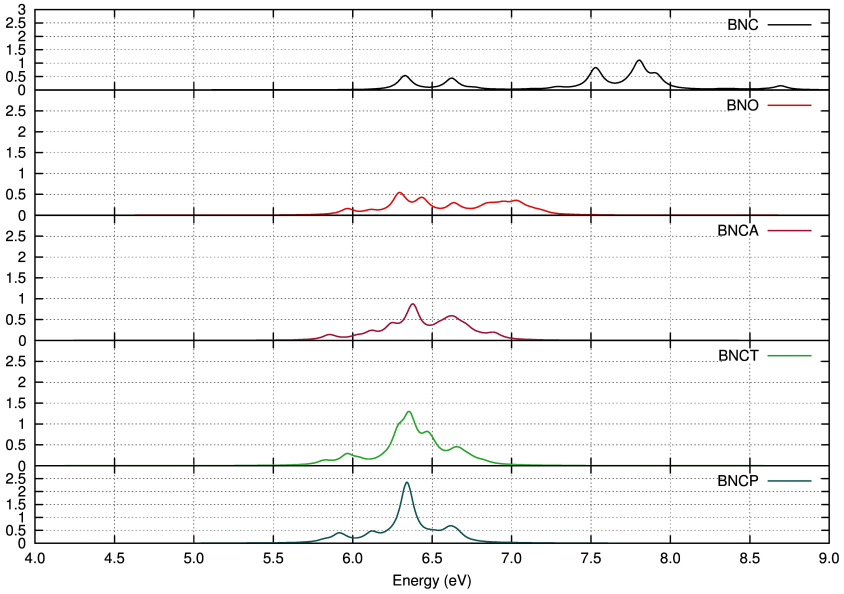

Figure 28: Absorption spectra (absorption cross-section [a.u.] as a function of energy [eV]) for the Boron-Nitride-made Circumacenes (from BN-Coronene to BN-Circumpentacene from top to bottom, respectively).

For the BN-clusters from Fig.28 and Tab. 9 we found that a general redshift of the optical onsets takes place as a function of the system size (from 6.22 eV (BNC) to 5.82 eV (BNCP)), with small variations dependently on the cluster size. The main peaks in the onset region are nearly localized around 6.4 eV. No BN-made molecule here studied absorb in the visible range: the absorption takes place in the UV. For the exciton-binding energies a reduction takes place as a function of the molecular size (going from 2.49 eV to 1.9 eV) (see Fig. 30) as verified for the C-made parents.

Going from C-made molecule to its corresponding BN-one, we observe a blueshift of the dominant peaks and the optical onsets (see Tab.9 and Fig. 27 and Fig. 28). In the case of the exciton-binding energy we confirm the decrease previously encountered for the C-made family, but with a minor slope. (see Tab. 9 and Fig. 30).
Concerning the dominant peaks, while for the BN-made molecules the position in energy of the main peak at the onset is almost fixed, for the C-made original parents a redshift, from the smallest (C) to the largest member (CP), takes place. Regarding the optical onsets, both the families are characterized by an homogeneous redshift as a function of the molecular size. On the contrary, dealing with the exciton-binding energies, a general decrease as the molecular dimension increases takes place in both the species.

As in the previous section, we propose a comparative analysis of the optical properties through a graphical depiction for the size effects, presenting the results for C to CP on one side and BNC and

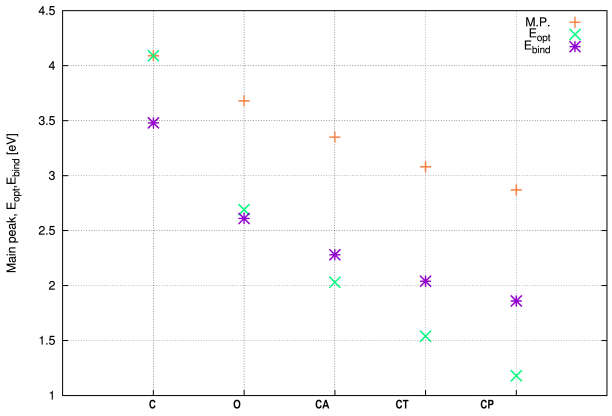

Figure 29: Computed optical properties as a function of size for Circumacenes. From top to bottom: energy relative to the main peak (M.P.), optical onset (E_{opt}) and exciton binding-energy (E_{bind}). All data are reported in eV in Tab.9.

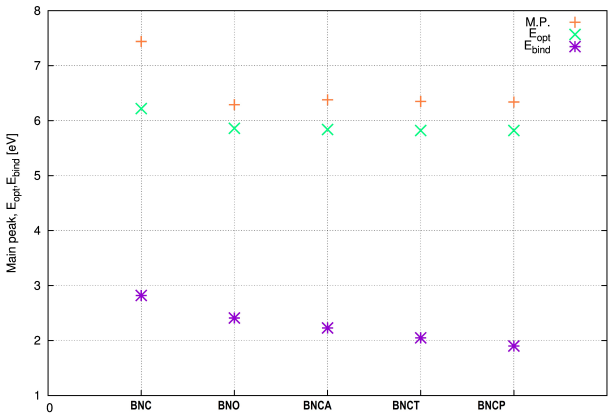

Figure 30: Computed optical properties as a function of size for BN-made Circumacenes. From top to bottom: energy relative to the main peak (M.P.), optical onset (E_{opt}) and exciton binding-energy (E_{bind}). All data are reported in eV in Tab. 9.

BNCP on the other (see Fig. 31). Passing from the smallest molecule C (BNC) to the largest one CP (BNCP), there is a lowering of the QP gap, a redshift of the optical onset and a reduction of the exciton-binding energy. The effect is slightly stronger in the C-made family, since the percentage decrease going from C to CP are $\sim -54\%$, -71% and -28% for the QP gap, E_{opt} and E_{bind}, respectively. For the same observables, we found in the case of the BN-made counterparts, going from BNC to BNCP, a deviation of the order of $\sim -11\%$, $+6\%$ and -24%, for the fundamental gap, the optical onset and the exciton binding-energy, respectively. Concerning the optical behavior comparison between the two species, the main results may be summarized as follows:

Table 9: Energies relative to the main peak position at the onset region (M.P.O.), optical onset (E_{opt}) and exciton-binding energy (E_{bind}) for C, O, CA, CT and CP molecules and their corresponding BN-made counterparts (BNC, BNO, BNCA, BNCT and BNCP). The (%) variation of each observable is computed with respect to the original C-made molecule. All the values are given in eV.

Molecule	M.P.O.	E_{opt}	E_{bind}
C	4.09	4.09	2.59
BNC	7.44 (+82%)	6.22 (+52%)	2.49 (-4%)
O	3.68	2.69	2.61
BNO	6.29 (+70.9%)	5.86 (+117.8%)	2.41 (-8%)
CA	3.35	2.03	2.28
BNCA	6.38 (+90.4%)	5.84 (+187%)	2.23 (-3%)
CT	3.08	1.54	2.04
BNCT	6.35 (+106.2%)	5.82 (+278%)	2.05 (–)
CP	2.87	1.18	1.86
BNCP	6.34 (+121.7%)	5.82 (+393%)	1.9 (+2%)

- The systems here analyzed are characterized by very different optical absorption structures, as observed in their spectra (see Figs. 27 and 28);
- while the C-based molecules spectra present a well definite dominant peak, roughly localized at the threshold of the visible, followed by some secondary peaks of minor amplitude, the BN-made compounds show spectra with a quite broaden absorption structure, located in a more restricted energy range.
- while in the case of the Circumacenes the absorption takes place in range that includes the IR, the visible and a portion of UV (1-7 eV), the BN-made counterparts present a characteristic absorption spectrum limited in the UV (5-9 eV).

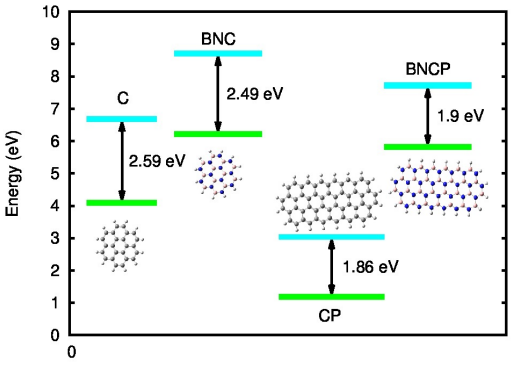

Figure 31: Fundamental gaps (light-blue lines), optical onsets (green lines) and exciton binding energies (black arrows) for C, BNC, CP and BNCP, from left to right, respectively.

4.5.1 *HOMO-LUMO levels*

In several situations in which the molecules are studied or used, e.g. optical or transport applications, one may be interested in a detailed knowledge of the charge spatial distribution for states around the gap: e.g. the HOMO and the LUMO states. Figs. 32 and 33 give a pictorial representation of the HOMO and LUMO states, as obtained after TDDFT calculations. Because of the large number of molecules involved in this systematic study, we only report the smallest and the largest molecule for each family, that is C and CP and their BN-made analogues. The plots represent the wave function of the charge density relative to the frontiers molecular orbitals (FMOs): HOMO is the acronym for the "highest occupied molecular orbital", while LUMO indicates the "lower unoccupied molecular orbital". These electronic levels are significant for both the establishment of the chemical bond and for the spectroscopic response.

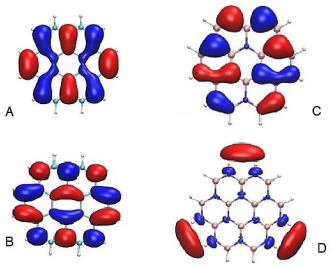

Figure 32: HOMO-LUMO states representation for Coronene and BN-Coronene. A and C indicate the two HOMO levels, while B and D refer to the LUMO ones, for the C-made and the BN-made molecules, respectively.

From Fig.32 we observe that passing from the C-made molecule to the BN-made one the shape of the wave function completely changes

for the LUMO level. In this last case, the LUMO level of BNC (D) present a redistribution of the charge density, which tend to be equal to zero in the innermost molecular areas, joining towards the peripheral ones. A similar behavior for the largest molecule takes place with a drastic change of the wave function's shape (see Fig. 33 B and D), characterized by a charge density accumulation on a side of the system. The FMOs figures show that the HOMO and LUMO are delocalized over the entire molecule in all the cases, while for the BNC (see D Fig. 32) and BNCP (see Fig. 33) the LUMO are localized on the edge atoms. We have found that our calculated isosurfaces of the C and BNC as shown in Fig.32 result in accordance with the data available from the literature, as obtained by Ref. [114] and [107]. In particular, we verified that our results are in agreement with respect to the HOMO and LUMO states representation for the BNC as presented in Ref. [114], despite of the slight difference in the computational details. It is clear from Figs.32 and 33 that the charge density distribution, either for the HOMO and LUMO states, differs in shape and symmetry going from C to BNC and from CP to BNCP. This occurrence could be the origin of the different nature of the optical onset transition in the BN clusters (H $\rightarrow$ L+1,2,3 transitions) with respect to their carbonaceous counterparts (H $\rightarrow$ L transitions). This fact is probably due to the more ionic nature of the BN structures as compared to the original C-based compounds. Moreover, as predicted in Ref. [114] the larger extent of orbital delocalization at the peripheral rings could have repercussions on the electronic gap, implicating its reduction.

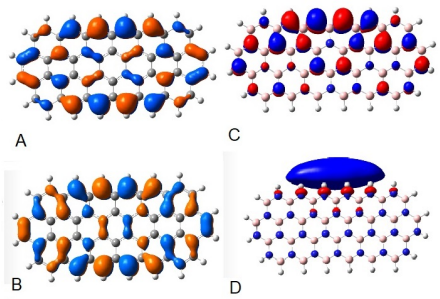

Figure 33: HOMO-LUMO states representation for Circumpentacene and BN-Circumpentacene. A and C indicate the two HOMO levels, while B and D refer to the LUMO ones, for the C-made and the BN-made molecules, respectively.

4.6 PERFLUORINATION EFFECT: THE CASE OF CORONENE

In the present section we have selected the Coronene molecule and its BN-made counterpart to study the effect provoked by the presence of halogen atoms (Fluorine, in this case) on the electronic and optical properties [1]. This part of the work has been the object of one of our previous published paper (see Ref. [94] for more details).

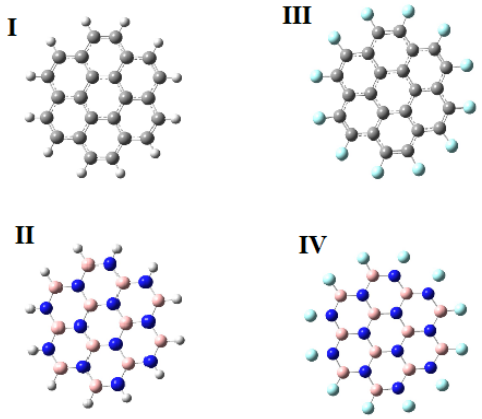

Figure 34: Coronene molecule (I) in its BN (II), perfluorinanted (III) and perfluorineted-BN-made (IV) counterparts. C atoms are indicated in grey, H in white, F in light-blue, N in blue and B in pink.

4.6.1 *Electronic Properties after Perfluorination*

In the following discussion, the analyzed molecules will be indicated by the acronyms in brackets, respectively: Coronene (C), BN-Coronene (BNC) and the two perfluorinated-species are denoted by the suffix "p". Tab. 10 presents the computed data of the electronic properties for all the molecules under study. For each observable the percentage variation, calculated with respect to the original parent (C), has been reported in brackets. Vertical electron affinity (EA_V), vertical ionization energy (IE_V) and fundamental gap (E_{gap}) are shown in Fig.35 (A) through a diagrammatic representation.

In the following lines, we have decided to focus in details in a comparative description on the electronic properties behavior, analyzing, in particular, what happens switching from C to BNC and from BNC to p-BNC. Considering the vertical electron affinity, going from C to BNC, a decrease nearly ∼-170% takes place. On the other hand, the perfluorination effect in BNC determines a large rise (of the order of +200%) of the same observable. On the contrary, for the vertical ion-

1 The perfluorination corresponds to the total substitution of H atoms with F atoms in the peripheral molecular areas. A similar analysis has been made by Ref. [72].

Table 10: Vertical electron affinity (EA_V), vertical ionization energy (IE_V) and fundamental gap (E_{gap}) for C, BNC, p-C and p-BNC. The (%) variation of each observable is computed with respect to the original C-made molecule (C). All the values are given in eV.

Molecule	EA_V	IE_V	E_{gap}
C	0.39	7.07	6.68
BNC	-0.26 (-167%)	8.45 (+19.5%)	8.71 (+30.4%)
p-C	1.77 (+354%)	8.25 (+16.7%)	6.49 (-2.8%)
p-BNC	0.35 (-10.3%)	9.68 (+36.9%)	9.33 (+39.7%)

ization energy, from C to its BN-counterpart, we have registered an increase of about 20%. For this observable, the presence of Fluorine (F) atoms produced a rise of similar entity in p-BNC (of about 15%), as compared to the corresponding original parent (BNC). For what concerns the fundamental gap, we observed an increase of ~ +30% from C to BNC. In this case, for p-BNC the QP gap increases of ~+7% with respect to its original analogue (BNC). The transition from the C-made molecule to the BN-made one provokes a lowering in EA_V, an increase of IE_V and a consequent rise of E_{gap}.The perfluorination effect, going to BNC to p-BNC, induces a general raise of all the above mentioned observables.

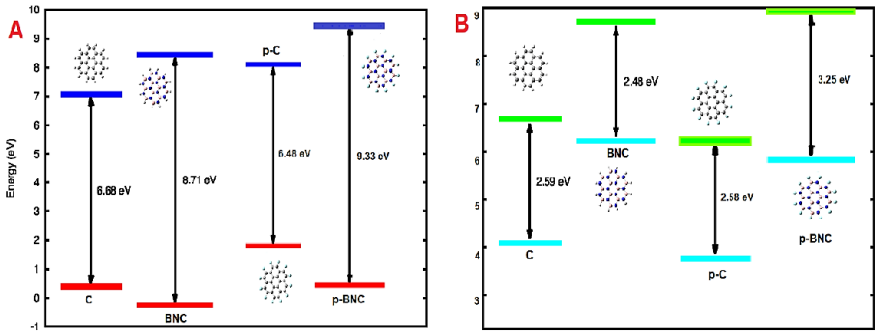

Figure 35: (A)Vertical electron affinities (red lines), vertical ionization energies (blue lines) and fundamental gaps (black arrows) for C, BNC, p-C and p-BNC, from left to right, respectively.
(B) Fundamental gaps (green lines), optical onsets (light-blue lines) and exciton binding energies (black arrows) for C, BNC, p-C and p-BNC, from left to right, respectively.

4.6.2 *Optical Properties after Perfluorination*

Tab. 11 reports the results for the optical properties, as obtained after TDDFT calculations, while Fig. 35 (B) shows the trend of some of the

Table 11: Energies relative to the main peak position (M.P.P.), optical onset (E_{opt}) and exciton-binding energy (E_{bind}) for C, BNC, p-C and p-BNC. The % variation of each observable is calculated with respect to the original C-made parent molecule. All values are given in eV.

Molecule	M.P.P.	E_{opt}	E_{bind}
C	4.09	4.09	2.59
BNC	7.44 (+82%)	6.22 (+52%)	2.49 (-4%)
p-C	6.44 (+57%)	3.91 (-4%)	2.59 (-)
p-BNC	6.38 (+56%)	6.07 (+48%)	3.26 (+26%)

previous observables through a diagrammatic representation. Also in this case, we focus in details on the comparison between C and BNC and BNC and p-BNC.

From the computed data, we noted that both the main peak and the optical onset of BNC are blueshifted of ~80% and ~ 50%, respectively, as compared to those of C. For what concerns the perfluorination effect, the presence of F-atoms implicates a redshift of the optical onset and the dominant peak in the p-BNC with respect to BNC and respectively of the order of 2% and 14%.

Regarding the exciton-binding energy, this observable remains almost constant from a molecule to the following one: in particular, a negligible reduction (~ 4%) from C to BNC takes place, while a rise of ~ 26% is determined as a consequence of the perfluorination in BNC.

Moreover, from Fig. 36 the optical onsets of the BNC and p-BNC are blueshifted with respect to their C-made original parents: the absorption is mainly shifted towards the UV region. The typical absorption structure of the C-based material, characterized by a peak close to 4 eV, in the BN-made molecules spectra is absent and a redistribution of the intensity at higher energies takes place. In the BN-system the presence of F-atom, produces a redshift for both the main peak (from 7.44 to 6.38 eV) and for the optical onset (6.22 from to 6.07 eV), as previously discussed.

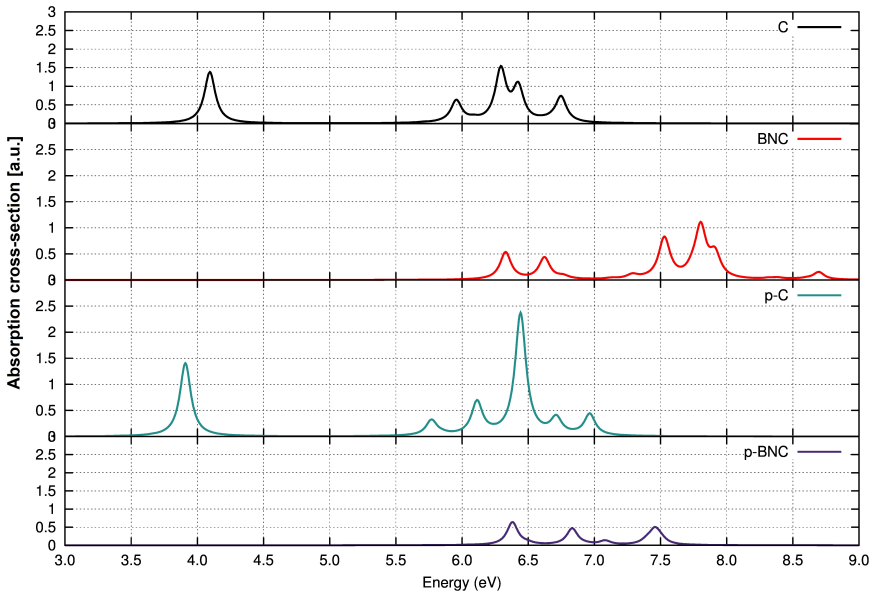

Figure 36: Absorption spectra (absorption cross-section [a.u.] vs energy [eV]) for C, BNC, p-C and p- BNC, from the top to the bottom, respectively.

4.7 FINAL DISCUSSION

We have presented a comparative study of Circumacenes and their BN analogues in the context of DFT and TDDFT methods. Dealing with the electronic properties, we have found that a lowering of the vertical electron affinities and a rise of either the ionization energies or QP gaps take place passing from the C-made to the BN-based systems.
Dealing with the morphological properties, we confirmed that all the BN molecules maintain a planar appearance, feature typical of the Circumacenes. For what concerns the optical properties, we observed that the absorption is localized in the UV for all the BN-based molecules, unlike their C-made parents which present absorption spectra located in the visible range aside for Coronene. We have verified a blueshift of the optical onsets and the dominant peaks for the BN-made molecules with respect to the original C-made parents.
Moreover, the perfluorination effect, here analyzed in the particular example only for the smallest member of the family, has similar behavior either for the Carbon or the BN compounds. Since one of the aim of this work is to give a contribution to improve the microscopic understanding of optoelectronic properties of novel 2D materials, a quantitative comparison of these Circumacenes compounds, could offer the possibility to predict new properties, through an approach based on ab-initio simulations.The tunable electronic and optical properties make these BN-nanostructures as promising candi-

dates for different technological devices, complementary but also innovative with respect to the successful Carbon-based counterpart.In particular, thanks to their UV-absorption feature here analysed, these BN nanomaterials keep a promising role in the technology linked to UV optoelectronics, beyond Graphene applications.One of the most relevant result in the present work is that the electronic observables and optical properties (e.g. ionization potentials or optical onset energies) of the BN Circumacenes here studied show slight dependence from the cluster size. This occurrence is in contrast with the results obtained for their Carbon counterpart, which, on the contrary, are strongly related to the molecular size. This fact could have important consequences on the strategies of choice of the best cluster for suitable application goals or devices.

5

C/SI/GE LINEAR CLUSTERS

5.1 INTRODUCTION

Since 2004 the discovery and the synthesis of Graphene [48] has opened the way to the new 2D-materials generation: its exotic and peculiar properties leads to the further exploration of its silicon-made and germanium-made counterparts (Silicene, Germanene)[60]. In fact, germanium, silicon and carbon are very similar, since all three IV group elements [1], even if each of them is characterized by its own significant peculiarities. For example, in their infinite structural appearance, unlike Graphene, the presence of buckling in Silicene and Germanene provides an added advantage for them to be integrated with substrates [60]. Secondly, because of the larger atomic number of Ge and Si as compared to C, these materials present a stronger spin–orbit coupling, which imply that also a small buckling may increase the spin–orbit coupling by orders of magnitude [1]. However, these materials exhibit favorable mechanical, electronic and optical properties (resistence, flexibility, planar feature, thermal nature, chemical response...)[90] so much to become ideal systems as for fundamental research and promising candidates for nanoelectronic applications [63].
Furthermore, in the optoelectronic context the position occupied by the linear acenes, compounds composed of laterally fused benzene rings [37] and the polyciclic aromatic hydrocarbons (PAHs), a large class of conjugated π—electron systems [85], should be considered since they are usually used, both in their crystalline and thin-film state, as active elements in many diverse optoelectronic devices, spacing from solar arrays, light emitting diodes (LEDs), flexible and trasparent displays to liquid crystals and organic thin-film field-effect transitors. In addition, these systems are of great importance and wide interest in several research field, ranging from astrochemistry to condensed matter physics and material science [86].
These molecules are here analyzed to be nanometric portions of their infinite counterparts, in their C-Si-Ge made shapes. In the present work, we consider the Si and Ge-made analogues of the carbon linear acenes clusters (e.g. Benzene, Naphtalene, Anthracene, Tetracene, Pentacene and Hexacene, see Fig. 37) up to the sixth member of each family, in order to explore the different behavior switching from C to Si and Ge, as compared to the passage from Graphene to Silicene and Germanene. We present a comparative computational investigation on the morphological, electronic and optical properties of the each

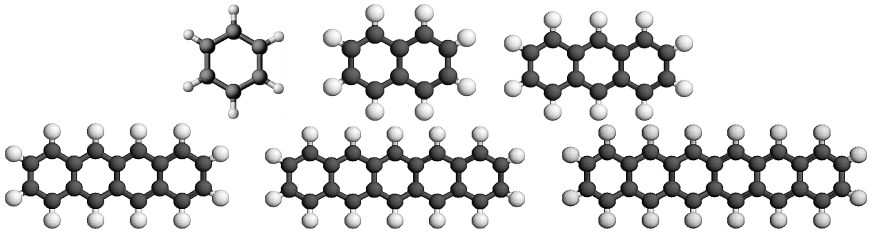

Figure 37: The linear Acenes family $C_{4n+2}H_{2n+4}$, with $n = 1, .., 6$ (Benzene, Naphthalene, Anthracene, Tetracene, Pentacene and Hexacene). C atoms are indicated in grey, while H atoms are in white.

above mentioned systems, analyzing the possible similarities and the differences existing between the various families and the trend characteristic of each cluster as a function of the molecular size.

5.2 COMPUTATIONAL DETAILS

For the ground/excited-state and optical absorption we used the same DFT and TDDFT as described in chapter 2.Geometry optimizations have been executed in this case using the B3PW91 hybrid exchange-correlation functional [7, 73, 138], combined with the TZVP basis-set, triple-zeta valence basis-sets that results in the extended set plus one set of d-functions on the heavy atoms and one set of p-functions on hydrogen from [36, 116, 117]. Previous DFT calculations at this level (B3PW91/TZVP) have demonstrated that this scheme produced best results showing, for example, that the puckering distortion of silicenes is preserved with the increasing molecular size [36, 95].
Finally, a possible link with the results of theoretical and experimental previous works could be proposed. In all the cases, structural optimizations have been obtained imposing tight convergence criteria. The minimum-energy configurations of Si and Ge species were found not to preserve the planar geometry of their parent original C-made molecules, from the first member of the family.

5.3 MORPHOLOGICAL PROPERTIES

In this section, we present an evaluation on the morphological effects linked to the change of the atomic type, going from C to Si to up to Ge, in the same molecular structures. What we have found, in fact, is that in Si and Ge-made clusters, considerable "out-of-plane" deformations take place, for all the considered molecules. On the other hand, in the C-made clusters, the planar appearance is preserved in all the six systems. The entity of the distortions in the Si/Ge-made clusters could be expressed in terms of the variation of the "out-of-plane" quota (that is the coordinate perpendicular to the molecular

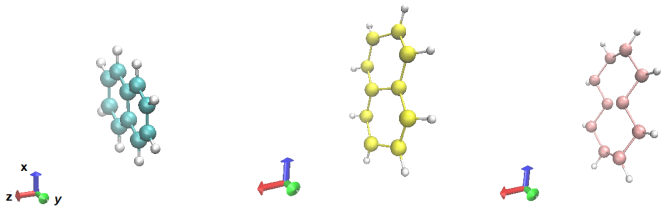

Figure 38: $C_{10}H_8$, $Si_{10}H_8$ and $Ge_{10}H_8$ from left ro right, respectively. C atoms are indicated in light-blue, Si atoms are in yellow, Ge atoms are in pink and H in white.

plane in the reference molecular system, which differs from one system to an other one, after the optimization), analyzing the optimized geometries derived from the DFT ground-state calculations. We have given an estimate on the average deviation from the out-of-plane direction for each cluster, considering the C, Si and Ge atoms and not the H peripheral atoms, and making a comparison among the different families. For what concerns the Linear Acenes clusters, we have found that globally each member of the family does not present deformations in the out-of-plane direction, maintaining a global flatness along the quota. As expected, this fact is confirmed by the literature (see Ref.[37]).

Considering, the silicene clusters, we have found that distortions (see Fig. 38) take place from the first family member, with a deviation of about 0.195 Åalong the z axis. The maximum deviation is, in this case, obtained for the 2^{nd}-molecule (with 2 rings), with a corresponding deviation of $\sim$ 0.1972 Å, in absolute value. On the average, as the molecular size increases, from 1 to 6 rings, the deviation is of the order of 0.1961 Å. Finally, for the germanene clusters, we have recorded that, also in this case, similarly to the Si-made molecules, distortions along the out-of-plane direction take place:the maximum deviation has been registered for the 1^{th} member of the family, with a deviation of $\sim$ 0.3161 Å. The average deviation along the out-of-plane direction in germanene clusters is of $\sim$ 0.307 Å. The Ge-made clusters show greatest distorsions in the out-of-plane direction, as compared to the Si-made and C-made ones.
All the data relative to the deviation along the out-of -plane directions (expressed in Å), for each member of each family (indicated by numbers form 1 to 6, that follow the rings numeration) are reported in Tab. 12. We do not report the data concering the C-made family since the deviation along the z axis are close to 0 ($\sim 10^{-4}$ Å) from the smallest to the largest molecular system.

As an illustrative example Fig.38 presents the 2 rings member for each cluster ($C_{10}H_8$, $Si_{10}H_8$ and $Ge_{10}H_8$, from left ro right, respectively) The C-made cluster maintains the planar geometry typical of

Table 12: Average deviations (expressed in Å) along the $\perp$-axis (with respect to the plane), quota corresponding to the out-of-plane direction, with respect to the reference molecular system, for the C-Si-Ge-made clusters (see Fig. 38). Each molecule is labeled by a number from 1 to 6, corresponing to the number of rings that composed each system.

Number of Rings	Si	Ge
1	0.1952	0.3161
2	0.1972	0.3127
3	0.1968	0.3081
4	0.1960	0.3044
5	0.1953	0.3015
6	0.1964	0.2993

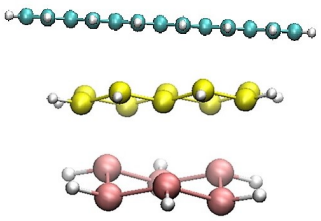

Figure 39: Lateral views of $C_{26}H_{16}$, $Si_{10}H_8$ and Ge_6H_6, from top to bottom, respectively. C atoms are in light-blue, Si in yellow, Ge in pink and H peripheral atoms in white.

the family: on the contrary, distrorsions in the out-of-plane directions are evident from the second molecule, for both the silicene and germanene clusters. Previous studies (e.g. see Ref [92] and Chapter 3), focused on Silicon insertions into C-made matrix, show that deformations of the original structure could take place after the substitutions of Silicon into a Carbon-based material. Fig. 39 shows the lateral views for $C_{26}H_{16}$, $Si_{18}H_{12}$ and $Ge_{14}H_{10}$: while in the C-made family even the largest member ($C_{26}H_{16}$) preserves the planar feature, typical of these compounds, in Si-made and Ge-made analogues the flatness is lost. $Si_{10}H_8$ (2^{nd} molecule) and Ge_6H_6 (1^{st} molecule) are shown as examples to present the largest distortions along the perpendicular axis with respect to the reference molecular system, as compared to the largest C-made molecule.

These results could be compared with the theoretical ones, present in the literature (see Tab. 13), obtained for the corresponding infinite systems (Graphene, Silicene and Germanene), through the evaluation of the "buckling amplitude", parameter which estimates the average

distortion into a solid medium, as calculated by Ref. [91]. Multiplying our calculated values by a factor of 2, we could make a comparison with the data for the corresponding infinite systems from Ref. [91], finding an average buckling of 0.39 Å(0.61 Å) for Silicon (Germanium). The percentage deviation with respect of the printout previous results (see Tab. 13) are of the order of 13 % (11%) in the case of Silicene (Germanene) cluster.

Table 13: Buckling amplitude (Δ) in Åcalculated for the infinite 2D systems (Graphene, Silicene and Germanene) as obtained by Ref. [91].

	C	**Si**	**Ge**
Δ (Å)	0.00	0.45	0.69

In any case, the sheet buckling in Silicene and Germanene exhibits strong deviations from the sp^2 hybridization of planar Graphene towards an sp^3 hybridization similarly to bulk Si and Ge crystallizing in diamond structure. Deviations from the planar geometry and sp^2 bonding are usually important for avoiding a metallic character of the 2D honeycomb crystals, in particular in the Ge case. Nevertheless, despite the buckling, the π and σ bands remain decoupled in Silicene and Germanene for symmetry reasons with the resulting gap to be zero as for Graphene [91].

Comparing Tab.12 and Tab. 13, we note that in the case of finite clusters deviations for planar geometry are always limited with respect to the infinite 2D systems.

5.4 ELECTRONIC PROPERTIES

Figures 40, 41 and 42 show the observables EA_v, IE_v and E_{gap} as a function of the number of rings for the C-Si-Ge linear acenes clusters, respectively.

For all the species, indipendently by the constituent atom, IE_v (EA_V) is found to decrease (increase) at increasing molecular size. Concerning the C-made family we noted that as the molecular size increases, EA_v rises (assuming negative values for the first two members of the family), while IE_v and E_{gap} tend to decrease. For the Si-made cluster, EA_v presents always positive values, showing an increase as a function of the molecular size. IE_v and E_{gap} have a reduction going from the smallest to the largest structure. Also for the Ge-based clusters we have registered that a rise of the EA_v is accompained with a decrease of both IE_v and E_{gap} as a function of the molecular size. The percentage deviations, calculated with respect the first-family member, are more pronounced for the electron affinities (from +76% to +209% for C-made clusters, from +65% to +170% for Si-made clusters and

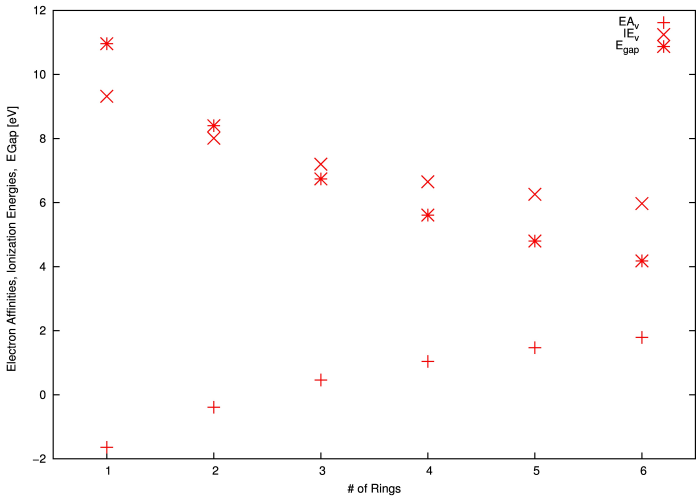

Figure 40: Computed electronic properties as a function of Linear Carbon Acenes size. Vertical electron affiniy (EA_V), vertical ionization energy (IE_V) and fundamental gap E_{gap}.

from +49% to +128% for Ge-made clusters) than the ionizations energies (from −14% to −36% for C-made clusters, from −9% to −23% for Si-made clusters and from −9% to −22% for Ge-made clusters). In particular, in the case of the IE_v the deviation range are similar passing from carbon, to silicon up to germanium.

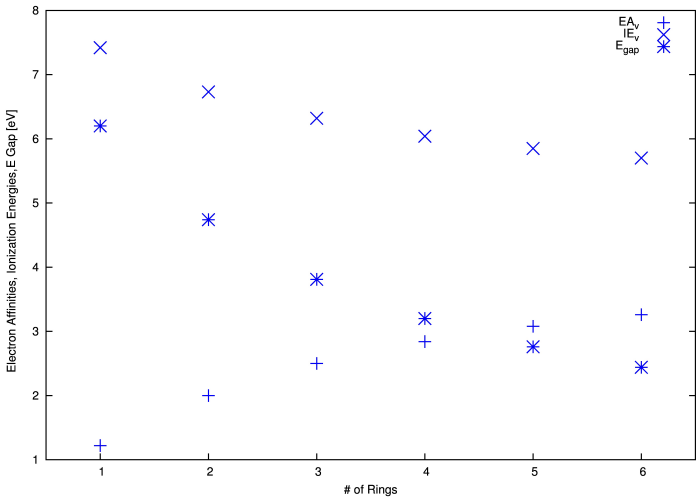

Figure 41: Computed electronic properties as a function of the Silicene cluster size. Vertical electron affiniy (EA_V), vertical ionization energy (IE_V) and fundamental gap E_{gap}.

Moreover, for the E_{gap} we only observed a similar trend: the reduction range is of the same order of magnitude in all the cases (from −62% to −23% for C-made clusters, from −61% to −23% for Si-made clusters and from −59% to −24% for Ge-made clusters). Analyzing these observed behaviors of the electronic properties we should conclude with the following statements:

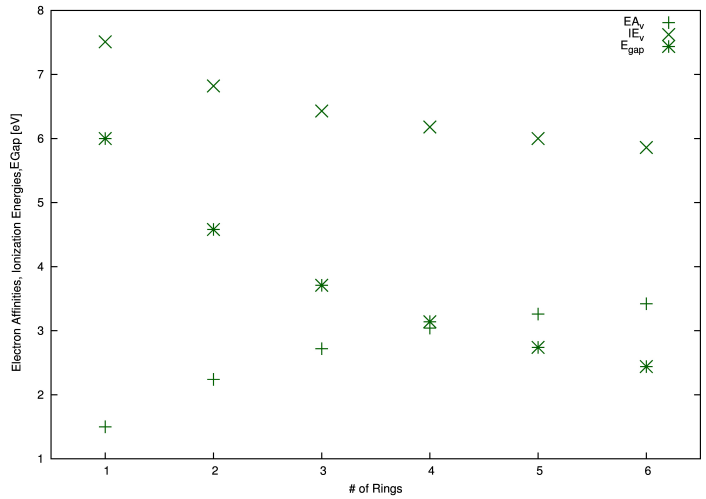

Figure 42: Computed electronic properties as a function of the Germanene cluster size. Vertical electron affiniy (EA_V), vertical ionization energy (IE_V) and fundamental gap E_{gap}.

- the rise of EA_v as a function of the molecular size implies a gain in terms of energy stability of the systems, since the number of electron involved in the molecular stucture grows;
- the decrease of IE_v, on the other hand, means that it is easier the estraction of electrons from the molecules as the dimension increases;
- the reduction of E_{gap} as the number of rings increases in the molecular structure is reflected in a lowering of the optical gap of the material (e.g. in the case of C, this is true for graphite, that is a zero band gap material).

5.5 OPTICAL PROPERTIES

For the optical absorption we have reported all the data, representing for each molecular family the corresponding spectra as obtained after TDDFT calculations and the details of the transitions in the following dedicated section. Figures 43, 44 and 45 show the absorption spectra for all the molecules considered. Firstly, we describe, separately, the observed trends for each family and then the global behavior, analyzing the possible similarities and differences among the atomic species considered. Tables 14, 15 and 16 report the optical onset and dominant peaks energies for all the systems considered.

From Fig.43, in the case of C linear acenes, we noted that as the number of the molecular rings increases, both the optical onsets and the main peaks are redshifted (for the first and the second system the onset and the dominant peak correspond). The absorption is extended in the visible range up to the UV (3-7.5 eV). The main peaks

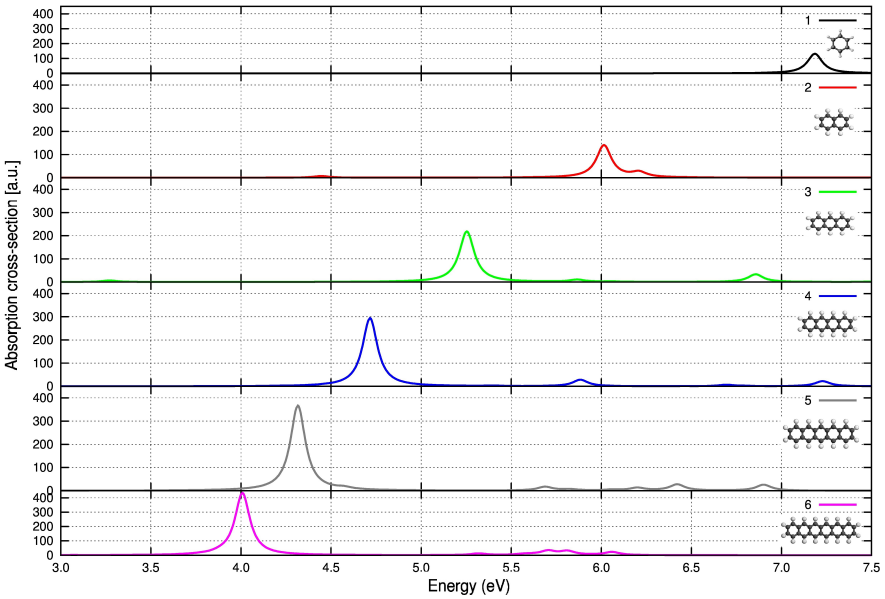

Figure 43: Absorption cross-section [a.u.] vs energy [eV] for the linear acenes cluster $C_{4n+2}H_{2n+4}$ ($n = 1, ..., 6$), from top to bottom, respectively.

amplitude increases as a function of the molecular size. The spectra do not show rich absorption structures, but they are caracterized by a single dominant peak and a series (2 or 3) of secondary structures with decreasing intensities, localized at higher energies.

Table 14: Energies relative to the optical onset (E_{opt}) and the main peak (M.P.) in the absorption spectrum for $C_{4n+2}H_{2n+4}$ ($n = 1, .., 6$). The percentage deviation, with respect to C_6H_6, is also reported.All the energies are reported in eV.

$C_{4n+2}H_{2n+4}$	E_{opt}	M. P.
1	7.18	7.18
2	4.44 (-16%)	6.01 (-16%)
3	3.27 (-54%)	5.25 (-27%)
4	2.49 (-65%)	4.72 (-34%)
5	1.93 (-73%)	4.32 (-39%)
6	1.53 (-79%)	4.01 (-44%)

From Tab. 14 we found that the optical onset redshifts by $10 - 80\%$ the value relative to the smallest cluster between. Similarly, for what concerns the main peaks, the redshift deviation oscillates between $10 - 80\%$.

From Fig. 44, also in the case of Si clusters, we have observed that as the molecular size increases, both the onset and the dominant peaks show a general redshfit. The absorption takes place between the IR and the UV (1-6.5 eV). The main peaks amplitude raises as a function of the number rings which constitute the molecules. The absorption spectra do not present variegated or rich absorption figures and they are characterized by the presence of an individual dominant peak and a series of some secondary peaks with lower amplitude, localized at higher energies.

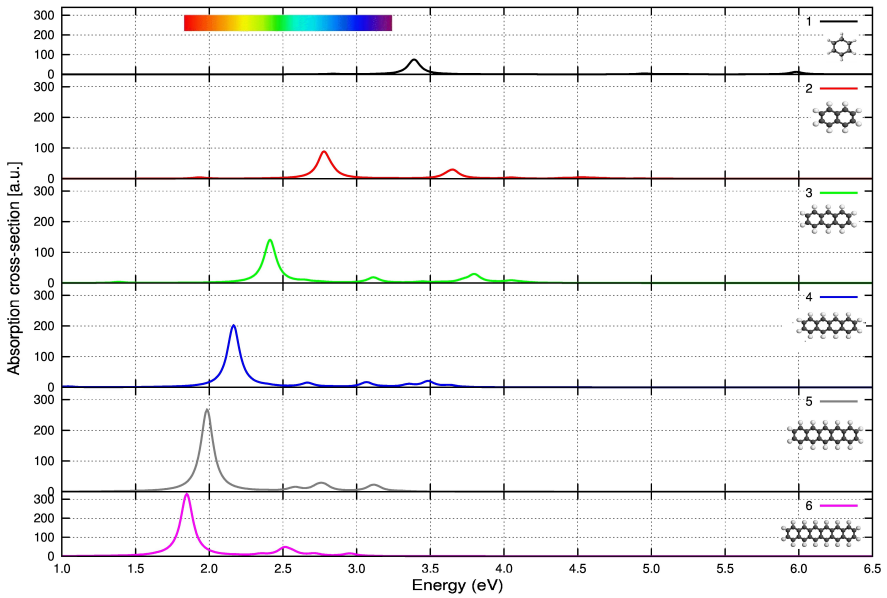

Figure 44: Absorption cross-section [a.u.] vs energy [eV] for the silicene cluster family $Si_{4n+2}H_{2n+4}$ ($n = 1, ..., 6$) from top to bottom, respectively. The visible range is also highlighted.

Considering the increase in the number of rings, the optical onsets redshift (see Tab. 15) in the range $\sim 30-80\%$, similar to the case of C-clusters, while the redshift range for the main peaks spaces from $\sim 20-50\%$ (values reduced with respect to the C-made linear acenes).

From Fig. 45 also for the Ge clusters, as the rings number increases in the molecular structure, both the optical onset and the main peaks are redshifted. The absorption ranges over the IR to the near UV (in the range $\sim$ 1-4 eV). The dominant peaks amplitude show an amplification as a function of the molecular dimensions. The absorption spectra are characterized by the presence of a single main peak and a group (2 or 3) secondary peaks of lower amplitude, localized at higher energies, as in the two previous cases.

From Tab.16 we have recorded that the redshift percentage range for the optical onset in germanene clusters oscillates between $30-75\%$. In the case of the dominant peak the redshift deviation is in-

Table 15: Energies relative to the optical onset (E_{opt}) and the main peak (M.P.) in the absorption spectrum for $Si_{4n+2}H_{2n+4}$ ($n = 1,..,6$). The percentage deviation, with respect to Si_6H_6, is also reported. All the energies are reported in eV.

$Si_{4n+2}H_{2n+4}$	E_{opt}	M.P.
1	2.84	3.39
2	1.93 (-32%)	2.78 (-18%)
3	1.39 (-51%)	2.41 (-29%)
4	1.04 (-63%)	2.16 (-36%)
5	0.81 (-71%)	1.98 (-41%)
6	0.64 (-77%)	1.85(-45%)

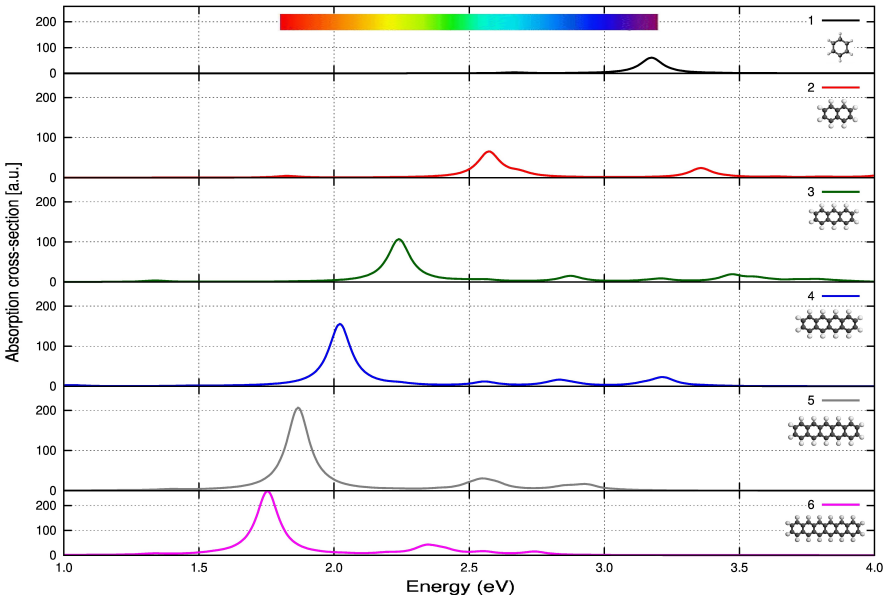

Figure 45: Absorption cross-section [a.u.] vs energy [eV] for germanene cluster family $Ge_{4n+2}H_{2n+4}$ ($n = 1, ..., 6$), from top to bottom, respectively. The visible range is also highlighted.

Table 16: Energies realtive to the optical onset (E_{opt}) and the main peak (M.P.) in the absorption spectrum for $Ge_{4n+2}H_{2n+4}(n = 1,..,6)$. The percentage deviation, with respect to Ge_6H_6, is also reported. All the energies are reported in eV.

$Ge_{4n+2}H_{2n+4}$	E_{opt}	M.P.
1	2.66	3.17
2	1.82 (-31%)	2.57 (-19%)
3	1.34 (-50%)	2.24 (-29%)
4	1.03 (-61%)	2.02 (-36%)
5	0.82 (-69%)	1.87 (-41%)
6	0.67 (-75%)	1.74 (-45%)

cluded in the range $20-45\%$. Also in this case the range is limited as compared to the linear acenes and the silicene clusters.

Therefore, the main trend, occuring in all the three families, is a redshift of the optical onsets and the dominant peaks as a function of the molecular dimension, going from the first to the last structure. Following the rise of the molecular size also the main peak amplitudes increase and this fact is valid for each cluster, due to the larger numbers of electrons at disposition for the optical transitions. Secondly, at fixed size of the cluster (going from to C-Si-Ge clusters), increasing the atomic type, the absorption moves toward lower energies. Considering the main absorption structure Carbon clusters are characterized by the more extended absorption range (about 3.5 eV), with respect to that of Si acenes ($\sim$ 2.7 eV) and that of the Ge clusters ($\sim$ 2 eV) (see Figs. 43, 44 and 45.) Moreover, an other point concerning the optical properties is that, while for all the members of C-linear acenes the absorption spectrum lies in the UV, for Si and Ge linear clusters, aside from Si_6H_6 and Ge_6H_6, all the other members do absorb in the visible. This is an important finding with respect to possible optical applications.

Within our scheme we are able also to estimate the exciton binding energy. In Tab. 17 the exciton binding energies relative to each cluster is reported. This observable is one of the key parameters that govern the optical absorption in many opto-electronic devices [81]. These data are also shown in Fig. 46 which presents the behavoir of E_{bind} for each family, in different colors (red=C, blue=Si, green=Ge clusters), as a function of the molecular size. Firstly, concerning the Carbon linear acenes, there is a decrease of E_{bind} as a function of the molecular size. The reduction oscillates between ~ -44 and -16%

Table 17: Exciton binding energies(E_{bind}) for $C_{4n+2}H_{2n+4}$, $Si_{4n+2}H_{2n+4}$ and $Ge_{4n+2}H_{2n+4}$ molecules, with $n = 1, ..., 6$, from left to right, respectively. The percentage deviation, going from the smallest member of each family to each other one, is also reported. All values are given in eV.

Exciton binding energy			
	$C_{4n+2}H_{2n+4}$	$Si_{4n+2}H_{2n+4}$	$Ge_{4n+2}H_{2n+4}$
1	3.78	3.36	3.34
2	3.96 (+4.7%)	2.81 (-16.4%)	2.76 (-17.4%)
3	3.47 (-8.2%)	2.42 (-27.9%)	2.37 (-29%)
4	3.12 (-17.5%)	2.16 (-35.6%)	2.11 (-36.8%)
5	2.87 (-24%)	1.95 (-41.9%)	1.92 (-42.5%)
6	2.65 (-29.9%)	1.8 (-46.4%)	1.77 (-47%)

with respect to E_{bind} for the smallest cluster [1] Analyzing the case of the Si-made molecules, a general reduction of the exciton binding energy takes place, from the smallest to the largest member and the deviation range is included between ~ -46 and -16%. A similar behavior has been verified also for the Ge-made linear clusters, in which we observe a lowering of E_{bind} as the molecular size increases, with a deviation range oscillating between ~ -47 -and -17%. We should conclude stating that a general decrease of the exciton binding energy takes place as a function of the molecular size, in all the three families. This fact could be ascribed to the decrease of confinement effects and a reduction of the screening as the molecular size increases [81]. While the Si/Ge-based clusters present the same variation range, the C-made family shows a slighlty smaller deviation range of the exciton binding energies.

5.5.1 *Details of optical transitions: α, β peaks and p band*

This subsection is dedicated to present other details linked to the optical transitions, after TDDFT calculations, making a comparison with previous results found in the literature (see Ref. [138] and Ref. [83]). We here compare our results to those from those of the above publications referred to C/Si Linear Acenes with n=1,..,6. The three principal spectral features in the absorption spectra, α, β and p-bands for

1 Please consider that (for the sake of consistency), we use for the calculation of the E_{bind} only for benzene as optical onset, the second root in the absorption spectrum as found also for the other single ring clusters. Even if this transition in benzene results of small oscillatory strength. This fact is also related to the lowering of the symmetry of the molecule going from benzene (D_{6H}) to the Si/Ge single ring cluster (D_{3D}).

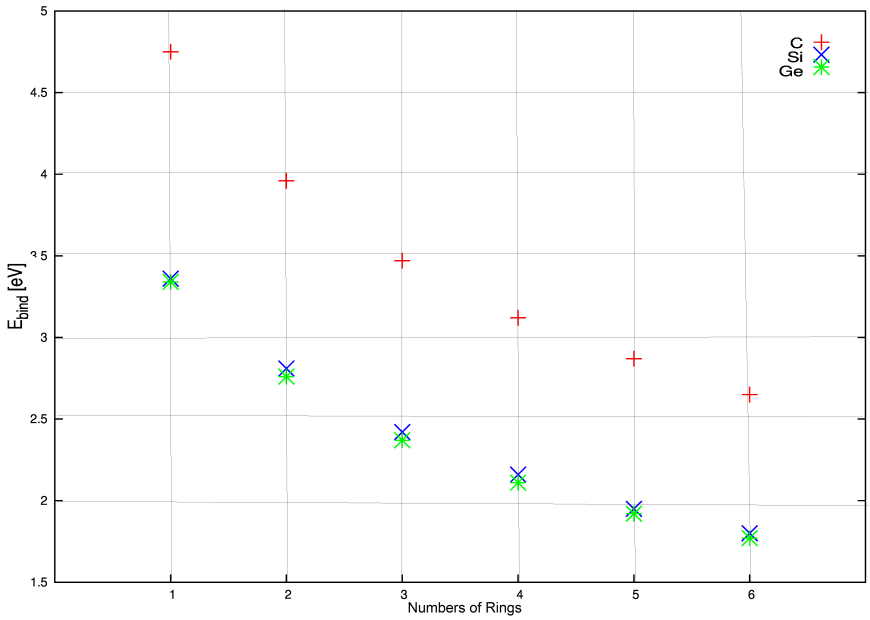

Figure 46: Exciton binding energy (E_{bind}) values as a function of the molecular size, for C/Si/Ge-made linear clusters in red, blue and green, respectively.

C-made linear acenes [83], could be found also in the case of silicene clusters. The α and β peaks arise from the same transition polarized along the long axis of the molecule. In particular, the β peak corresponds to the main peak of the absorption spectrum, while the α peak corresponds to a transition with lower oscillator strength (often this peak is not observable in the absorption spectrum because of its negligible oscillator strength [138]). On the other hand, the p-band is originated by the transition polarized along the short axis of the molecule and corresponds to the optical onset of the absorption spectrum. In the C linear acenes, the β peak is found to fall in the UV region, while the α and p-bands are in the visible range, with characteristic lower oscillator strengths [138]. The slight deviation could be ascribed to the differences in the computational scheme and the code used. A detailed comparison for the C-made clusters with previous results by Ref. [83] available from the 2^{nd} member of the family is reported in Tabs. 18, 19 and 20, since the excited state symmetries of the first molecule could not be determined.

All the data are in a good agreement with the tabulated ones, except for the β peak belonging to the largest member of the family (see Tab. 19), that according to Ref. [83] is not identifiable. In particular, we have found that our data differ from the tabulated ones, on the average, of $\sim 2\%, 3\%$ and 2%, respectively for the α, β peaks and p-band. For the Carbon linear acenes we have registered that as a function of the molecular size the peaks tend to redshift, showing greater oscillator strengths, with increasing dimension of the cluster.

Table 18: Excitation energies, oscillatory strenghts (O.S.), transitions and associate weights corresponding to the α peaks of Carbon linear acenes (in red the results as obtained by Ref. [83]).

$C_{4n+2}H_{2n+4}$	α (eV)	O.S.	Transition
2	4.52 4.44	0.001 <0.001	H→ L+1 (0.25)
3	3.91 3.85	0.0002 <0.001	H-1 → L (0.25)
4	3.52 3.47	0.0014 0.002	H-2 → L (0.27)
5	3.26 3.21	0.0041 0.005	H-2→ L (0.27)
6	3.07 3.02	0.0087 0.01	H-2 → L (0.27)

Table 19: Excitation energies, oscillatory strenghts (O.S.), transitions and associate weights corresponding to the β peaks of Carbon linear acenes (the results as obtained by Ref. [83] are presented in red).

$C_{4n+2}H_{2n+4}$	β (eV)	O.S.	Transition
2	6.01 5.85	1.27 1.26	H-1 → L (0.25)
3	5.25 5.14	1.98 1.99	H → L+1 (0.26)
4	4.72 4.62	2.68 2.69	H → L+2 (0.26)
5	4.32 4.24	3.34 3.35	H → L+3 (0.27)
6	4.01 -	3.95 -	H → L+3 (0.28)

Table 20: Excitation energies, oscillatory strenghts (O.S.), transitions and associate weights corresponding to the p band of Carbon linear acenes (the results as obtained by Ref. [83] are presented in red).

$C_{4n+2}H_{2n+4}$	p-band (eV)	O.S.	Transition
2	4.44 4.36	0.06 0.061	H → L (0.47)
3	3.27 3.21	0.06 0.058	H → L (0.49)
4	2.49 2.45	0.05 0.049	H →L (0.50)
5	1.93 1.91	0.04 0.041	H → L (0.50)
6	1.53 1.51	0.03 0.034	H → L (0.50)

It is important to find possible corresponding features for Si-made clusters typical of the C-made analogues. A similar comparison can be proposed only partially for the Silicon-made clusters. In particular, a brief discussion on the p-band of the polysilo-acenes is difficult, as verified by Ref. [138], who observed a close analogy analyzing just the case of $Si_{10}H_8$ and $C_{10}H_8$.

About that, we report only the complete comparable results with the data found in literature (see Ref.[138]) for the α and β peaks (this last corresponding to the dominant peak of the absorption spectrum). Tabs. 21 and 22 report our results for the silicene cluster as compared from those available from literature (previous results are shown in blue).

Table 21: Excitation energies, oscillatory strenghts (O.S.), transitions and associate weights corresponding to the α peaks of buckled polysilo-acene (in blue the results as obtained by ref. [138]).

$Si_{4n+2}H_{2n+4}$	α(eV)	O.S.	Transition
2	1.98 1.79	0.0001 >0.0001	H→ L+1 (0.25)
3	1.71 1.52	>0.0001 0.0003	H-1 → L (0.25)
4	1.54 1.35	0.0002 0.0018	H-2 →L (0.25)
5	1.43 1.24	0.0011 0.0048	H-2 → L(0.25)
6	1.35 1.16	0.003 0.0099	H-3→ L (0.25)

Table 22: Excitation energies, oscillatory strenghts (O.S.), involved transitions and associate weights corresponding to the β peaks of buckled polysilo-acene (in blue the results as obtained by ref. [138]).

$Si_{4n+2}H_{2n+4}$	β(eV)	O.S.	Transition
2	2.78 2.56	0.76 0.549	H-1 → L (0.25)
3	2.41 2.18	1.27 0.942	H → L+1 (0.25)
4	2.16 1.92	1.83 1.16	H →L+2 (0.26)
5	1.98 1.71	2.41 1.27	H → L+2 (0.27)
6	1.85 1.56	2.98 1.30	H → L+2 (0.27)

A satisfactory agreement with the tabulated data can be found also in this case, confirming that, despite the different computational framework, the results are consitent, especially for what concerns the α peaks. In this case, our calculated data differ from those coming by the literature of average values of 2% and 12%, respectively for the α and β peaks.
Similarly to the C-made linear acenes, we noted that both the α and

β peaks also in the case of Silicene clusters are redshifted as a function of the molecular size with increasing values of the amplitude. For what concerns the Ge-made clusters we have not found in the literature the same feature typical of the C-based counterpart and partially found in Silicon-based cluster spectra. Therefore, this is the first systematic study of these Ge-made cluster (as far as we know). We propose a similar study, showing our calculated data, considering the same feature in the Ge-made clusters. We only report the values for the presumed α peaks (see Tab. 23), since those relative to the β peaks (main peaks) and the p-band (optical onset) have been treated in the dedicated section (see section 5.5). Also in this last case the main peaks positions are redshifted as the molecular size increases, showing growing values of the oscillator strengths.

Table 23: Excitation energies, oscillatory strenghts (O.S.), transitions and weights, corresponding to the α peaks of the Germanene cluster.

$Ge_{4n+2}H_{2n+4}$	α(eV)	O.S.	Transition
2	1.87	<0.0001	H→ L+1 (0.25)
3	1.63	0.0013	H-1 → L (0.26)
4	1.49	0.006	H-2 →L (0.26)
5	1.39	0.017	H-2 → L(0.27)
6	1.33	0.035	H-3→ L (0.29)

The general trend, after the present outcomes, is that the α peak is located in all the cases at lower energies with respect to the β one, even if it has the same symmetry and it is characterized by a lower value of the oscillatory strength. Moreover, the characteristic spectral features of linear acenes can be also found in the Si/Ge-made linear clusters.

In Fig.47 the wavelength of the β peaks, the strangest structure in the absoprtion spectra of the clusters under study, as a function of the length of the clusters, i.e. the number hexagonal rings, has been reported. In Tab. 24 it has been also reported the straight line fitting the data after the present simulations with the corresponding formula. For all the families here studied a linear relationship between the β peak positions and the length of the Carbon linear acenes, silicene and germanene clusters may be observed.

In the case of the Si-made clusters, the depicted results are in fair agreement with those after Dimuthu *e*t al. in Ref. [138], for the case of the buckled polysilo-acenes. In the case of the Si-made clusters and Ge-made ones, the fitting lines show almost the same slope with the peak positions for the Si clusters positioned at lower wavelength with respect to the Germanium ones. On the other hand, the posi-

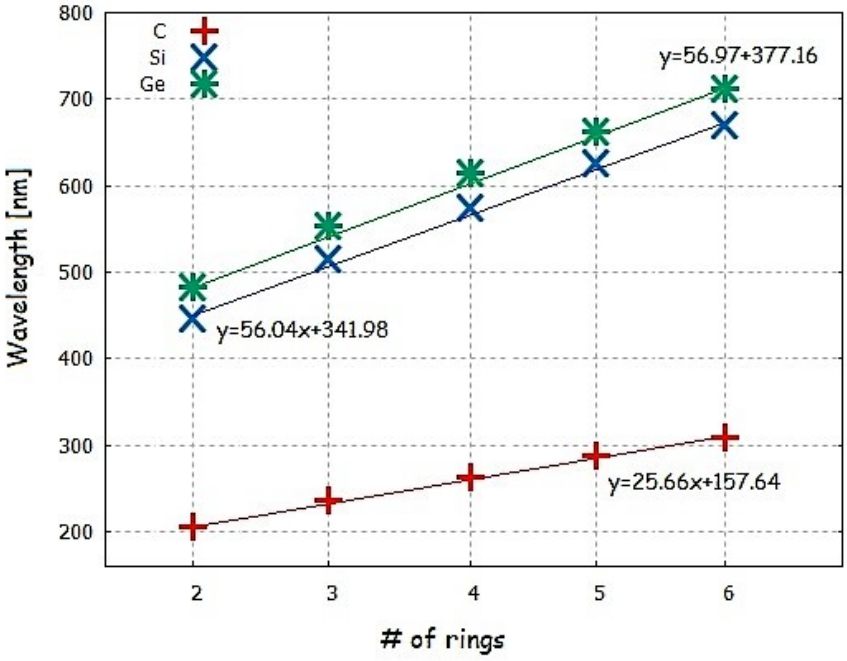

Figure 47: β peak excitation wavelengths of C-Si-Ge Acenes from two to six rings. The linear-relationship between the wavelengths of the β peak and the clusters size (number of rings) can be observed.

Table 24: β peak excitation wavelength (nm) for the C, Si, Ge linear clusters under study as a function of the rings number. The straight lines (S.L.) fitting the data after the present simulations with the corresponding formula have been reported.

	C	**Si**	**Ge**
2	206.3	445.9	482.4
3	236.2	514.4	553.5
4	262.7	574.0	613.8
5	287.0	626.2	663.0
6	309.2	670.2	712.5
S.L.	y=25.66x+157.64	y=56.04x+341.98	y=56.97x+377.16

tions of the β peaks for the Carbon acenes are at shorter wavelengths distributed along a straight line with a slightly lower angular coefficient. The presents outcomes demonstate than for all the families of linear clusters here considered the strongest structure in the absorption spectrum report similar behavior with respect to the longitudinal plasmon peak found for noble metals linear nanostructures [138].

5.6 FINAL DISCUSSION

The outcomes of the present chapter propose a systematic comparative study on the morphological, electronic and optical properties of C-Si-Ge-made linear clusters. Within DFT and TDDFT schemes, we have computed electron affinities, ionization energies, fundamental gaps and optical absorption spectra.
The analysis on the morphological properties confirmed that, while the C-based compounds preserve the planar appareance from the smallest to the largest system, for both the Si-made and Ge-made clusters, distortions in the out-of-plane direction take place ever for the smallest molecule of the family.
For what concerns the electronic properties, we have found for each species, a general increase (decrease) of the vertical electron affinities (ionization energies) as a function of the molecular size and deviations of the fundamental gaps of the same order of magnitude. Considering the systems at fixed dimension, we verified that for Si and Ge based clusters the above observables (EA_V and IE_V) result smaller that those of the Carbon Acenes; the same happens for the fundamental gap.
Dealing with the optical properties, we have observed a general redshift for both the optical onsets and the dominant peaks positions as a function of the molecular size indipendently by the nature of the constituent atom. In particular, for the wavelength positions of the main absorption peaks (β structures), a linear dependence with respect to the number of the rings composing the linear systems has been found. For the Si/Ge acenes we found nearly parallel straigth lines. At fixed dimension of the clusters, we found for both the dominat peaks and the optical onsets, a redshift in the case of Si and Ge made family, with respect to the Carbon counterpart.
A similar behavior, at the same size, could be found for the exciton-binding energies. The present investigation focused on the effect of atoms substitutions in linear acenes cluster, could be of interest for the search of complementary materials to carbon structures for new applications and devices.

6

CONCLUSIONS

In this Thesis, using different forefort computational techniques, we performed a systematic comparative study, focused on the effects of partial/total chemical substitutions on the electronic, optical and morphological properties of several Polycyclic Aromatic Hydrocarbons (PAHs) compounds. In particular, we have widely analyzed the effects of partial or total substitutions with atoms of different nature (Si, B, N, Ge) into Circumacenes and Linear Carbon Acenes. This study has been connected with the intriguing world of 2D materials, since the systems analyzed could be considered as finite portions (with a nanometric size) of their infinite counterparts (Graphene, Silicene, Germanene,..). We have selected the hybrid exchange-correlation functional B3LYP in combination with a gaussian localized basis set as implemented in two of the most actually performing all-electrons codes: *NWChem* and *Gaussian*. We computed the electron affinity (EA), ionization energy (IE), Quasi-Particle (QP) gap, exciton binding energies, and the optical absorption spectra for the various systems under study.

The inclusion of Si atoms into Coronene and Ovalene has provoked larger values of the ground-state energies for all the substituted configurations with respect to the original counterparts. In both Coronene and Ovalene molecules, we recorded a general reduction of the QP gap and optical onset energies as a consequence of the chemical modification.
Concerning the optical properties, for each type of substitution, the absorption spectra show a redshift of the optical onsets and a remodeling of the main peaks intensity. For the morphological properties, we observed that some trimer insertions (as for Coronene and Ovalene) deform consistently the molecule in the out-of-plane directions.

The comparative study of Circumacenes and their BN analoguos give rise to the following results: dealing with the electronic properties, we have found that a lowering of EA and a rise of IE and QP gap take place passing from the C-made to the BN-based systems.
Dealing with the morphological properties, we verified that all the BN molecules maintain a planar appearance, as their carbonaceous parents. For the optical properties, we observed that the absorption is localized in the UV for all the BN-based molecules, unlike their C-made analogues which present an absorption spectrum located in the visible range (except for Coronene). In this case we have verified a blueshift of the optical onsets and the dominant peaks for the

BN-made molecules with respect to the original C-made parents. In particular, thanks to their UV-absorption feature here analysed, the BN nanomaterials keep a promising role in the technology related to UV optoelectronics.
One of the most relevant result in the present work is that the electronic observables and optical properties (e.g. IE or optical onset energies) of the BN Circumacenes here studied show slight dependence from the dimension of the cluster. This is in contrast with the results obtained for their Carbon counterparts, which are strongly related to the molecular size. This occurrence could have important consequences on the strategies of choice of the best cluster for suitable applications or devices.

Considering the linear C/Si/Ge clusters, the analysis on the morphological properties confirms that, while the C-based compounds preserve the planar appareance from the first to the last molecule, for both the silicon-made and germanium-made clusters distortions in the out-of-plane direction take place ever since from the smallest member of the family. Extending ideally to the infinite dimension, the previous molecules could form a rippled Si/Ge-surfaces, in accordance with the experimental finding. For what concerns the electronic properties, as a function of the molecular size, we have found for each species, a general increase (decrease) of EA (IE) and deviations of the QP gaps of the same order of magnitude. Moreover, a general redshift for both the optical onsets and the dominant peaks positions, as a function of the molecular size, indipendently by the nature of the constituent atom, takes place. At fixed dimension of the clusters, for both the dominat peaks and the optical onsets, a redshift in the case of Si and Ge made family, with respect to the Carbon counterpart has been observed. Also for the exciton binding energy a similar behavior for Si and Ge clusters has been found.

Overall, the present investigation, focused on the effect of different atomic substitutions in Carbon-based clusters, could be interesting for the search of new and complementary materials for many modern applications and possible future optoelectronic devices.

BIBLIOGRAPHY

[1] A Acun et al. "Germanene: the germanium analogue of graphene." In: *Journal of Physics: Condensed Matter* 27.44 (2015), p. 443002. URL: http://stacks.iop.org/0953-8984/27/i=44/a=443002.

[2] Bernard Aufray, Abdelkader Kara, Sébastien Vizzini, Hamid Oughaddou, Christel Léandri, Benedicte Ealet, and Guy Le Lay. "Graphene-like silicon nanoribbons on Ag(110): A possible formation of silicene." In: *Applied Physics Letters* 96.18 (2010), p. 183102. DOI: 10.1063/1.3419932. eprint: https://doi.org/10.1063/1.3419932. URL: https://doi.org/10.1063/1.3419932.

[3] Foresman J B and Frisch A E. "Exploring Chemistry with Electronic Structure Methods." In: *Gaussian Inc. Pittsburgh* (1996).

[4] Rüdiger Bauernschmitt and Reinhart Ahlrichs. "Treatment of electronic excitations within the adiabatic approximation of time dependent density functional theory." In: *Chemical Physics Letters* 256.4 (1996), pp. 454 –464. ISSN: 0009-2614. DOI: https://doi.org/10.1016/0009-2614(96)00440-X. URL: http://www.sciencedirect.com/science/article/pii/000926149600440X.

[5] F. Bechstedt, R. Del Sole, G. Cappellini, and Lucia Reining. "An efficient method for calculating quasiparticle energies in semiconductors." In: *Solid State Communications* 84.7 (1992), pp. 765 –770.

[6] Axel D. Becke. "Density-functional thermochemistry. III. The role of exact exchange." In: *Journal of Chemical Physics* 98 (1993), p. 5648.

[7] Axel D. Becke. "Density-functional thermochemistry. III. The role of exact exchange." In: *The Journal of Chemical Physics* 98.7 (1993), pp. 5648–5652. DOI: 10.1063/1.464913. eprint: https://doi.org/10.1063/1.464913. URL: https://doi.org/10.1063/1.464913.

[8] M. Bernardi, C. Ataca, M. Palummo, and J. C. Grossman. "Optical and Electronic Properties of Two-Dimensional Layered Materials." In: *Nanophotonics* 6, 30 (Mar. 2017), p. 30. DOI: 10.1515/nanoph-2015-0030.

[9] Marco Bernardi, Maurizia Palummo, and Jeffrey C. Grossman. "Optoelectronic Properties in Monolayers of Hybridized Graphene and Hexagonal Boron Nitride." In: *Phys. Rev. Lett.* 108 (22 2012), p. 226805. DOI: 10.1103/PhysRevLett.108.226805. URL: https://link.aps.org/doi/10.1103/PhysRevLett.108.226805.

[10] Elisabeth Bianco, Sheneve Butler, Shishi Jiang, Oscar D. Restrepo, Wolfgang Windl, and Joshua E. Goldberger. "Stability and Exfoliation of Germanane: A Germanium Graphane Analogue." In: *ACS Nano* 7.5 (2013). PMID: 23506286, pp. 4414–4421. DOI: 10.1021/nn4009406. eprint: https://doi.org/10.1021/nn4009406. URL: https://doi.org/10.1021/nn4009406.

[11] M. Born and J. R. Oppenheimer. "Zur Quantentheorie der Molekeln." German. In: *Annalen der Physik* 84 (1927), pp. 457–484.

[12] Michael J.D Bosdet and Warren E Piers. "B-N as a C-C substitute in aromatic systems." In: *Canadian Journal of Chemistry* 87.1 (2009), pp. 8–29. DOI: 10.1139/v08-110. eprint: https://doi.org/10.1139/v08-110. URL: https://doi.org/10.1139/v08-110.

[13] S. F. Boys. "Electronic Wave Functions. I. A General Method of Calculation for the Stationary States of Any Molecular System." In: *Proceedings of the Royal Society of London A: Mathematical, Physical and Engineering Sciences* 200.1063 (1950), pp. 542–554.

[14] Sheneve Z. Butler et al. "Progress, Challenges, and Opportunities in Two-Dimensional Materials Beyond Graphene." In: *ACS Nano* 7.4 (2013). PMID: 23464873, pp. 2898–2926. DOI: 10.1021/nn400280c. eprint: https://doi.org/10.1021/nn400280c. URL: https://doi.org/10.1021/nn400280c.

[15] MARK E. CASIDA. "Time-Dependent Density Functional Response Theory for Molecules." In: *Recent Advances in Density Functional Methods*, pp. 155–192. DOI: 10.1142/9789812830586_0005. eprint: https://www.worldscientific.com/doi/pdf/10.1142/9789812830586_0005. URL: https://www.worldscientific.com/doi/abs/10.1142/9789812830586_0005.

[16] S. Cahangirov and M. Topsakal. "Two- and One-Dimensional Honeycomb Structures of Silicon and Germanium." In: *Phys. Rev. Lett.* 102 (23 2009), p. 236804. URL: https://link.aps.org/doi/10.1103/PhysRevLett.102.236804.

[17] G. Cappellini, G. Malloci, and G. Mulas. "Electronic excitations of oligoacenes: A time dependent density functional theory study." In: *Superlattices and Microstructures* 46.1 (2009). NanoSEA2008, pp. 14 –18. ISSN: 0749-6036. DOI: https://doi.org/10.1016/j.spmi.2008.12.019. URL: http://www.sciencedirect.com/science/article/pii/S0749603608002784.

[18] G Cappellini, Guido Satta, K Tenelsen, and F Bechstedt. "Pressure and Strain-Dependent Quasiparticle Energies of Cubic, Wurtzite and Hexagonal BN." In: *Physica Status Solidi B-basic Solid State Physics - PHYS STATUS SOLIDI B-BASIC SO* 217

(Feb. 2000), pp. 861–867. DOI: 10.1002/(SICI)1521-3951(200002)217:2<861::AID-PSSB861>3.0.CO;2-H.

[19] Giancarlo Cappellini, Guido Satta, Maurizia Palummo, and Giovanni Onida. "Optical properties of BN in cubic and layered hexagonal phases." In: *Phys. Rev. B* 64 (3 2001), p. 035104. DOI: 10.1103/PhysRevB.64.035104. URL: https://link.aps.org/doi/10.1103/PhysRevB.64.035104.

[20] R. Cardia. "Computational investigation on Polycyclic Aromatic Hydrocarbons in in the molecular and solid state phases." PhD thesis. -, 2016.

[21] R. Cardia, G. Malloci, A. Mattoni, and G. Cappellini. "Effects of TIPS-Functionalization and Perhalogenation on the Electronic, Optical, and Transport Properties of Angular and Compact Dibenzochrysene." In: *The Journal of Physical Chemistry A* 118.28 (2014). PMID: 24946056, pp. 5170–5177. DOI: 10.1021/jp502022t. eprint: https://doi.org/10.1021/jp502022t. URL: https://doi.org/10.1021/jp502022t.

[22] R. Cardia, G. Malloci, G.-M. Rignanese, X. Blase, E. Molteni, and G. Cappellini. "Electronic and optical properties of hexathiapentacene in the gas and crystal phases." In: *Phys. Rev. B* 93 (23 2016), p. 235132. DOI: 10.1103/PhysRevB.93.235132. URL: https://link.aps.org/doi/10.1103/PhysRevB.93.235132.

[23] A. U. Carsten. *Time-Dependent Density Functional Theory: concept and applications*. Oxford University Press, 2012.

[24] M. E. Casida and Huix Rotllant M. "Progress in Time-Dependent Density Functional Theory." In: *Annu. Rev. Phys. Chem.* 63.- (2012), pp. 287–323.

[25] Franco Cataldo, Susana Iglesias-Groth, and Arturo Manchado. "Electronic absorption spectroscopy of polycyclic aromatic hydrocarbons (PAHs) radical cations generated in oleum: a superacid medium." In: *Spectrochimica acta. Part A, Molecular and biomolecular spectroscopy* 77.5 (2010), 998—1004. ISSN: 1386-1425. DOI: 10.1016/j.saa.2010.08.037. URL: https://doi.org/10.1016/j.saa.2010.08.037.

[26] Wei Chen, Yafei Li, Guangtao Yu, Chen-Zhong Li, Shengbai B. Zhang, Zhen Zhou, and Zhongfang Chen. "Hydrogenation: A Simple Approach To Realize Semiconductor-Half-Metal-Metal Transition in Boron Nitride Nanoribbons." In: *Journal of the American Chemical Society* 132.5 (2010). PMID: 20085366, pp. 1699–1705. DOI: 10.1021/ja908475v. eprint: https://doi.org/10.1021/ja908475v. URL: https://doi.org/10.1021/ja908475v.

[27] Zhi-Gang Chen and Jin Zou. "Field emitters: ultrathin BN nanosheets protruded from BN fibers." In: *J. Mater. Chem.* 21 (4 2011), pp. 1191–1195. DOI: 10.1039/C0JM02955F. URL: http://dx.doi.org/10.1039/C0JM02955F.

[28] Reza Dabestani and Ilia Ivanov. "Invited Review A Compilation of Physical, Spectroscopic and Photophysical Properties of Polycyclic Aromatic Hydrocarbons." In: *Photochemistry and Photobiology - PHOTOCHEM PHOTOBIOL* 70 (Jan. 1999). DOI: 10.1562/0031-8655(1999)070<0010:IRACOP>2.3.CO;2.

[29] Nicolas Dardenne, Roberto Cardia, Jing Li, Giuliano Malloci, Giancarlo Cappellini, Xavier Blase, Jean-Christophe Charlier, and Gian-Marco Rignanese. "Tuning Optical Properties of Dibenzochrysenes by Functionalization: A Many-Body Perturbation Theory Study." In: *The Journal of Physical Chemistry C* 121.44 (2017), pp. 24480–24488. DOI: 10.1021/acs.jpcc.7b08601. eprint: https://doi.org/10.1021/acs.jpcc.7b08601. URL: https://doi.org/10.1021/acs.jpcc.7b08601.

[30] P. H. Dederichs, S. Blügel, R. Zeller, and H. Akai. "Ground States of Constrained Systems: Application to Cerium Impurities." In: *Phys. Rev. Lett.* 53 (26 1984), pp. 2512–2515.

[31] Hugo Dil, Jorge Lobo-Checa, Robert Laskowski, Peter Blaha, Simon Berner, Jürg Osterwalder, and Thomas Greber. "Surface Trapping of Atoms and Molecules with Dipole Rings." In: *Science* 319.5871 (2008), pp. 1824–1826. ISSN: 0036-8075. DOI: 10.1126/science.1154179. eprint: http://science.sciencemag.org/content/319/5871/1824.full.pdf. URL: http://science.sciencemag.org/content/319/5871/1824.

[32] Yun Ding, Marcella Iannuzzi, and Jürg Hutter. "Investigation of Boron Nitride Nanomesh Interacting with Water." In: *The Journal of Physical Chemistry C* 115.28 (2011), pp. 13685–13692. DOI: 10.1021/jp110235y. eprint: https://doi.org/10.1021/jp110235y. URL: https://doi.org/10.1021/jp110235y.

[33] R. Ditchfield, W. J. Hehre, and J. A. Pople. "Self-Consistent Molecular-Orbital Methods IX. An Extended Gaussian-Type Basis for Molecular-Orbital Studies of Organic Molecules." In: *The Journal of Chemical Physics* 54.2 (1971), pp. 724–728.

[34] Shokoofeh Dolati, Abdolhossein Fereidoon, and Kazem Reza Kashyzadeh. "A Comparison Study between Boron nitride Nanotubes and Carbon Nanotubes." In: *International Journal of Emerging Technology and Advanced Engineering* 2.10 (2012), pp. 470–474.

[35] Mehdi N Ebrahimy, Mohammad Naziri, Alireza Andalib, and Ziaddin Daie Kuzekanani. "Ultrasensitive and compact tunable electro-optic filter in a 2D silicon photonic-crystal cavity."

In: *Laser Physics* 26.6 (2016), p. 066202. URL: http://stacks.iop.org/1555-6611/26/i=6/a=066202.

[36] Luis Echegoyen and Lourdes E. Echegoyen. "Electrochemistry of Fullerenes and Their Derivatives." In: *Accounts of Chemical Research* 31.9 (1998), pp. 593–601. DOI: 10.1021/ar970138v. eprint: https://doi.org/10.1021/ar970138v. URL: https://doi.org/10.1021/ar970138v.

[37] *Electronic structure of higher acenes and polyacenes: The perspective developed by theoretical analysis*. https://pdfs.semanticscholar.org/70df/f93e28fc47a64633a7dd0ff0ded5ae12428d.pdf. Accessed: 2018-12-22.

[38] Matthias Ernzerhof and Gustavo E. Scuseria. "Assessment of the Perdew–Burke–Ernzerhof exchange-correlation functional." In: *The Journal of Chemical Physics* 110.11 (1999), pp. 5029–5036. DOI: 10.1063/1.478401. eprint: https://doi.org/10.1063/1.478401. URL: https://doi.org/10.1063/1.478401.

[39] E. Fermi. "Eine statistische Methode zur Bestimmung einiger Eigenschaften des Atoms und ihre Anwendung auf die Theorie des periodischen Systems der Elemente." German. In: *Zeitschrift für Physik* 48.1-2 (1928), pp. 73–79.

[40] R. P. Feynman. "Forces in Molecules." In: *Phys. Rev.* 56 (4 1939), pp. 340–343.

[41] Alessio Filippetti, Vincenzo Fiorentini, G Cappellini, and Andrea Bosin. "Ionicity and Relaxation Anomalies at III-V Nitride Surfaces." In: *Physica Status Solidi (a)* 170 (Dec. 1998), pp. 265–269. DOI: 10.1002/(SICI)1521-396X(199812)170:2<265::AID-PSSA265>3.0.CO;2-N.

[42] V. Fock. "Näherungsmethode zur Lösung des quantenmechanischen Mehrkörperproblems." German. In: *Zeitschrift für Physik* 61.1-2 (1930), pp. 126–148. DOI: 10.1007/BF01340294.

[43] R. F. Frindt. "Single Crystals of MoS2 Several Molecular Layers Thick." In: *Journal of Applied Physics* 37.4 (1966), pp. 1928–1929. DOI: 10.1063/1.1708627. eprint: https://doi.org/10.1063/1.1708627. URL: https://doi.org/10.1063/1.1708627.

[44] M. J. Frisch et al. *Gaussian~16 Revision B.01*. Gaussian Inc. Wallingford CT. 2016.

[45] Min Gao, Andrey Lyalin, and Tetsuya Taketsugu. "Catalytic Activity of Au and Au2 on the h-BN Surface: Adsorption and Activation of O2." In: *The Journal of Physical Chemistry C* 116.16 (2012), pp. 9054–9062. DOI: 10.1021/jp300684v. eprint: https://doi.org/10.1021/jp300684v. URL: https://doi.org/10.1021/jp300684v.

[46] Xingfa Gao, Zhen Zhou, Yuliang Zhao, Shigeru Nagase, S. B. Zhang, and Zhongfang Chen. "Comparative Study of Carbon and BN Nanographenes: Ground Electronic States and Energy Gap Engineering." In: *The Journal of Physical Chemistry C* 112.33 (2008), pp. 12677–12682. DOI: 10.1021/jp801679j. eprint: https://doi.org/10.1021/jp801679j. URL: https://doi.org/10.1021/jp801679j.

[47] Iryna Garkusha, Jan Fulara, Peter J. Sarre, and John P. Maier. "Electronic Absorption Spectra of Protonated Pyrene and Coronene in Neon Matrixes." In: *The Journal of Physical Chemistry A* 115.40 (2011). PMID: 21861507, pp. 10972–10978. DOI: 10.1021/jp206188a. eprint: https://doi.org/10.1021/jp206188a. URL: https://doi.org/10.1021/jp206188a.

[48] Andre K. Geim. "Nobel Lecture: Random walk to graphene." In: *Rev. Mod. Phys.* 83 (3 2011), pp. 851–862. DOI: 10.1103/RevModPhys.83.851. URL: https://link.aps.org/doi/10.1103/RevModPhys.83.851.

[49] O. Gunnarsson and B. I. Lundqvist. "Exchange and correlation in atoms, molecules, and solids by the spin-density-functional formalism." In: *Phys. Rev. B* 13 (10 1976), pp. 4274–4298.

[50] D. R. Hartree. "The Wave Mechanics of an Atom with a Non-Coulomb Central Field. Part I. Theory and Methods." In: *Mathematical Proceedings of the Cambridge Philosophical Society* 24 (01 Jan. 1928), pp. 89–110.

[51] D. R. Hartree. "The Wave Mechanics of an Atom with a Non-Coulomb Central Field. Part II. Some Results and Discussion." In: *Mathematical Proceedings of the Cambridge Philosophical Society* 24 (01 Jan. 1928), pp. 111–132.

[52] So Hirata and Martin Head-Gordon. "Time-dependent density functional theory for radicals: An improved description of excited states with substantial double excitation character." In: *Chemical Physics Letters* 302.5 (1999), pp. 375 –382. ISSN: 0009-2614. DOI: https://doi.org/10.1016/S0009-2614(99)00137-2. URL: http://www.sciencedirect.com/science/article/pii/S0009261499001372.

[53] So Hirata and Martin Head-Gordon. "Time-dependent density functional theory within the Tamm-Dancoff approximation." English (US). In: *Chemical Physics Letters* 314.3-4 (Dec. 1999), pp. 291–299. ISSN: 0009-2614. DOI: 10.1016/S0009-2614(99)01149-5.

[54] P. Hohenberg and W. Kohn. "Inhomogeneous Electron Gas." In: *Phys. Rev.* 136 (3B 1964), B864–B871.

[55] Wei Hu, Xiaojun Wu, Zhenyu Li, and Jinlong Yang. "Porous silicene as a hydrogen purification membrane." In: *Phys. Chem. Chem. Phys.* 15 (16 2013), pp. 5753–5757. DOI: 10.1039/C3CP00066D. URL: http://dx.doi.org/10.1039/C3CP00066D.

[56] Ángel J Pérez-Jiménez and Juan C Sancho-García. "Using circumacenes to improve organic electronics and molecular electronics: design clues." In: *Nanotechnology* 20.47 (2009), p. 475201. URL: http://stacks.iop.org/0957-4484/20/i=47/a=475201.

[57] E. Jennings, W. Montgomery, and Ph. Lerch. "Stability of Coronene at High Temperature and Pressure." In: *The Journal of Physical Chemistry B* 114.48 (2010). PMID: 21067207, pp. 15753–15758. DOI: 10.1021/jp105020f. eprint: https://doi.org/10.1021/jp105020f. URL: https://doi.org/10.1021/jp105020f.

[58] Frank Jensen. *Introduction to Computational Chemistry*. 2rd. Wiley, 2007.

[59] Per Joensen, R.F. Frindt, and S.Roy Morrison. "Single-layer MoS2." In: *Materials Research Bulletin* 21.4 (1986), pp. 457 – 461. ISSN: 0025-5408. DOI: https://doi.org/10.1016/0025-5408(86)90011-5. URL: http://www.sciencedirect.com/science/article/pii/0025540886900115.

[60] Rita John and Benita Merlin. "Optical properties of graphene, silicene, germanene, and stanene from IR to far UV – A first principles study." In: 110 (2017). Exported from https://app.dimensions.ai on 2018/12/22, pp. 307–315. DOI: 10.1016/j.jpcs.2017.06.026. URL: https://app.dimensions.ai/details/publication/pub.1086139573.

[61] R. O. Jones. "Density functional theory: Its origins, rise to prominence, and future." In: *Rev. Mod. Phys.* 87 (3 2015), pp. 897–923.

[62] R. O. Jones and O. Gunnarsson. "The density functional formalism, its applications and prospects." In: *Rev. Mod. Phys.* 61 (3 1989), pp. 689–746. DOI: 10.1103/RevModPhys.61.689. URL: https://link.aps.org/doi/10.1103/RevModPhys.61.689.

[63] Deepthi Jose and Ayan Datta. "Structures and electronic properties of silicene clusters: a promising material for FET and hydrogen storage." In: *Phys. Chem. Chem. Phys.* 13 (16 2011), pp. 7304–7311. DOI: 10.1039/C0CP02580A. URL: http://dx.doi.org/10.1039/C0CP02580A.

[64] Deepthi Jose and Ayan Datta. "Understanding of the Buckling Distortions in Silicene." In: *The Journal of Physical Chemistry C* 116.46 (2012), pp. 24639–24648. DOI: 10.1021/jp3084716. eprint: https://doi.org/10.1021/jp3084716. URL: https://doi.org/10.1021/jp3084716.

[65] Saban Kalay, Zehra Yilmaz, Ozlem Sen, Melis Emanet, Emine Kazanc, and Mustafa Culha. "Synthesis of boron nitride nanotubes and their applications." In: *Beilstein Journal of Nanotechnology* 6.1 (2015), pp. 84–102. DOI: doi:10.3762/bjnano.6.9. URL: https://www.ingentaconnect.com/content/doaj/21904286/2015/00000006/00000001/art00009.

[66] Umar Khan, Peter May, Arlene O'Neill, Alan P. Bell, Elodie Boussac, Arnaud Martin, James Semple, and Jonathan N. Coleman. "Polymer reinforcement using liquid-exfoliated boron nitride nanosheets." In: *Nanoscale* 5 (2 2013), pp. 581–587. DOI: 10.1039/C2NR33049K. URL: http://dx.doi.org/10.1039/C2NR33049K.

[67] Keun Soo Kim, Yue Zhao, Houk Jang, Sang Yoon Lee, Jong Min Kim, Kwang S Kim, Jong-Hyun Ahn, Philip Kim, Jae-Young Choi, and Byung Hee Hong. "Large-scale pattern growth of graphene films for stretchable transparent electrodes." In: *Nature* 457.7230 (2009), 706—710. ISSN: 0028-0836. DOI: 10.1038/nature07719. URL: https://doi.org/10.1038/nature07719.

[68] W. Kohn and L. J. Sham. "Self-Consistent Equations Including Exchange and Correlation Effects." In: *Phys. Rev.* 140 (4A 1965), A1133–A1138.

[69] Walter Kohn. "Electronic structure of matter-wave functions and density functionals (NOBEL Lecture)." In: *Review of Modern Physics* 71 (1999), p. 1253.

[70] J. C. Kotz, P. M. Treichel, J. R. Townsend, and D. A. Treichel. *Chimica*. EDISES, 2013.

[71] A. Kumar, R. Cardia, and G. Cappellini. "Electronic and optical properties of chromophores from bacterial cellulose." In: *Cellulose* 25.4 (2018). cited By 0, pp. 2191–2203. DOI: 10.1007/s10570-018-1728-0. URL: https://www.scopus.com/inward/record.uri?eid=2-s2.0-85044740130&doi=10.1007$\%$2fs10570-018-1728-0&partnerID=40&md5=d5760f42b4e58eaa35aed7c9b3f3804a.

[72] Lin Lai, Wei Song, Jing Lu, Zhengxiang Gao, Shigeru Nagase, Ming Ni, W. N. Mei, Jianjun Liu, Dapeng Yu, and Hengqiang Ye. "Structural and Electronic Properties of Fluorinated Boron Nitride Nanotubes." In: *The Journal of Physical Chemistry B* 110.29 (2006). PMID: 16854105, pp. 14092–14097. DOI: 10.1021/jp061203y. eprint: https://doi.org/10.1021/jp061203y. URL: https://doi.org/10.1021/jp061203y.

[73] Chengteh Lee, Weitao Yang, and Robert G. Parr. "Development of the Colle-Salvetti correlation-energy formula into a functional of the electron density." In: *Phys. Rev. B* 37 (2 1988), pp. 785–789. DOI: 10.1103/PhysRevB.37.785. URL: https://link.aps.org/doi/10.1103/PhysRevB.37.785.

[74] Hai Li, Zongyou Yin, Qiyuan He, Hong Li, Xiao Huang, Gang Lu, Derrick Wen Hui Fam, Alfred Iing Yoong Tok, Qing Zhang, and Hua Zhang. "Fabrication of Single- and Multilayer MoS2 Film-Based Field-Effect Transistors for Sensing NO at Room Temperature." In: *Small* 8.1 (2012), pp. 63–67. DOI: 10.1002/smll.201101016. eprint: https://onlinelibrary.wiley.com/doi/pdf/10.1002/smll.201101016. URL: https://onlinelibrary.wiley.com/doi/abs/10.1002/smll.201101016.

[75] Yafei Li, Dihua Wu, Zhen Zhou, Carlos R. Cabrera, and Zhongfang Chen. "Enhanced Li Adsorption and Diffusion on MoS2 Zigzag Nanoribbons by Edge Effects: A Computational Study." In: *The Journal of Physical Chemistry Letters* 3.16 (2012). PMID: 26295774, pp. 2221–2227. DOI: 10.1021/jz300792n. eprint: https://doi.org/10.1021/jz300792n. URL: https://doi.org/10.1021/jz300792n.

[76] Chun-Liang Lin, Ryuichi Arafune, Kazuaki Kawahara, Mao Kanno, Noriyuki Tsukahara, Emi Minamitani, Yousoo Kim, Maki Kawai, and Noriaki Takagi. "Substrate-Induced Symmetry Breaking in Silicene." In: *Phys. Rev. Lett.* 110 (7 2013), p. 076801. DOI: 10.1103/PhysRevLett.110.076801. URL: https://link.aps.org/doi/10.1103/PhysRevLett.110.076801.

[77] Yi Lin and John W. Connell. "Advances in 2D boron nitride nanostructures: nanosheets, nanoribbons, nanomeshes, and hybrids with graphene." In: *Nanoscale* 4 (22 2012), pp. 6908–6939. DOI: 10.1039/C2NR32201C. URL: http://dx.doi.org/10.1039/C2NR32201C.

[78] Yi Lin, Christopher E. Bunker, K. A. Shiral Fernando, and John W. Connell. "Aqueously Dispersed Silver Nanoparticle-Decorated Boron Nitride Nanosheets for Reusable, Thermal Oxidation-Resistant Surface Enhanced Raman Spectroscopy (SERS) Devices." In: *ACS Applied Materials & Interfaces* 4.2 (2012). PMID: 22280102, pp. 1110–1117. DOI: 10.1021/am201747d. eprint: https://doi.org/10.1021/am201747d. URL: https://doi.org/10.1021/am201747d.

[79] Yi-Tao Liu, Xu-Ming Xie, and Xiong-Ying Ye. "Tuning the solubility of boron nitride nanosheets in organic solvents by using block copolymer as a "Janus" modifier." In: *Chem. Commun.* 49 (4 2013), pp. 388–390. DOI: 10.1039/C2CC36623A. URL: http://dx.doi.org/10.1039/C2CC36623A.

[80] Alejandro Lopez-Bezanilla, Wu Zhou, and Juan-Carlos Idrobo. "Electronic and Quantum Transport Properties of Atomically Identified Si Point Defects in Graphene." In: *The Journal of Physical Chemistry Letters* 5.10 (2014). PMID: 26270371, pp. 1711–1718. DOI: 10.1021/jz500403h. eprint: https://doi.org/10.1021/jz500403h. URL: https://doi.org/10.1021/jz500403h.

[81] Knupfer M. *Exciton binding energies in organic semiconductors*. Springer, 2003.

[82] Gerald D. Mahan. *Many-Particle Physics*. 2rd. Kluwer Academic / Plenum Press, 2000.

[83] G. Malloci, G. Mulas, G. Cappellini, and C. Joblin. "Time-dependent density functional study of the electronic spectra of oligoacenes in the charge states -1, 0, +1, and +2." In: *Chemical Physics* 340.1 (2007), pp. 43 –58. ISSN: 0301-0104. DOI: https://doi.org/10.1016/j.chemphys.2007.07.046. URL: http://www.sciencedirect.com/science/article/pii/S0301010407003084.

[84] G. Malloci, G. Cappellini, G. Mulas, and A. Mattoni. "Electronic and optical properties of families of polycyclic aromatic hydrocarbons: A systematic (time-dependent) density functional theory study." In: *Chemical Physics* 384.1 (2011), pp. 19 –27. ISSN: 0301-0104. DOI: https://doi.org/10.1016/j.chemphys.2011.04.013. URL: http://www.sciencedirect.com/science/article/pii/S0301010411001327.

[85] Giuliano Malloci, Christine Joblin, and Giacomo Mulas. "Online database of the spectral properties of polycyclic aromatic hydrocarbons." In: *Chemical Physics* 332.2 (2007), pp. 353 –359. ISSN: 0301-0104. DOI: https://doi.org/10.1016/j.chemphys.2007.01.001. URL: http://www.sciencedirect.com/science/article/pii/S0301010407000031.

[86] Giuliano Malloci, Christine Joblin, and Giacomo Mulas. "Online database of the spectral properties of polycyclic aromatic hydrocarbons." In: *Chemical Physics* 332 (Jan. 2007), pp. 353–359. DOI: 10.1016/j.chemphys.2007.01.001.

[87] Giuliano Malloci, Giancarlo Cappellini, Giacomo Mulas, and Guido Satta. "Quasiparticle effects and optical absorption in small fullerenelike GaP clusters." In: *Phys. Rev. B* 70 (20 2004), p. 205429. DOI: 10.1103/PhysRevB.70.205429. URL: https://link.aps.org/doi/10.1103/PhysRevB.70.205429.

[88] Giuliano Malloci, Letizia Chiodo, Angel Rubio, and Alessandro Mattoni. "Structural and Optoelectronic Properties of Unsaturated ZnO and ZnS nanoclusters." In: *J. Phys. Chem. C* 116 (2012), pp. 8741–8746.

[89] M.A.L. Marques and E.K.U. Gross. "TIME-DEPENDENT DENSITY FUNCTIONAL THEORY." In: *Annual Review of Physical Chemistry* 55.1 (2004), pp. 427–455.

[90] Rubén Mas-Ballesté, Cristina Gómez-Navarro, Julio Gómez-Herrero, and Félix Zamora. "2D materials: to graphene and beyond." In: *Nanoscale* 3 (1 2011), pp. 20–30. DOI: 10.1039/C0NR00323A. URL: http://dx.doi.org/10.1039/C0NR00323A.

[91] Lars Matthes, Paola Gori, Olivia Pulci, and Friedhelm Bechstedt. "Universal infrared absorbance of two-dimensional honeycomb group-IV crystals." In: *Phys. Rev. B* 87 (3 2013), p. 035438. DOI: 10.1103/PhysRevB.87.035438. URL: https://link.aps.org/doi/10.1103/PhysRevB.87.035438.

[92] P Mocci, R Cardia, and G Cappellini. "Inclusions of Si-atoms in Graphene nanostructures: a computational study on the ground-state electronic properties of Coronene and Ovalene." In: *Journal of Physics: Conference Series* 956.1 (2018), p. 012020. URL: http://stacks.iop.org/1742-6596/956/i=1/a=012020.

[93] P Mocci, R Cardia, and G Cappellini. "Si-atoms substitutions effects on the electronic and optical properties of coronene and ovalene." In: *New Journal of Physics* 20.11 (2018), p. 113008. URL: http://stacks.iop.org/1367-2630/20/i=11/a=113008.

[94] P Mocci, R Cardia, and G Cappellini. "A computational investigation on the electronic and optical properties of coronene and its Boron-Nitride (BN) and perfluorinated counterparts." In: *Journal of Physics: Conference Series* 1226.012016 (2019), pp. 1–6. DOI: 10.1088/1742-6596/1226/1/012016.

[95] Junais Habeeb Mokkath and Udo Schwingenschlögl. "Tunable optical absorption in silicene molecules." In: *J. Mater. Chem. C* 4 (31 2016), pp. 7387–7390. DOI: 10.1039/C6TC02186G. URL: http://dx.doi.org/10.1039/C6TC02186G.

[96] Alessandro Molle, Joshua Goldberger, Michel Houssa, Yong Xu, Shou-Cheng Zhang, and Deji Akinwande. "Buckled two-dimensional Xene sheets." In: 16.2 (2017). Exported from https://app.dimensions.ai on 2018/12/19, p. 163. DOI: 10.1038/nmat4802. URL: https://app.dimensions.ai/details/publication/pub.1013071627andhttps://lirias.kuleuven.be/bitstream/123456789/601108/1/Perspective-Final-Accepted.pdf.

[97] *NIST-standard reference data*. https://www.nist.gov/srd. Accessed: 2017-09-30.

[98] Noushin Nasiri, Dayong Jin, and Antonio Tricoli. "Nanoarchitechtonics of Visible-Blind Ultraviolet Photodetector Materials: Critical Features and Nano-Microfabrication." In: *Advanced Optical Materials* 0.0 (), p. 1800580. DOI: 10.1002/adom.201800580. eprint: https://onlinelibrary.wiley.com/doi/pdf/10.1002/adom.201800580. URL: https://onlinelibrary.wiley.com/doi/abs/10.1002/adom.201800580.

[99] Fabian Donat Natterer, Fran çois Patthey, and Harald Brune. "Ring State for Single Transition Metal Atoms on Boron Nitride on Rh(111)." In: *Phys. Rev. Lett.* 109 (6 2012), p. 066101. DOI: 10.1103/PhysRevLett.109.066101. URL: https://link.aps.org/doi/10.1103/PhysRevLett.109.066101.

[100] G. A. Nemnes, Camelia Visan, D. V. Anghel, and A. Manolescu. "Molecular dynamics of halogenated graphene - hexagonal boron nitride nanoribbons." In: *Journal of Physics: Conference Series* 738.1 (2016), p. 012027. URL: http://stacks.iop.org/1742-6596/738/i=1/a=012027.

[101] K. S. Novoselov, A. K. Geim, S. V. Morozov, D. Jiang, Y. Zhang, S. V. Dubonos, I. V. Grigorieva, and A. A. Firsov. "Electric Field Effect in Atomically Thin Carbon Films." In: *Science* 306.5696 (2004), pp. 666–669. ISSN: 0036-8075. DOI: 10.1126/science.1102896. eprint: http://science.sciencemag.org/content/306/5696/666.full.pdf. URL: http://science.sciencemag.org/content/306/5696/666.

[102] G. Onida, L. Reining, and A. Rubio. "Electronic excitations: density-functional versus many-body Green's-function approaches." In: *Rev. Mod. Phys.* 74 (2002), p. 601.

[103] Giovanni Onida, Lucia Reining, and Angel Rubio. "Electronic excitations: density-functional versus many-body Green's-function approaches." In: *Rev. Mod. Phys.* 74 (2 2002), pp. 601–659. DOI: 10.1103/RevModPhys.74.601. URL: https://link.aps.org/doi/10.1103/RevModPhys.74.601.

[104] L. Pan, H. J. Liu, X. J. Tan, H. Y. Lv, J. Shi, X. F. Tang, and G. Zheng. "Thermoelectric properties of armchair and zigzag silicene nanoribbons." In: *Phys. Chem. Chem. Phys.* 14 (39 2012), pp. 13588–13593. DOI: 10.1039/C2CP42645E. URL: http://dx.doi.org/10.1039/C2CP42645E.

[105] John P. Perdew, Kieron Burke, and Matthias Ernzerhof. "Generalized Gradient Approximation Made Simple." In: *Phys. Rev. Lett.* 77 (18 1996), pp. 3865–3868.

[106] John P. Perdew, J. A. Chevary, S. H. Vosko, Koblar A. Jackson, Mark R. Pederson, D. J. Singh, and Carlos Fiolhais. "Atoms, molecules, solids, and surfaces: Applications of the generalized gradient approximation for exchange and correlation." In: *Phys. Rev. B* 46 (11 1992), pp. 6671–6687.

[107] I.K. Petrushenko and K.B. Petrushenko. "Optical properties of bilayer quantum dot models based on coronene and its BN analogues with a BODIPY dye: Theoretical TD-CAM-B3LYP-D3 investigation." In: *Spectrochimica Acta Part A: Molecular and Biomolecular Spectroscopy* 206 (2019), pp. 498 –505. ISSN: 1386-1425. DOI: https://doi.org/10.1016/j.saa.2018.08.033. URL: http://www.sciencedirect.com/science/article/pii/S1386142518308060.

[108] Max Pinheiro, Luiz F. A. Ferrão, Fernanda Bettanin, Adélia J. A. Aquino, Francisco B. C. Machado, and Hans Lischka. "How to efficiently tune the biradicaloid nature of acenes by chem-

ical doping with boron and nitrogen." In: *Phys. Chem. Chem. Phys.* 19 (29 2017), pp. 19225–19233. DOI: 10.1039/C7CP03198J. URL: http://dx.doi.org/10.1039/C7CP03198J.

[109] Jason Potticary, Lui R. Terry, Christopher Bell, Andrew M. Collins, Claudio Fontanesi, Gabriele Kociok-Kohn, Simon Crampin, Enrico Da Como, and Simon R. Hall. "Control of polymorphism in coronene by the application of magnetic fields." In: *arXiv e-prints*, arXiv:1509.04120 (Sept. 2015), arXiv:1509.04120. arXiv: 1509.04120 [cond-mat.mtrl-sci].

[110] Maria Stella Prete, Adriano Mosca Conte, Paola Gori, Friedhelm Bechstedt, and Olivia Pulci. "Tunable electronic properties of two-dimensional nitrides for light harvesting heterostructures." In: *Applied Physics Letters* 110.1 (2017), p. 012103. DOI: 10.1063/1.4973753. eprint: https://doi.org/10.1063/1.4973753. URL: https://doi.org/10.1063/1.4973753.

[111] A Bosin R Cardia G Malloci and G Cappellini. "Electronic and optical properties of functionalized polyaromatic hydrocarbons: a computational investigation on perfluorinated circumacenes." In: *Proc.SPIE* 9895 (2016), pp. 9895 –9895–8. DOI: 10.1117/12.2229744. URL: https://doi.org/10.1117/12.2229744.

[112] Erich Runge and E. K. U. Gross. "Density-Functional Theory for Time-Dependent Systems." In: *Phys. Rev. Lett.* 52 (12 1984), pp. 997–1000.

[113] Ernesto D. Sandoval, Samad Hajinazar, and Aleksey N. Kolmogorov. "Stability of two-dimensional BN-Si structures." In: *Phys. Rev. B* 94 (9 2016), p. 094105. DOI: 10.1103/PhysRevB.94.094105. URL: https://link.aps.org/doi/10.1103/PhysRevB.94.094105.

[114] Somananda Sanyal, Arun Manna, and Swapan Pati. "BN-decorated graphene nanoflakes with tunable opto-electronic and charge transport properties." In: *Journal of Materials Chemistry C* 2 (July 2014), p. 11.

[115] Guido Satta, Giancarlo Cappellini, Valerio Olevano, and Lucia Reining. "Many-body effects in the electronic spectra of cubic boron nitride." In: *Phys. Rev. B* 70 (19 2004), p. 195212.

[116] Ansgar Schäfer, Hans Horn, and Reinhart Ahlrichs. "Fully optimized contracted Gaussian basis sets for atoms Li to Kr." In: *The Journal of Chemical Physics* 97.4 (1992), pp. 2571–2577. DOI: 10.1063/1.463096. eprint: https://doi.org/10.1063/1.463096. URL: https://doi.org/10.1063/1.463096.

[117] Ansgar Schäfer, Christian Huber, and Reinhart Ahlrichs. "Fully optimized contracted Gaussian basis sets of triple zeta valence quality for atoms Li to Kr." In: *The Journal of Chemical Physics* 100.8 (1994), pp. 5829–5835. DOI: 10.1063/1.467146. eprint: https://doi.org/10.1063/1.467146. URL: https://doi.org/10.1063/1.467146.

[118] Mariyappan Shanmugam, Tanesh Bansal, Chris A. Durcan, and Bin Yu. "Molybdenum disulphide/titanium dioxide nanocomposite-poly 3-hexylthiophene bulk heterojunction solar cell." In: *Applied Physics Letters* 100.15 (2012), p. 153901. DOI: 10.1063/1.3703602. eprint: https://doi.org/10.1063/1.3703602. URL: https://doi.org/10.1063/1.3703602.

[119] J. C. Slater. "Atomic Shielding Constants." In: *Phys. Rev.* 36 (1 1930), pp. 57–64.

[120] J. C. Slater. "Note on Hartree's Method." In: *Phys. Rev.* 35 (2 1930), pp. 210–211.

[121] Sasha Stankovich, Dmitriy A. Dikin, Geoffrey H.B. Dommett, Kevin M. Kohlhaas, Eric J. Zimney, Eric A. Stach, Richard D. Piner, SonBinh Nguyen, and Rodney S. Ruoff. "Graphene-based composite materials." English (US). In: *Nature* 442.7100 (July 2006), pp. 282–286. ISSN: 0028-0836. DOI: 10.1038/nature04969.

[122] Maria Stella Prete, Olivia Pulci, and Friedhelm Bechstedt. "Strong in- and out-of-plane excitons in two-dimensional InN nanosheets." In: *Physical Review B* 98 (Dec. 2018), pp. –. DOI: 10.1103/PhysRevB.98.235431.

[123] Maria Stella Prete, Davide Grassano, Olivia Pulci, Igor Kupchak, and Friedhelm Bechstedt. "Excitonic effects in absorption and emission of 2D group-III nitrides." In: (Mar. 2019), pp. –.

[124] P. J. Stephens, F. J. Devlin, C. F. Chabalowski, and M. J. Frisch. "Ab Initio Calculation of Vibrational Absorption and Circular Dichroism Spectra Using Density Functional Force Fields." In: *The Journal of Physical Chemistry* 98.45 (1994), pp. 11623–11627. DOI: 10.1021/j100096a001. eprint: https://doi.org/10.1021/j100096a001. URL: https://doi.org/10.1021/j100096a001.

[125] Qing Tang and Zhen Zhou. "Graphene-analogous low-dimensional materials." In: *Progress in Materials Science* 58.8 (2013), pp. 1244–1315. ISSN: 0079-6425. DOI: https://doi.org/10.1016/j.pmatsci.2013.04.003. URL: http://www.sciencedirect.com/science/article/pii/S0079642513000376.

[126] M. Terrones et al. "Experimental and Theoretical Studies Suggesting the Possibility of Metallic Boron Nitride Edges in Porous Nanourchins." In: *Nano Letters* 8.4 (2008). PMID: 18333621, pp. 1026–

1032. DOI: 10.1021/nl072713m. eprint: https://doi.org/10.1021/nl072713m. URL: https://doi.org/10.1021/nl072713m.

[127] L. H. Thomas. "The calculation of atomic fields." In: *Mathematical Proceedings of the Cambridge Philosophical Society* 23 (05 1927), pp. 542–548.

[128] Sergio Tosoni, Christian Tuma, Joachim Sauer, Bartolomeo Civalleri, and Piero Ugliengo. "A comparison between plane wave and Gaussian-type orbital basis sets for hydrogen bonded systems: Formic acid as a test case." In: *The Journal of Chemical Physics* 127.15 (2007), p. 154102. DOI: 10.1063/1.2790019. eprint: https://doi.org/10.1063/1.2790019. URL: https://doi.org/10.1063/1.2790019.

[129] Noach Treitel 1, Roy Shenhar, Ivan Aprahamian, Tuvia Sheradsky, and Mordecai Rabinovitz. "Calculations of PAH anions: When are diffuse functions necessary?" In: *Phys. Chem. Chem. Phys.* 6 (6 2004), pp. 1113–1121. DOI: 10.1039/B315069K. URL: http://dx.doi.org/10.1039/B315069K.

[130] S. Trivedi, A. Srivastava, and R. Kurchania. "Silicene and Germanene: A First Principle Study of Electronic Structure and Effect of Hydrogenation-Passivation." In: *Journal of Computational and Theoretical Nanoscience, vol. 11, issue 3, pp. 781-788* 11 (Mar. 2014), pp. 781–788. DOI: 10.1166/jctn.2014.3428.

[131] Giovanni Tronci, Federico Raffone, and Giancarlo Cicero. "Theoretical Study of Nanoporous Graphene Membranes for Natural Gas Purification." In: *Applied Sciences* 8 (Sept. 2018), p. 1547. DOI: 10.3390/app8091547.

[132] M. Valiev et al. "NWChem: A comprehensive and scalable open-source solution for large scale molecular simulations." In: *Computer Physics Communications* 181.9 (2010), pp. 1477 – 1489. ISSN: 0010-4655. DOI: https://doi.org/10.1016/j.cpc.2010.04.018. URL: http://www.sciencedirect.com/science/article/pii/S0010465510001438.

[133] S. H. Vosko, L. Wilk, and M. Nusair. "Accurate spin-dependent electron liquid correlation energies for local spin density calculations: a critical analysis." In: *Canadian Journal of Physics* 58.8 (1980), pp. 1200–1211.

[134] Ashcroft N W and Mermin D N. *Solid State Physics*. CENGAGE learning, 2010.

[135] Bin Wang and Marie-Laure Bocquet. "Monolayer Graphene and h-BN on Metal Substrates as Versatile Templates for Metallic Nanoclusters." In: *The Journal of Physical Chemistry Letters* 2.18 (2011), pp. 2341–2345. DOI: 10.1021/jz201047c. eprint: https://doi.org/10.1021/jz201047c. URL: https://doi.org/10.1021/jz201047c.

[136] Liancheng Wang, Changhui Sun, Liqiang Xu, and Yitai Qian. "Convenient synthesis and applications of gram scale boron nitride nanosheets." In: *Catal. Sci. Technol.* 1 (7 2011), pp. 1119–1123. DOI: 10.1039/C1CY00191D. URL: http://dx.doi.org/10.1039/C1CY00191D.

[137] Rui Wang, Brian A. Ruzicka, Nardeep Kumar, Matthew Z. Bellus, Hsin-Ying Chiu, and Hui Zhao. "Ultrafast and spatially resolved studies of charge carriers in atomically thin molybdenum disulfide." In: *Phys. Rev. B* 86 (4 2012), p. 045406. DOI: 10.1103/PhysRevB.86.045406. URL: https://link.aps.org/doi/10.1103/PhysRevB.86.045406.

[138] K. L. Dimuthu M. Weerawardene and Christine M. Aikens. "Strong Tunable Visible Absorption Predicted for Polysilo-acenes Using TDDFT Calculations." In: *The Journal of Physical Chemistry Letters* 6.17 (2015). PMID: 26266968, pp. 3341–3345. DOI: 10.1021/acs.jpclett.5b01446. eprint: https://doi.org/10.1021/acs.jpclett.5b01446. URL: https://doi.org/10.1021/acs.jpclett.5b01446.

[139] Roland Widmer, Daniele Passerone, Thomas Mattle, Hermann Sachdev, and Oliver Gröning. "Probing the selectivity of a nanostructured surface by xenon adsorption." In: *Nanoscale* 2 (4 2010), pp. 502–508. DOI: 10.1039/B9NR00431A. URL: http://dx.doi.org/10.1039/B9NR00431A.

[140] E. Wigner. "On the Interaction of Electrons in Metals." In: *Phys. Rev.* 46 (11 1934), pp. 1002–1011.

[141] Heejun Yang, Jinseong Heo, Seongjun Park, Hyun Jae Song, David H. Seo, Kyung-Eun Byun, Philip Kim, Inkyeong Yoo, Hyun-Jong Chung, and Kinam Kim. "Graphene barristor, a triode device with a gate-controlled Schottky barrier." In: *Science* 336 6085 (2012), pp. 1140–3.

[142] Haibo Zeng, Chunyi Zhi, Zhuhua Zhang, Xianlong Wei, Xuebin Wang, Wanlin Guo, Yoshio Bando, and Dmitri Golberg. ""White Graphenes": Boron Nitride Nanoribbons via Boron Nitride Nanotube Unwrapping." In: *Nano Letters* 10.12 (2010). PMID: 21028887, pp. 5049–5055. DOI: 10.1021/nl103251m. eprint: https://doi.org/10.1021/nl103251m. URL: https://doi.org/10.1021/nl103251m.

[143] Fawei Zheng, Gang Zhou, Zhirong Liu, Jian Wu, Wenhui Duan, Bing-Lin Gu, and S B. Zhang. "Half metallicity along the edge of zigzag boron nitride nanoribbons." In: *Physical Review B - PHYS REV B* 78 (Nov. 2008). DOI: 10.1103/PhysRevB.78.205415.

[144] Wu Zhou, Myron D. Kapetanakis, Micah P. Prange, Sokrates T. Pantelides, Stephen J. Pennycook, and Juan-Carlos Idrobo. "Direct Determination of the Chemical Bonding of Individual Impurities in Graphene." In: *Phys. Rev. Lett.* 109 (20 2012), p. 206803. DOI: 10.1103/PhysRevLett.109.206803. URL: https://link.aps.org/doi/10.1103/PhysRevLett.109.206803.

[145] Yingchun Zhu, Yoshio Bando, Longwei Yin, and Dmitri Golberg. "Field Nanoemitters: Ultrathin BN Nanosheets Protruding from Si 3 N 4 Nanowires." In: *Nano letters* 6 (Jan. 2007), pp. 2982–6. DOI: 10.1021/nl061594s.

[146] Zafer Çiplak, Nuray Yildiz, and Ayla Çalimli. "Investigation of Graphene/Ag Nanocomposites Synthesis Parameters for Two Different Synthesis Methods." In: *Fullerenes, Nanotubes and Carbon Nanostructures* 23.4 (2015), pp. 361–370. DOI: 10.1080/1536383X.2014.894025. eprint: https://doi.org/10.1080/1536383X.2014.894025. URL: https://doi.org/10.1080/1536383X.2014.894025.

COLOPHON

This document was typeset using the typographical look-and-feel `classicthesis` developed by André Miede. The style was inspired by Robert Bringhurst's seminal book on typography "*The Elements of Typographic Style*". `classicthesis` is available for both LaTeX and LyX:

https://bitbucket.org/amiede/classicthesis/

Happy users of `classicthesis` usually send a real postcard to the author, a collection of postcards received so far is featured here:

http://postcards.miede.de/